

## **General Disclaimer**

### **One or more of the Following Statements may affect this Document**

- This document has been reproduced from the best copy furnished by the organizational source. It is being released in the interest of making available as much information as possible.
- This document may contain data, which exceeds the sheet parameters. It was furnished in this condition by the organizational source and is the best copy available.
- This document may contain tone-on-tone or color graphs, charts and/or pictures, which have been reproduced in black and white.
- This document is paginated as submitted by the original source.
- Portions of this document are not fully legible due to the historical nature of some of the material. However, it is the best reproduction available from the original submission.

# **NASA Contract Report 145368**

(NASA-CR-145368) THERMAL-STRUCTURAL DESIGN  
STUDY OF AN AIRFRAME-INTEGRATED SCRAMJET  
Interim Summary Report, Jun. 1975 - Mar.  
1977 (AiResearch Mfg. Co., Los Angeles,  
Calif.) 126 p HC A07/MF A01

N79-15045

CSSL 21A G3/07

Unclas  
42060

## **Interim Summary Report Thermal-Structural Design Study of an Airframe - Integrated Scramjet**

**J.J. Killackey, E.A. Katinsky,  
S. Tepper, A.A. Vuigner**

**AIRESEARCH MANUFACTURING COMPANY OF CALIFORNIA  
A Division of The Garrett Corporation**

**CONTRACT NAS 1-13984  
December 1978**

**NASA**

National Aeronautics and  
Space Administration

**Langley Research Center  
Hampton, Virginia 23665**

## FOREWORD

This interim report of an analytical study of an airframe-integrated Scramjet is submitted to the National Aeronautics and Space Administration in accordance with NASA Contract NAS1-13984. The work was performed between June 1975 and March 1977, by the AiResearch Manufacturing Company of California, a division of The Garrett Corporation.

The Project Manager for NASA was Mr. A. R. Wieting, Thermal Structures Branch, Structures and Dynamics Division, NASA Langley Research Center. The AiResearch Program Manager was Mr. O. A. Buchmann. The principal contributors to the study were Messrs. J. J. Killackey (Program Engineer), E. A. Katinszky and S. Tepper (Structural Analysis), A. A. Vuigner (Thermal Analysis), and M. Cooke (Engine Design).

Values for the physical quantities are given in both SI and U.S. Customary units. Calculations were made in U.S. Customary units.

# CONTENTS

	Page
INTRODUCTION .....	1
SYMBOLS .....	2
ENGINE DESCRIPTION .....	3
DESIGN CONDITIONS .....	10
Internal Flow Properties .....	10
Pressure Loads .....	13
Inertia Loads .....	13
Structural Design Criteria .....	13
Fuel/Coolant Conditions .....	17
DESIGN LOADING .....	18
Aerodynamic Heating .....	18
Heat Load Summary .....	21
Leading Edge Heat Flux .....	21
Corner Flow Heating .....	23
Strut Pressure Loads .....	24
Panel Pressure Loads .....	24
DESIGN APPROACH .....	26
Cooling System .....	26
Fuel Injection Struts .....	27
Engine Primary Structure .....	28
Transient Behavior .....	29
Engine-Aircraft Interface .....	29
Fuel System .....	29
Layout Design .....	29
DESIGN AND PERFORMANCE .....	30
Material Selection .....	30
Coolant Flow Routing .....	34
Flight Envelope Cooling Requirements .....	43
Thermal Protection System (TPS) .....	47
Leading Edges .....	61
Fuel Injection Struts .....	70
Primary Structure .....	83
ENGINE-AIRCRAFT INTERFACE .....	104

## CONTENTS (Continued)

	Page
HYDROGEN FLOW CONTROL .....	107
Coolant Flow Routing .....	107
Fuel System .....	108
CONCLUDING REMARKS .....	115
Cooled Structure .....	115
Coolant Flow Routing .....	115
Thermal Protection System .....	115
Leading Edges .....	116
Fuel Injection Struts .....	116
Engine-Aircraft Interface .....	116
Hydrogen Flow Control .....	116
REFERENCES .....	117

## LIST OF ILLUSTRATIONS

Figure		Page
1	Scramjet Engine Configuration and Installation .....	4
2	Scramjet Thermal-Structural Design .....	7
3	Typical Construction of Primary Support Structure .....	8
	and the Thermal Protection System (TPS)	
4	Altitude-Mach Number Envelope .....	11
5	Flow Properties for Internal Surfaces of an Outboard .....	12
	Module (Condition H)	
6	Engine Unstart Pressure Distributions .....	14
7	Aerodynamic Heating Rates on Engine Internal Surfaces .....	19
8	External Surface Thermal Loading .....	20
9	Comparison of Laminar and Turbulent Heating in a Corner; .....	24
	Sharp Leading Edge (ref. 9)	
10	Strut Loads, Transient Unstart Conditions .....	25
11	Panel Flow Routing Schemes .....	35
12	Primary Structure Temperature Profiles .....	37
13	Sidewall Shunt Coolant Distribution Concept .....	40
14	Coolant Flow Conditions .....	42
15	Heat Load Split Between Engine Sections .....	46
16	Inlet Heating Fraction .....	46
17	TPS Heat Exchanger Configurations .....	48
18	TPS Heat Exchanger Performance .....	49
19	Elastic-plastic Cycle .....	53
20	TPS Structural Design Fin Configurations .....	54
21	Finite Element Model .....	55
22	Effective Stresses (ksi) in Plate-Fin Structure .....	56
23	TPS Response to Thermal Gradient .....	57
24	Cycle Life for Formed-Fin TPS .....	59
25	Cycle Life for Machined-Fin TPS .....	60
26	TPS Configuration .....	63
27	Cooling Options .....	64
28	Typical Temperature Gradients Around Sidewall and .....	67
	Side Strut Leading Edge	
29	Center Strut Fuel/Coolant Passages .....	71
30	Midspan Tie Design .....	74
31	Finite Element Model of Three-Strut Assembly .....	76
32	Effective (von Mises) Stresses--Highly Stressed Areas .....	79
	with Midspan Tie	
33	Absolute Deformation with Midspan Tie, Perpendicular to .....	80
	Flow, Due to Pressure Only	
34	Absolute Deformation with Midspan Tie, Parallel to Flow, .....	81
	Due to Pressure Only	
35	Modified Strut Structural Design with Midspan Tie .....	82
36	Side Strut Structure for Increased-Cooling Analysis .....	84
37	Primary Support Structure for Swept Beam Model .....	85
38	Plate-Beam Element Sliding Connection Simulation .....	87
39	Honeycomb Thickness Variation (All-Honeycomb Model) .....	88

LIST OF ILLUSTRATIONS (Continued)

Figure		Page
40	Finite Element Models .....	90
41	Sidewall Performance .....	91
42	Topwall Performance .....	92
43	Cowl Performance .....	93
44	Sidewall Distorted Geometry .....	95
45	Nozzle Deformation .....	96
46	Model for Transient Temperature Analysis .....	99
47	Mission Profile .....	101
48	Coolant Outlet Temperature .....	101
49	Structural Temperature Response .....	102
50	Sidewall Honeycomb Panel Temperature Profiles .....	103
51	Engine Mounting Considerations .....	105
52	Engine Fuel System .....	109

## LIST OF TABLES

Table		Page
1	Inertia Loading, G Units .....	16
2	Heat Loads at Condition H .....	22
3	Leading Edge Heat Fluxes at Condition H .....	22
4	Material Properties for TPS Candidate Alloys (SI Units) .....	31
5	Materials Selected for Design .....	33
6	Flight Envelope Coolant Requirements .....	44
7	Sidewall TPS Temperature Gradient and Pressure Drop .....	50
	(SI Units)	
8	TPS Performance .....	62
9	Leading Edge Thermal Performance Hastelloy X Material .....	68
10	Leading Edge Cycle Life .....	69
11	Tubular Manifold Performance .....	73
12	Corner Displacements .....	97
13	Weight Comparison .....	97
14	Fuel System Components (Two Groups of Three Modules; .....	110
	Six Modules Total)	
15	Turbopump Subsystem, Three Modules .....	111
16	Fuel System Plumbing Line Size .....	114



## INTRODUCTION

The Langley Research Center of NASA has been involved in a research program for the development of airframe-integrated Scramjet concepts. These concepts use the entire undersurface of the aircraft to process the engine airflow. The forebody of the aircraft serves as an extension of the engine inlet and the afterbody serves as an extension of the engine nozzle.

The NASA Hypersonic Research Engine (HRE) program (ref. 1) was a major contributor to the development of Scramjet technology. This program culminated in two major milestones: (1) successful development of the first flight-weight, hydrogen-cooled engine structure, including verification tests in the NASA-Langley 8-Foot High-Temperature Structures Tunnel; and (2) confirmation of dual-mode (subsonic/supersonic combustion) aero-thermodynamic performance at Mach 5 to 7 in the NASA-Lewis facility at Plum Brook.

Subsequent research at NASA-Langley has led to a lightweight, fixed-geometry, modular, airframe-integrated Scramjet engine concept that promises high installed performance (net thrust) over a wide Mach number range. Performance predictions for this hydrogen-fueled, regeneratively cooled Scramjet indicate a cooling requirement that is less than the heat sink available in the hydrogen fuel up to at least a flight Mach number of 10. This provides a potential for actively cooling the airframe.

This study is an extension of the preliminary thermal-structural design of an airframe-integrated Scramjet conducted by NASA (ref. 2). The current objective is to define a practical engine concept that has a sound basis in materials and manufacturing technology. Emphasis is placed on the engine thermal-structural design although consideration is given to the fuel subsystem and the aircraft interface. The thermal-structural design evolved in the ref. 2 study and the HRE technology form the basis for this effort. The aerodynamic lines were defined by NASA and remained unchanged during the study.

Engine design is based on a research-size aircraft to provide a focal point; however, technological development is aimed at more advanced applications. The importance of hypersonic technology, its potential applications, and the case for a hypersonic research vehicle are described by Hearth and Preyss (ref. 3).

A major portion of the design study has been completed. Analyses are continuing to refine the strut and primary structure and to establish thermal transient characteristics. In a separate effort, NASA is examining the strut dynamic response to unstart. This interim report is being issued to make available the results obtained to date. Some of these are preliminary and may change in the course of the continuing effort.

## SYMBOLS

$E$	Young's modulus
$h$	heat transfer coefficient
$k$	thermal conductivity
$M_{\infty}$	free-stream Mach number
$q_{\infty}$	free-stream dynamic pressure
$RA$	reduction in area
$R_x$	local Reynolds number
$V_{\infty}$	free-stream velocity
$\alpha$	coefficient of thermal expansion
$\sigma_y$	yield stress
$\phi_c$	cooling equivalence ratio (fuel used for regenerative engine cooling as fraction of fuel burned)
$\phi_f$	fuel equivalence ratio burned

## ENGINE DESCRIPTION

A typical installation of a Scramjet engine on a high-speed research airplane is shown in fig. 1. The rectangular modular engine is attached directly to the vehicle undersurface. The aircraft forebody serves as the air inlet compression ramp and the afterbody serves as an extension on the engine nozzle; the entire undersurface is integrated into the engine design. The modular engines provide maximum capture of the air flow between the body and bow shock with minimum external drag.

Since the Scramjet does not operate at low speeds, some form of takeoff and acceleration system is required. In the research application, the vehicle is air launched at Mach 0.8, rocket boosted to Mach 4, and flown on the hydrogen-fueled Scramjets over the prescribed envelope.

As a baseline, the Scramjets were sized for one concept of a hypersonic research vehicle that has a weight after rocket burn-out of 9720 kg (21,430 lbf). The aircraft is 20.3 m (66.7 ft) long and requires six Scramjet engine modules that are located 12.2 m (39.9 ft) from the aircraft nose. Two inner Scramjet modules are shown in fig. 1; the side wall of one module is removed to show the internal engine surfaces. The Scramjet module is 45.7 cm (18.0 in.) high by 36.6 cm (14.4 in.) wide with an overall length of 314.3 cm (123.742 in.). External aerodynamic lines are defined in detail on Drawing 190062.

Sidewall leading edges are swept to provide an "open window" upstream of the cowl leading edge to spill flow downward during the inlet starting process at the low end of the Mach number range (ref. 2). This important design feature circumvents variable geometry. Consequently, sidewall leading edges are swept at 48 deg and the cowl does not begin until engine station 49.031. Three fuel injection struts are used to minimize the combustor length and heat flux to the internal surfaces. Heat release distribution is tailored by the use of combined parallel and perpendicular fuel injection (ref. 2).

To provide accessibility and replaceability of parts, each Scramjet module is comprised of four structural panels: topwall, cowl, sidewalls, and three fuel injection struts. The two side struts are identical, asymmetric, and have 3/2 of the chord of the symmetric center strut.

The module structural design concept is shown in figs. 2 and 3. All engine internal and external surfaces exposed to gas flow are cooled regeneratively by circulating hydrogen fuel through a thermal protection system (TPS) prior to injection. Coolant is introduced at the leading and trailing edges (low heat load) and flows toward the engine throat (highest heat load) where it is collected in manifolds and directed to the fuel plenum. From there, it is routed to fuel manifolds in each strut and injected into the air stream.

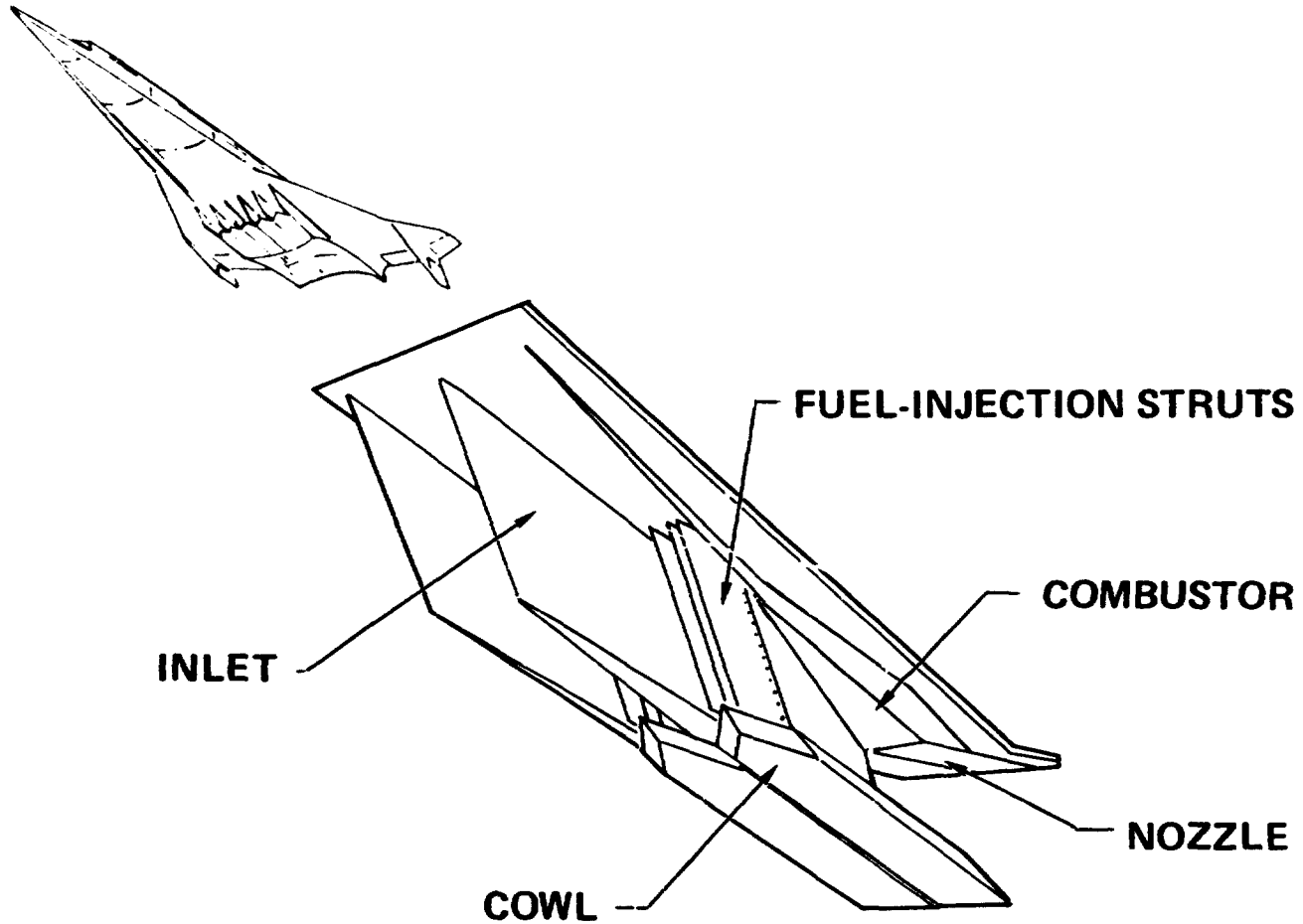
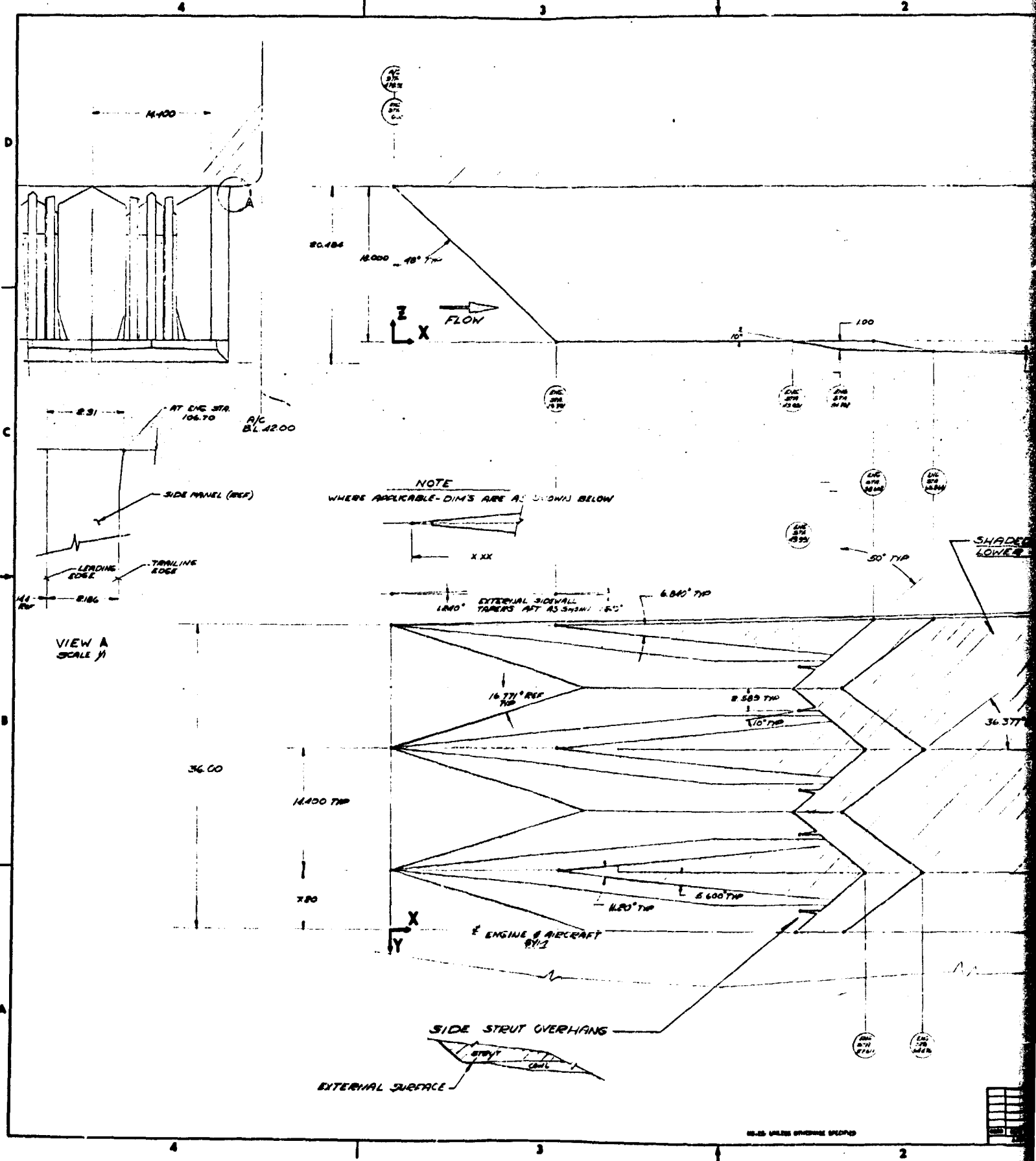


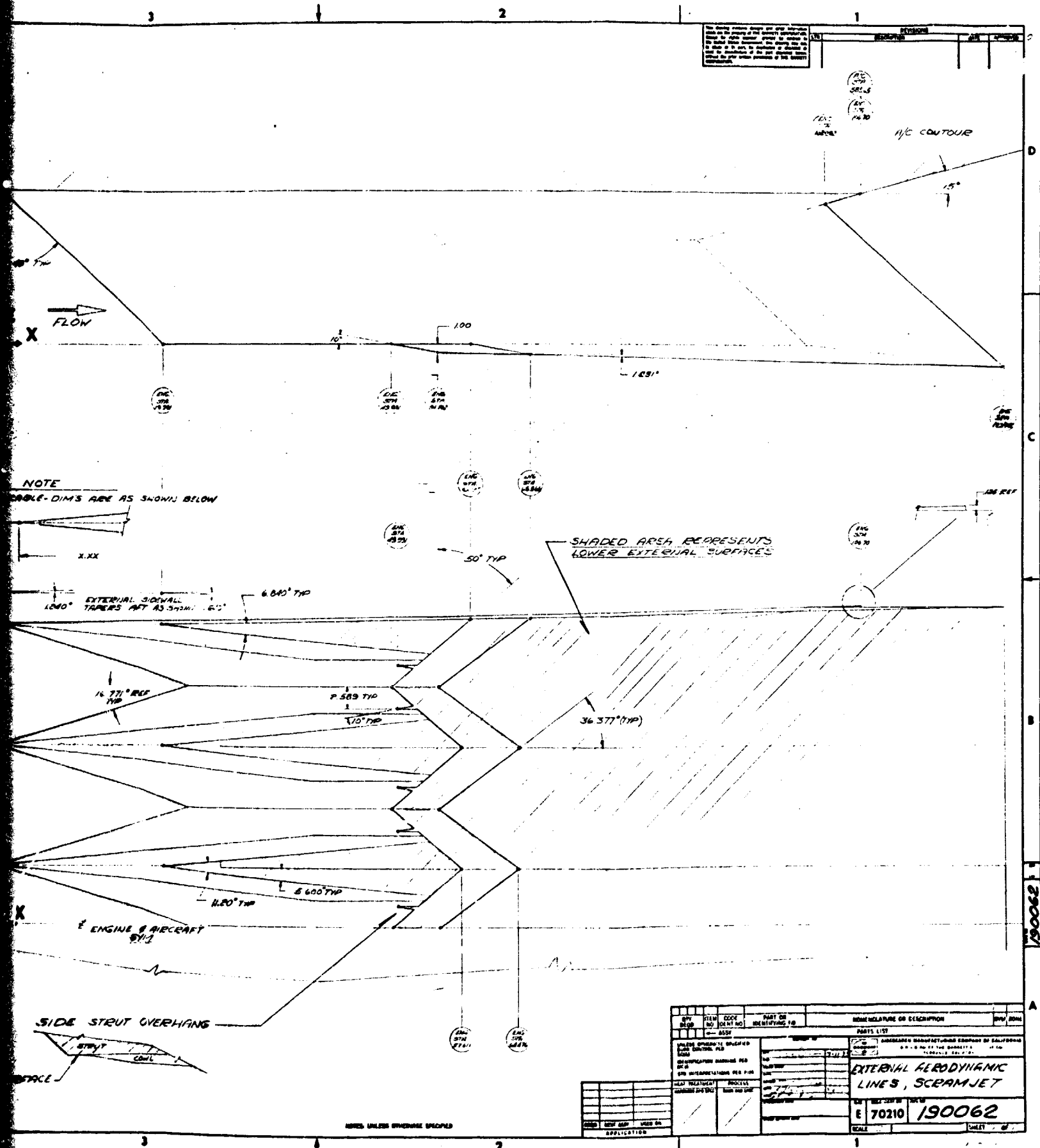
Figure 1.--Scramjet Engine Configuration and Installation.

S-2606

**SOLIDOUT FRAME**

ORIGINAL PAGE IS  
OF POOR QUALITY





NOTE  
DOUBLE-DIMS ARE AS SHOWN BELOW  
X.XX

SHADE AREA REPRESENTS LOWER EXTERNAL SURFACES

ITEM	QTY	DESCRIPTION	UNIT
1	1	EXTERNAL AERODYNAMIC LINES, SCRAMJET	
PART OR IDENTIFYING NO. MANUFACTURE OR DESCRIPTION PARTS LIST EXTERNAL AERODYNAMIC LINES, SCRAMJET E 70210 190062			
DATE	BY	CHKD	APP'D
SCALE	SHEET NO. OF TOTAL SHEETS		

UNLESS OTHERWISE SPECIFIED

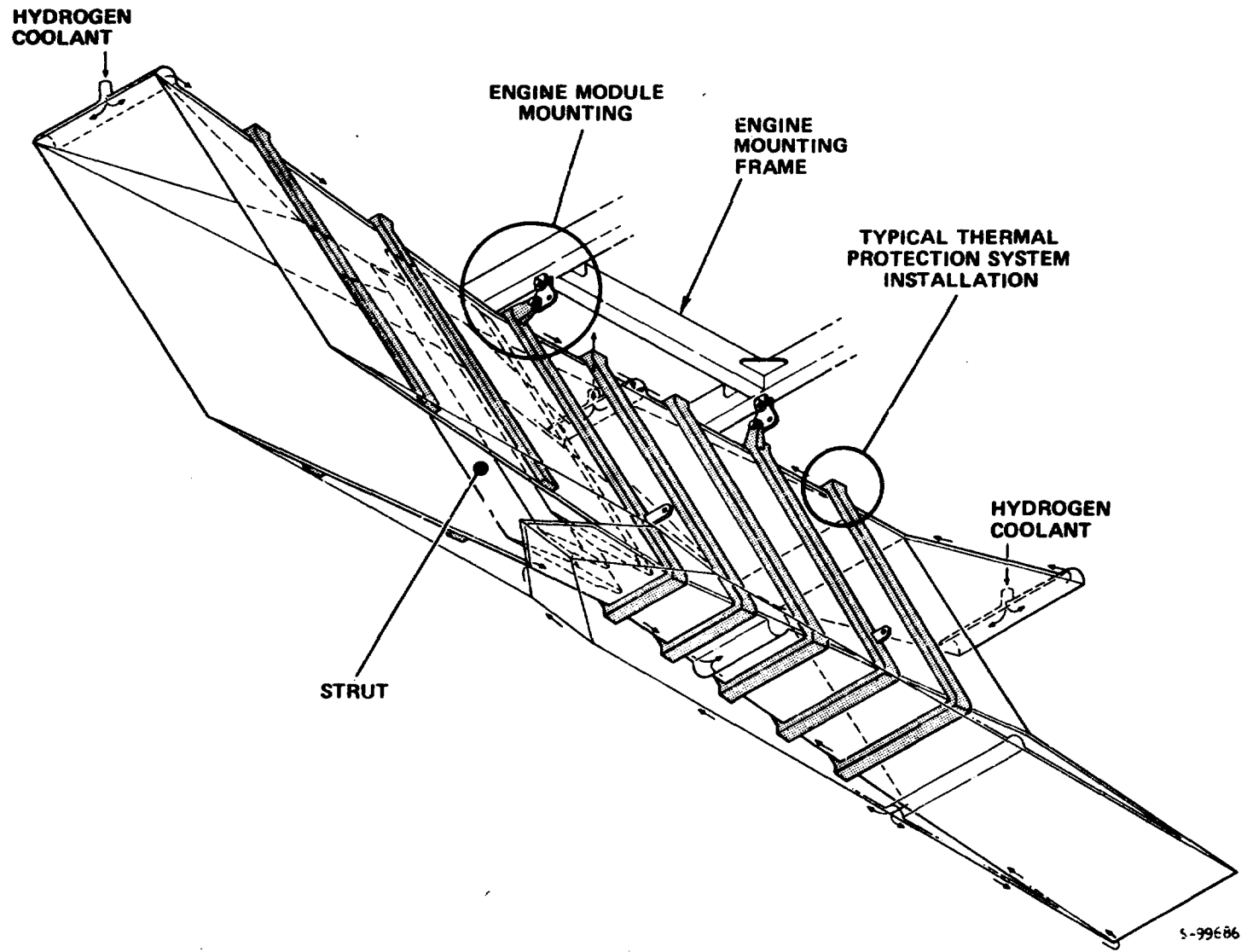


Figure 2---Scramjet Thermal-Structural Design.

All leading edges are impingement cooled. Coolant is injected through multiple slots and impinges directly on the inside surface of the leading edge, turns, and then flows through the TPS surface. Impingement cooling using cryogenic hydrogen provides a maximum possible cooling effect in these areas of maximum heat flux.

Pressure and thermal loads acting on the panels are accommodated by a honeycomb primary structure in the selected structural configuration. The panels are rigidly joined at the corners using a bolted connection and static seals to contain the gas flow. The struts are inserted through openings in the topwall and secured by a fixed mount in the topwall and a sliding support in the cowl. Bulkheads within the struts provide separate manifolds and contain the high-pressure hydrogen fuel and coolant.

The TPS is not considered as part of the primary load-carrying structure although it must contain the high-pressure hydrogen coolant at elevated temperature conditions. In the combustor section, the heat flux is intense and the temperature gradient across the TPS high. Under these conditions, the TPS goes into a plastic state and the controlling factor in structural design becomes cyclic life. The cooling flow passages are parallel channels in the panels and an offset pin fin geometry in the struts. The passages are formed using photochemical machining techniques.

Scramjet modules are assembled and joined to a separate support frame that transmits engine thrust, drag, and inertia to the aircraft. The support frame can also serve to mount coolant and fuel plenums and control valves. Differential thermal growths between the engine modules, support frame, and aircraft are accommodated by swing and sliding links. The engine compartment is sealed to prevent entry of hot gases.

Materials of construction used in design are: honeycomb panels (topwall, sidewalls, and cowl), Hastelloy X and Inconel 718; strut primary structure, Inconel 718; clips and beams, Inconel 718; manifolds and the leading and trailing edge support structure, Hastelloy X; TPS, Nickel-200 and Hastelloy X; and the mounts and mounting frame, Inconel 718.

**PRECEDING PAGE BLANK NOT FOLLOWS**



## DESIGN CONDITIONS

Normal engine operation is from Mach 4 to 10 with cruise at a dynamic pressure of 23.9 kPa (500 psf) and ascent at a dynamic pressure of 71.8 kPa (1500 psf). The engine also has the capability of undergoing a 2g powered maneuver at any condition within this envelope. The altitude-Mach number envelope is shown in fig. 4. It is assumed that the engine can reach steady-state operation at any point within the envelope. Transient conditions such as startup or a throttle chop can dictate structural design and are, therefore, considered in the study. All engine operating conditions (A through I) are taken from the contract statement of work (SOW).

Flight conditions resulting in maximum thermal loads and aero-pressure loading received special attention. Maximum thermal loading to the engine surfaces occurs during a 2g maneuver at a flight Mach number of 10, a dynamic pressure of 71.8 kPa (1500 psf), and a combustion equivalence ratio of 1.5 (Condition H). Maximum aerodynamic pressure loading occurs during an engine unstart condition resulting from thermal choking in the combustor. For a combustion equivalence ratio of 1.0, a 2g maneuver, and a dynamic pressure of 71.8 kPa (1500 psf), this condition occurs at a flight Mach number of 5.1 (Condition G). This is a transient condition that produces a pressure pulse during the transition from supersonic to subsonic flow.

In addition to these conditions, several other conditions within the flight envelope were considered with regard to cooling requirements. Engine cooling performance throughout the envelope must be examined to substantiate the feasibility of using the excess capacity for aircraft cooling. Condition B requires maximum coolant utilization. Conditions A, D, E, and F are typical cruise conditions. The Mach 10, zero fuel equivalence ratio point, Condition I, represents a possible maneuver after a throttle chop. At Mach 4, Condition C, fuel is assumed to be injected from both the struts and from the sidewalls within the combustor section to gain additional thrust.

### Internal Flow Properties

Inviscid flow properties for the engine internal surfaces were provided by NASA. Flow properties within the engine are constant along the 48-deg sweepline.

Typical flow properties along the internal surface of an external sidewall are presented in fig. 5. The abscissa in fig. 5 is the distance measured along the X-axis from the sidewall leading edge for all vertical elevations from  $Z = 0.0$  to 45.7 cm (18.00 in.). This provides for constant properties along a 48-deg sweepline in the inlet and combustor sections.

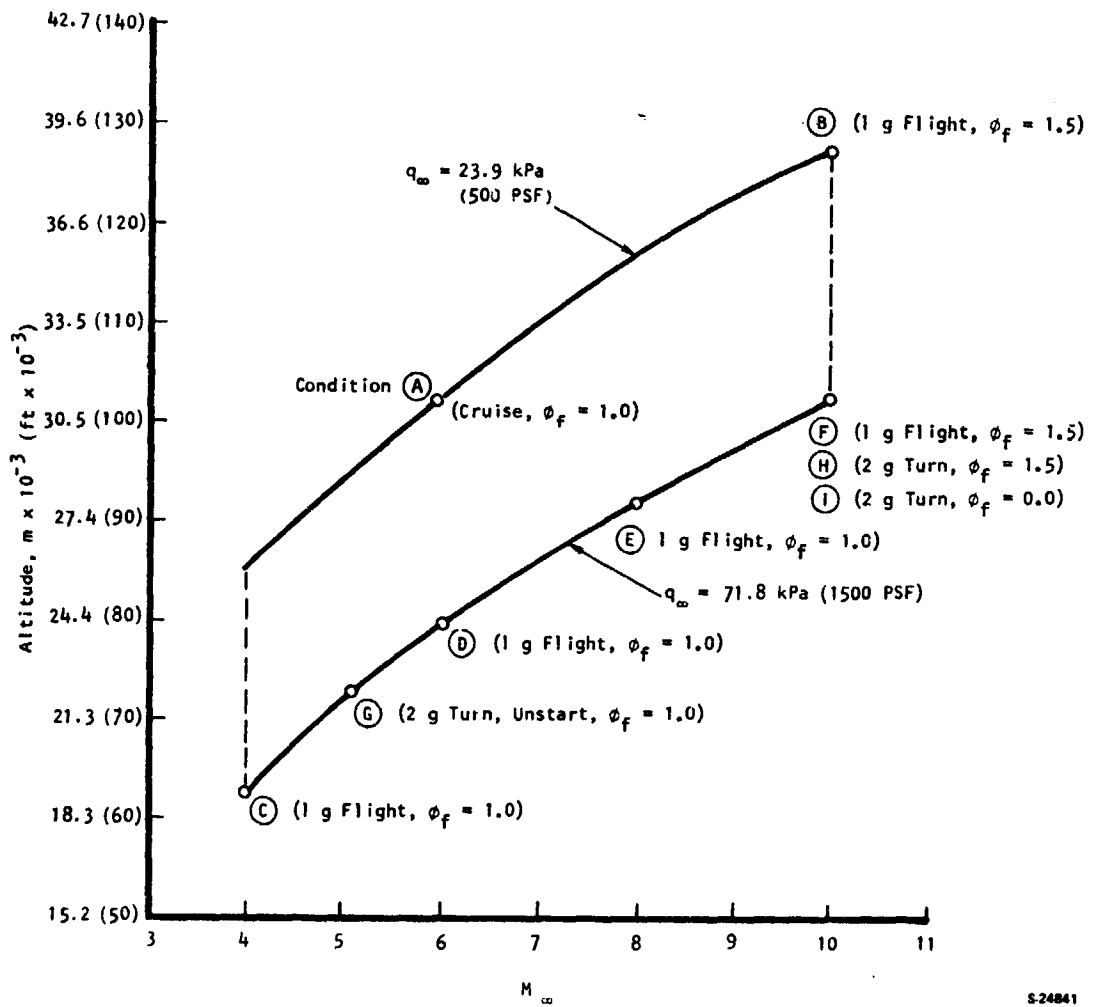
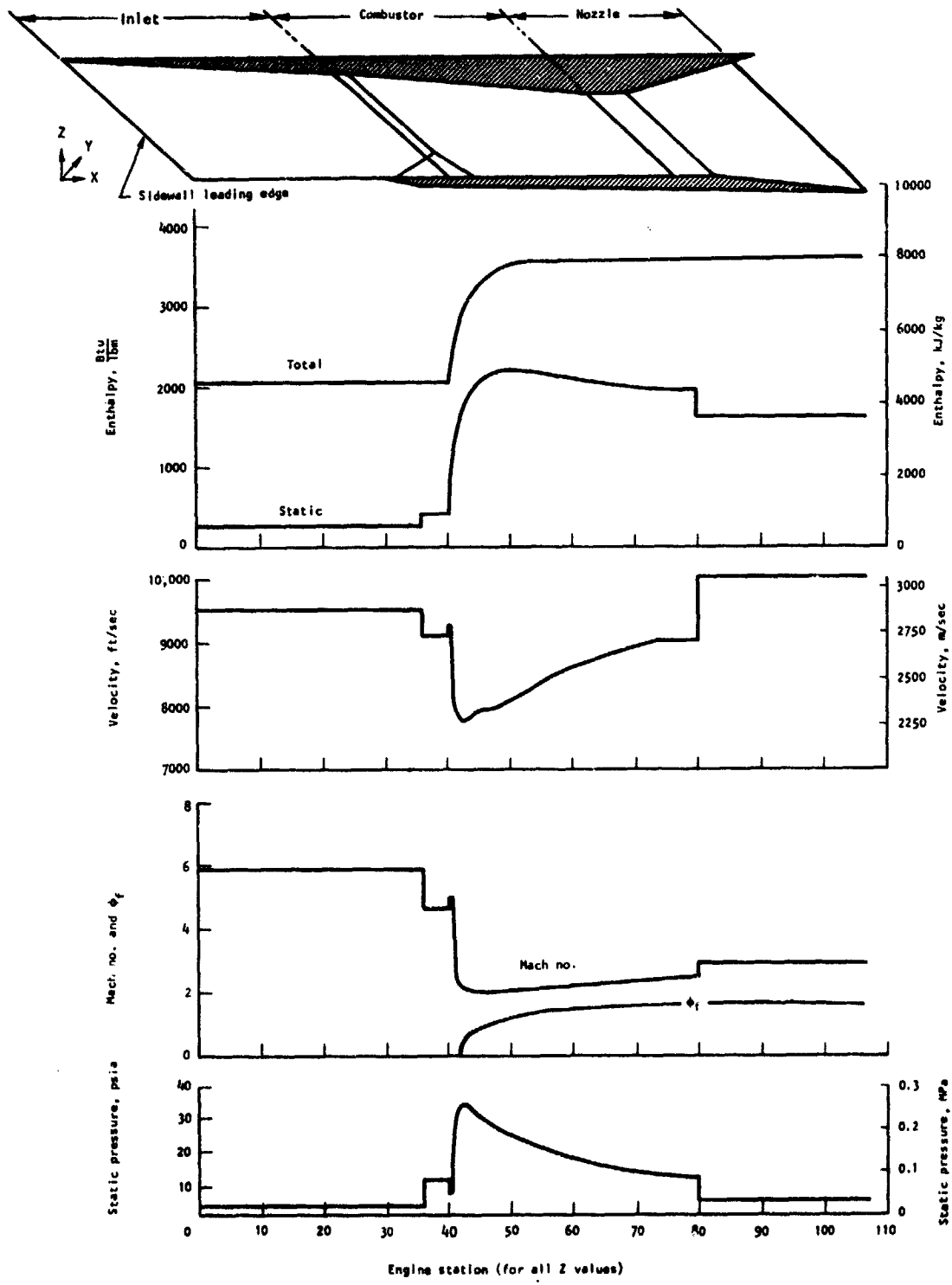


Figure 4.--Altitude-Mach Number Envelope.



S-15705-B

Figure 5.--Flow Properties for Internal Surfaces of an Outboard Module (Condition H).

## Pressure Loads

Maximum pressures through most of the engine are expected to occur during an engine unstart at Mach 5.1 (Condition G). Experimental data (ref. 4) indicate that the maximum unstart pressures are transient pressures, occurring as a shock wave moves upstream through the engine from the thermal choke line. Since the transient pressure pulse is not defined fully, the design pressure loading is taken conservatively as the envelope of the peak transient pressure. Pressure loads acting on the respective panels and struts are shown in fig. 6. The isobars are vertical upstream of the thermal choke line.

For this analysis, it is assumed that the unstart pressure pulse is equivalent to a steady-state load. A pulse period close to the natural frequency of the panels on the struts could cause greatly increased loading. Dynamic loading is especially critical in the case of the struts, which are slender structural elements. More complete definition of the unstart dynamics is especially desirable for these reasons.

It is assumed that as a possibility, albeit remote, an unsymmetrical unstart condition can exist on the side strut. That is, the flow is started (supersonic) on one side of the strut and unstarted (subsonic) on the other.

## Inertia Loads

Inertia loads used in the analysis are defined in Table 1. These loads are typical for a research airplane that is air launched, accelerated by rocket power, and lands without thrust. The effect of the inertia loads on the engine panels is not significant. These loads are of primary concern for the engine mounting design.

## Structural Design Criteria

The basic design objective for the engine is to minimize engine mass and cooling requirements and maintain structural integrity during all flight conditions, including any engine unstarts and any periods of high heat flux to the engine with or without combustion. Design life goals are 100 hours of hot operation with 1000 operational cycles. In addition, the engine must withstand 10 engine unstarts during the 100-hr lifetime at the maximum aero-pressure loading condition. Thermal and mechanical distortions that occur during normal service are limited and can change the flow area by no more than 5 percent or an angle by no more than 0.4 deg.

In the combustor section and at the leading edges, the heat flux is intense and the temperature gradient across the TPS high. It is not possible to keep the TPS material within elastic limits and the material goes into a plastic state. The controlling structural design criterion is low-cycle fatigue. For the primary support structure, however, the accepted design practice is to stay within the elastic limit and the material yield strength becomes the governing design criterion.

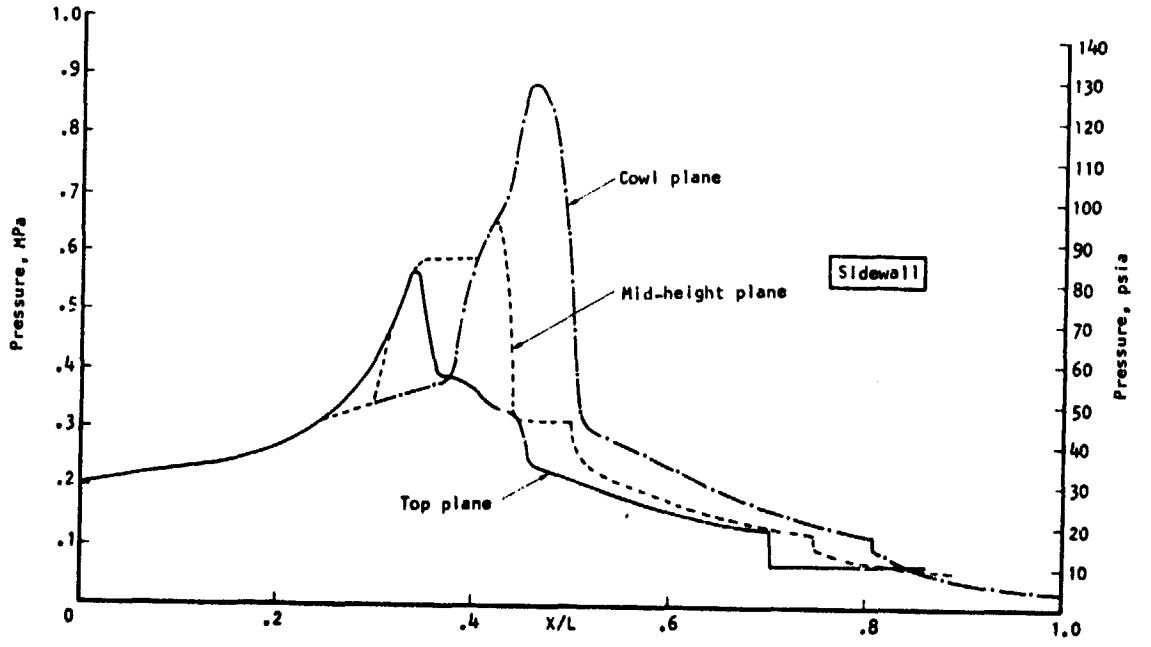
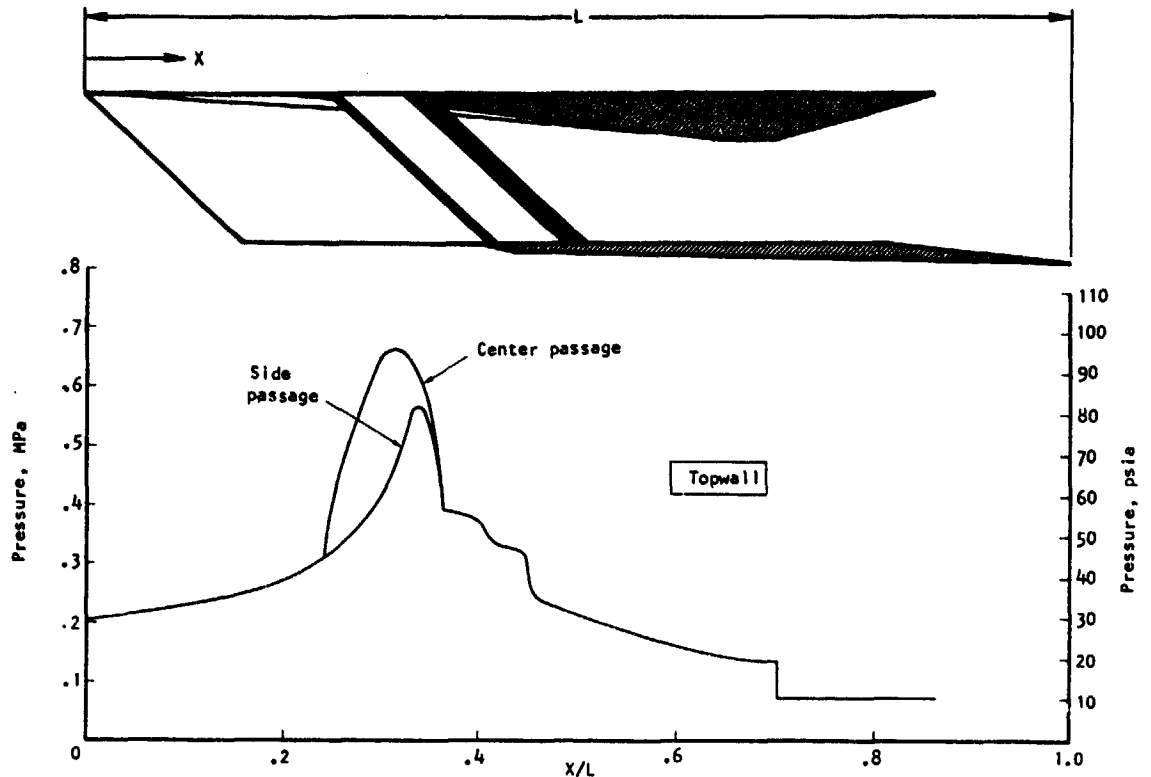


Figure 6.--Engine Unstart Pressure Distributions.

S-26387

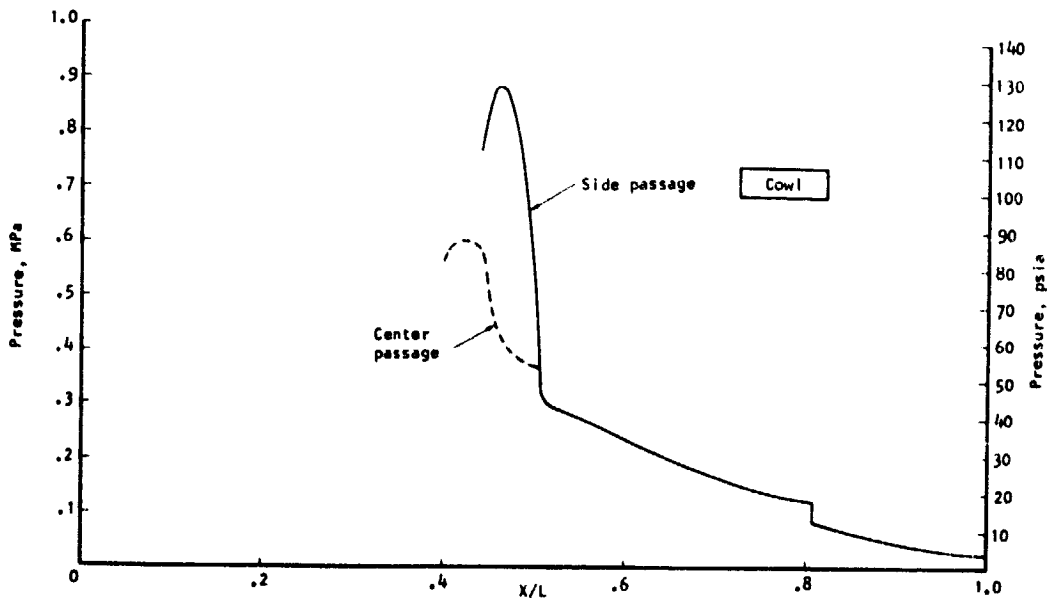
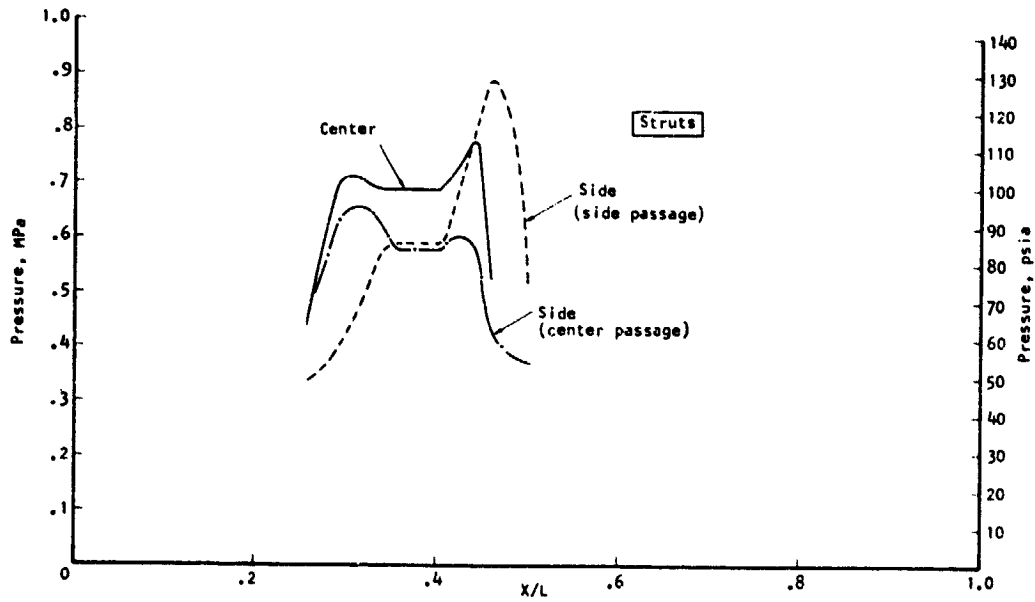
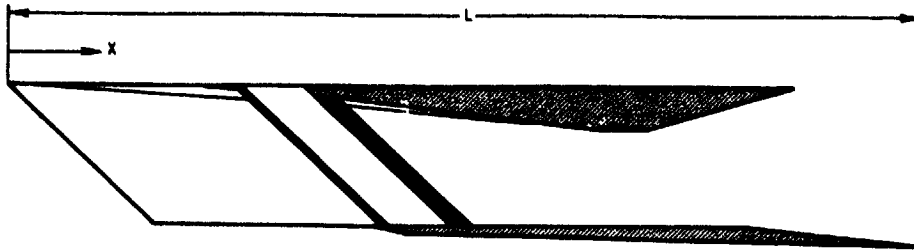


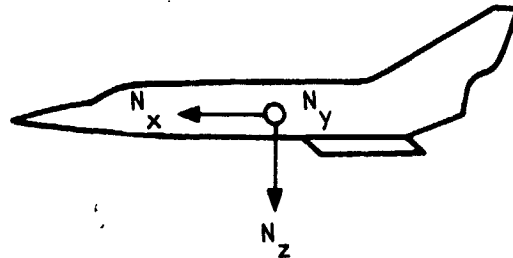
Figure 6.--(Concluded).

S-25308

TABLE 1.--INERTIA LOADING, G UNITS

Condition	Vertical (Z)	Maximum load, g	
		Side (Y)	Fore-aft (X)
Thrust or no thrust			
1) Pull-up after B-52 drop	2.5	<u>+0.5</u>	+1.5 -0.5
2) Nose over after climb and burnout	-1.0	<u>+0.5</u>	+3.0 -0.5
3) Turn at Mach 10	2.0	<u>+0.5</u>	<u>+0.5</u>
Attached to B-52, no thrust (*)	+6.0 -2.0	<u>+2.0</u>	<u>+2.0</u>
Research plane landing, no thrust	+6.8	<u>+1.0</u>	<u>+1.0</u>

(\*) Used only for aircraft engine interface design, cold conditions.



Baseline thermal-structural concepts and materials are derived from technology developed primarily on the NASA Hypersonic Research Engine (HRE) project (ref. 1) and hydrogen-cooled panel studies (refs. 5 and 6). Maximum operating temperature in these structures was limited to 870°C (1600°F) based on creep-rupture and low-cycle fatigue structural design criteria. This maximum temperature occurs in the outer fiber of the thermal protection system (TPS). Minimum operating temperature is equal to the hydrogen coolant supply temperature, 20°K (37°R). Reduced maximum operating temperatures are specified for the primary support structure to ensure meeting the elastic behavior design criteria.

The Scramjet structure and the associated operating conditions based on the above criteria are summarized below.

Structure Element	Operating Conditions
Thermal protection system	20° to 1144°K (37° to 2060°R), exposed to hot products of combustion and high-pressure hydrogen coolant
Primary structure (honeycomb)	20° to 890°K (37° to 1600°R), exposed to hydrogen coolant (hot face)
Clips and support beams	56° to 667°K (100° to 1200°R), ambient air

Because of the wide range of operating conditions, a single material will not necessarily be optimum for all areas.

#### Fuel/Coolant Conditions

The fuel/coolant is parahydrogen stored cryogenically as a liquid at 20°K (37°R) and 138 kPa (20 psia). Hydrogen temperature at the engine inlet is taken as 56°K (100°R) to allow for pump work and aerodynamic heating effects. For maximum utilization of the hydrogen heat sink capability, the design objective is to heat the hydrogen coolant to 890°K (1600°R) (primary structure temperature limit) within any cooling circuit.

Fuel flows are specified by NASA. Minimum fuel injection pressure is specified as 4.83 MPa (700 psia) to obtain the proper fuel flow rate and penetration into the airstream. The pressure drop across any cooling circuit is assumed to be 1.72 Mpa (250 psi) with 0.34 MPa (50 psi) allowed across the control valves and distribution system. The resulting engine coolant inlet manifold pressure is 6.9 MPa (1000 psia), which is compatible with the pressure containment capability of candidate structures and turbopump delivery pressures. It does not necessarily represent an upper limit for either.



## DESIGN LOADING

### Aerodynamic Heating

Aerodynamic heating of the internal engine surfaces (sidewall, top surface, cowl), strut sides, and external surfaces was determined for the Condition H maximum thermal load case. Calculations were performed by the adiabatic wall reference enthalpy method (ref. 7). Results are presented in Figures 7 and 8.

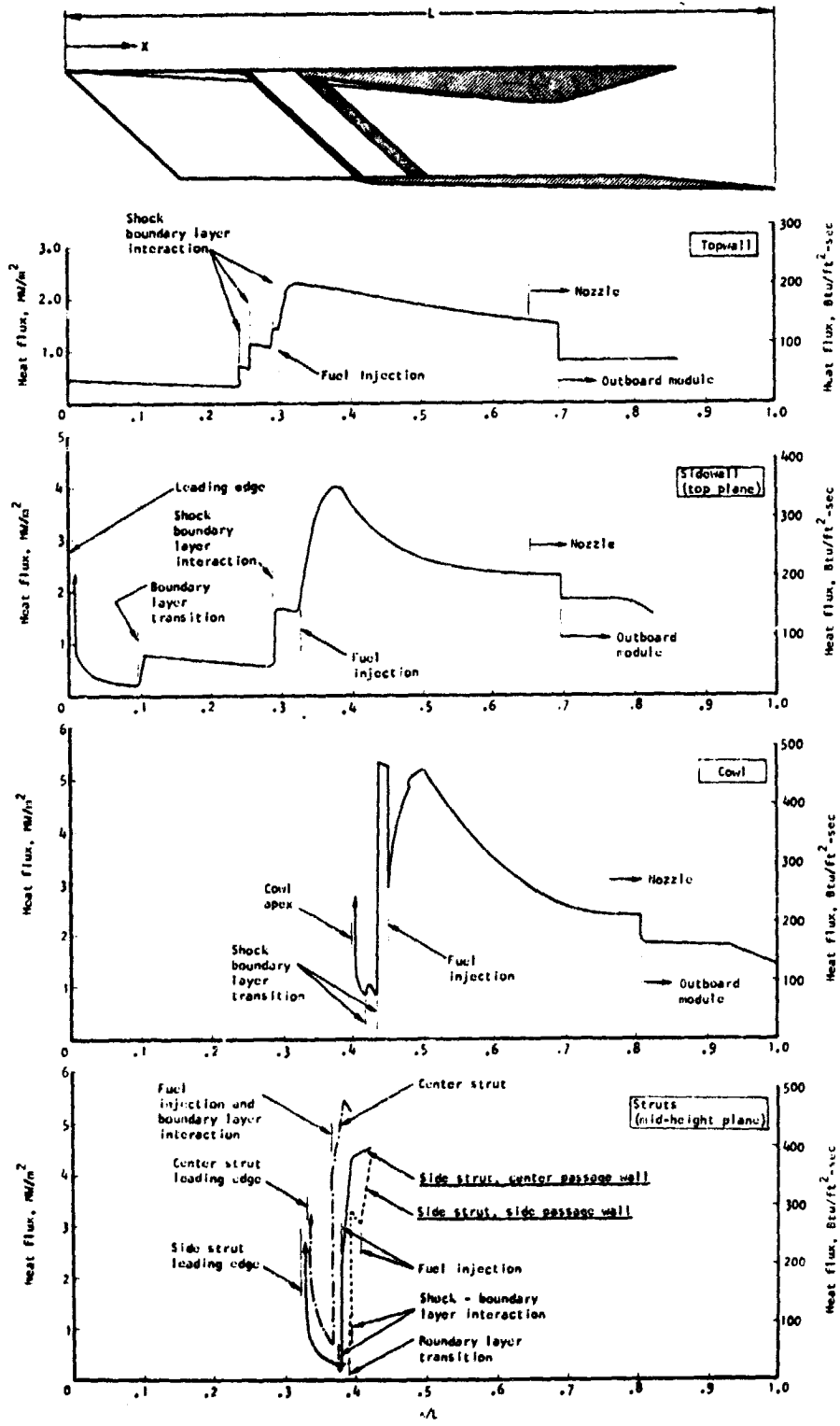
The peak combustor heat fluxes for the top surface, sidewall, and internal cowl of 2.27, 4.03, and 5.22 MW/m<sup>2</sup> (200, 355, and 460 Btu/sec sq ft), respectively, reflect the location of the virtual origin of the boundary layer. For the top surface, the virtual origin of the boundary layer was taken as 1016 cm (400 in.) upstream of the engine inlet, based on engine installations ranging from 1219 to 965 cm (480 in. to 380 in.) aft of the aircraft nose. Because of this, it was assumed that the flow transitioned upstream of the engine inlet and that the flow on the engine top surface was turbulent. On the side surface, internal cowl surface, and side struts, a laminar-to-turbulent transition Reynolds number of  $3 \times 10^6$  was used. The locations where transition occurs are indicated in Figures 7 and 8. On the center strut, the Reynolds number based on running length from leading edge was less than  $3 \times 10^6$  at the perpendicular injectors, so a transition to turbulent flow was imposed on the boundary layer at the injector location.

The top surface and internal cowl surfaces are exposed to a complex pattern of shock wave bays in the engine inlet. Each bay has a unique and constant set of inlet flow properties within it. This produces a heat loading on these surfaces that is both width- and axial-dependent. The loading definition on other surfaces of the engine is governed by one-dimensional flow properties that vary in the engine axial direction only. To facilitate the loading definition and the subsequent design, the various inlet streamlines produced by the complex shock bay pattern were reduced to one streamline. This one streamline was a composite of those producing maximum heating along the engine axis. Alternate paths through the inlet would yield a different and possibly more precise design heat load, but the variation is not considered significant. The maximum heat load in the inlet portion of the top surface is about 148 kW (140 Btu/sec) compared with a total module heat load of 7380 kW (7000 Btu/sec). Thus, the maximum variation in heat load due to path selection is less than 2 percent. The path presently specified results in a conservative design and is adequate for flow routing studies.

As part of the continuing analysis, a separate, detail analysis will be performed for the top wall panel in which the variation in heat flux along parallel streamlines is considered. Results will be included in the final report on the program.

Effects of shock wave-boundary layer interaction were considered. They occurred in turbulent flow for topwall, sidewall, and strut (side passage wall) surfaces and induced transition to turbulent flow on the internal cowl and side strut (center passage wall) surface.

ORIGINAL PAGE IS  
OF POOR QUALITY



5-24846

Figure 7.-- Aerodynamic Heating Rates on Engine Internal Surfaces.

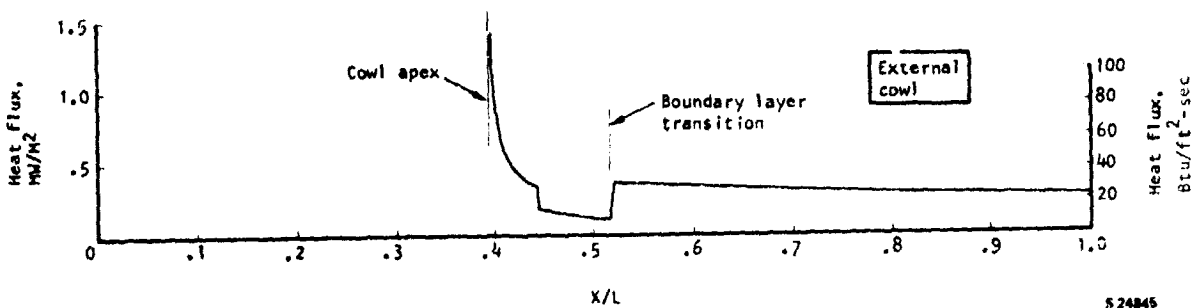
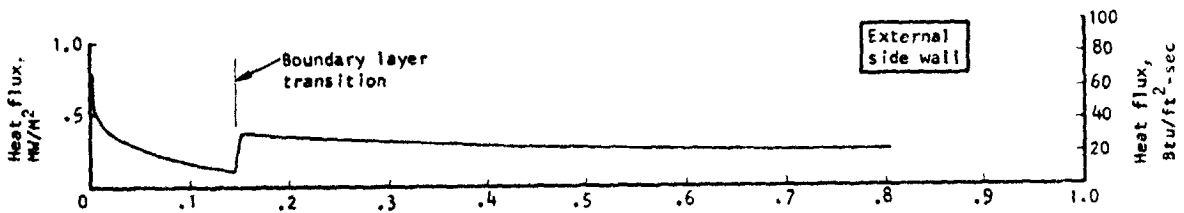
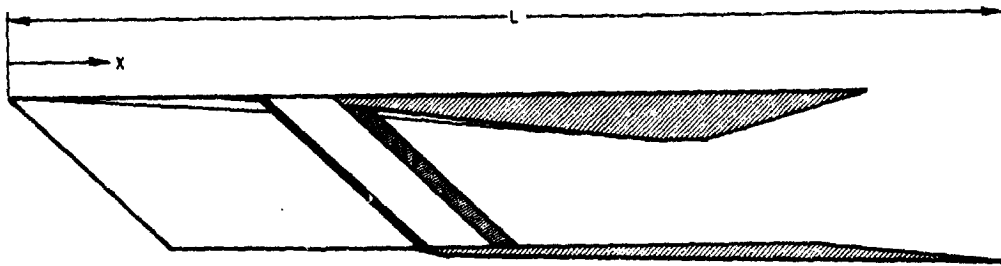


Figure 8.--External Surface Thermal Loading.

Aerodynamic heating on the side strut is not symmetrical. Hence, different distributions are shown in fig. 7 for each face of the side strut.

Results of aerodynamic heating analyses on the external surfaces of the sidewall (outboard module) and external cowl surfaces (all modules) are presented in fig. 8.

Estimates of wall temperature distributions were made to determine panel aerodynamic loadings in figs. 7 and 8. This was done to obtain estimates of overall loading levels and to determine aerodynamic heat transfer coefficients that are relatively insensitive to wall temperature, particularly with the adiabatic wall reference enthalpy method. Detailed wall temperature distributions for each panel can only be determined after a definition of coolant flow routing, TPS coolant passage geometry, and a thermal performance analysis using the aerodynamic heat transfer coefficients and hydrogen coolant coefficients. Results of these analyses are presented in a subsequent section.

#### Heat Load Summary

A summary of the heat loads is presented in Table 2. These are the area integrated results of figs. 7 and 8 for internal and external surfaces.

#### Leading Edge Heat Flux

Aerodynamic heating rates at the sidewall, cowl, and strut leading edges are presented in Table 3 (Condition H). Heat fluxes were calculated using the normal stagnation point method of Fay-Riddell (ref. 8) modified for the 48-deg sweep of the sidewall and struts and the 50-deg sweep of the cowl lip. The effect of sweep angle was considered by using the normal component of total pressure in the calculation of leading edge velocity gradient. The wall temperature at the stagnation line was assumed to be 833°K (1500°R). Two prospective radii were considered; increasing the radius from 0.8 to 1.3 mm (0.030 to 0.050 in.) reduces the heat flux by about 23 percent.

The cowl apex is a special case because it is the intersection of two cylindrical leading edges. For design, the apex was assumed hemispherical and unswept, both of which produce higher heat fluxes than the cylindrical swept leading edges on the sidewall, struts, and cowl. In addition, there is a point of sidewall shock wave intersection where the heat flux is intense.

Experimental evidence obtained during HRE testing has indicated that 0.8 to 1.3 mm (0.030 to 0.050 in.) radius leading edges can be adequately cooled with hydrogen up to stagnation heat fluxes of about 23 MW/m<sup>2</sup> (2000 Btu/sec sq ft). Higher and very localized heat fluxes produced by shock impingement on leading edges have also been accommodated when the impingement width is much smaller than leading edge radius; however, cowl leading edge fluxes of 45 to 60 MW/m<sup>2</sup> (4000 to 5000 Btu/sec sq ft) over a significant part of the radius is a definite departure from existing experimental data.

TABLE 2.--HEAT LOADS AT CONDITION H  
 ( $M_\infty = 10$ ,  $q_\infty = 1500$ , 2g TURN,  $\phi_f = 1.5$ )

Location	Maximum flux	Average flux	Heat load
	MW/m <sup>2</sup> (Btu/sec-sq ft)		MW (Btu/sec)
Top surface	2.27 (200)	1.06 (93)	0.827 (784)
Sidewalls	4.03 (355)	1.79 (156)	2.918 (2768)
Internal cowl	7.32 (645)	2.50 (220)	1.286 (1220)
Center strut	5.45 (480)	2.62 (231)	0.479 (454)
Side strut - center	4.54 (400)	2.09 (184)	0.578 (548)
- side	4.31 (380)	1.50 (132)	0.413 (392)
External cowl	-	0.45 (40)	0.297 (282)
Bottom of sidewalls	-	0.68 (60)	0.055 (52)
Outboard sidewall	-	0.45 (40)	0.865 (819)*
Total heat load, inboard module			6.853 (6500)
Total heat load, outboard module			7.618 (7319)

\*0.57 MW (540 Btu/sec) on external surface, 0.295 MW (279 Btu/sec) on extended internal surface

TABLE 3.--LEADING EDGE HEAT FLUXES AT CONDITION H

Leading edge	Heat flux, MW/m <sup>2</sup> (Btu/sec-sq ft)	
	0.8 mm (0.030 in.) radius	1.3 mm (0.050 in.) radius
Sidewall	13.7 (1206)	10.6 (935)
Side strut	19.5 (1718)	15.1 (1331)
Center strut	26.3 (2313)	20.3 (1792)
Cowl lip	18.5 (1634)	14.4 (1266)
Cowl apex	59.2 (5218)	45.9 (4042)

## Corner Flow Heating

The effect of corner-flow fields on the aerodynamic heating rate was investigated to determine if this condition would control the thermal protection system design.

Ref. 9 was used as the primary basis of the investigation; however, results are primarily for laminar flow for unswept leading edges, with and without wedge angles. Turbulent flow was treated on a limited basis in ref. 9 because of the limited test data available. The data are sufficient, however, to make judgments for this study.

One of the configurations from ref. 9 that was used in this study is shown in fig. 9. This configuration was selected because it has unwedged, ninety-degree corners, approach Mach numbers similar to the engine, and a comparable number of data points for turbulent flow as for laminar flow. This configuration is still different from the engine corners because (1) all engine corners have swept leading edges, (2) all engine corners have one surface that extends upstream from the origin of the corner so that this one surface already has an established boundary layer, and (3) all engine leading edges have leading edge radii of 0.8 to 1.3 mm (0.030 to 0.050 in.). These differences are thought to diminish the corner heating effect relative to results in ref. 9. The basic behavior of the aerodynamic heat transfer coefficient ( $h$ ) for laminar and turbulent flow at approach Mach numbers of 5 and 8 is included in fig. 9 for the selected configuration. For laminar flow, the corner effect on  $h$  is noticeable and also Reynolds number (and flow length) dependent. The  $h$  in the corner is less than predicted by laminar flat plate theory but increases to a peak value of 1.4 to 1.5 times the flat plate value 10 mm from the corner before diminishing to the flat plate value. For turbulent flow there is no corner effect on  $h$ , i.e., the  $h$  profile is flat with distance from the corner. This result does not appear to be affected by Reynolds number. In addition, the flat profile is approximately independent of approach Mach number, at least at the two values examined.

From these data, peak corner heating is not expected to be significantly higher than the laminar flat plate values in the laminar flow region of the cowl inlet. In addition, laminar flow heating is only about 15 to 25 percent of the corresponding heating if turbulent flow existed. Therefore, corner heating should not affect the design because the TPS will be selected primarily on the basis of turbulent flow heating in the cowl/strut section of the inlet. In the turbulent flow region, no increase in heating is expected due to corners. Laminar corner heating can be significant if a large portion of the corner is heated by laminar flow, regardless of turbulence level, but this is not the present case.

## Strut Pressure Loads

Pressure loads acting on the struts during the unstart condition (see fig. 6) were integrated and the results are shown in fig. 10 for the possible combinations. It was assumed that the unstarted pressure acts on the base of the trailing edge. Because the isobars are vertical on the unstarted side and swept on the started side, a torsional load is produced.

Using the resultant (net) lateral load, an average pressure load may be calculated by dividing the magnitude of the lateral (y directional) load resultant by the strut area projected on the x-z plane. The pressure intensity on this basis is 0.464 MPa (67.3 psi) for center passage unstart and 0.447 MPa (64.9 psi) for side passage unstart.

## Panel Pressure Loads

The pressure distributions shown in fig. 6 were used directly in the various analyses. Load calculations were internal to these analyses and were not separately performed as for the struts.

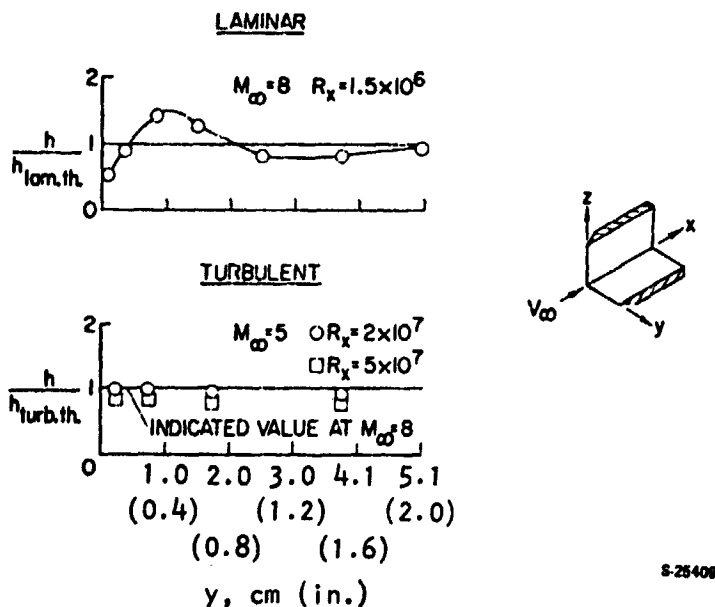
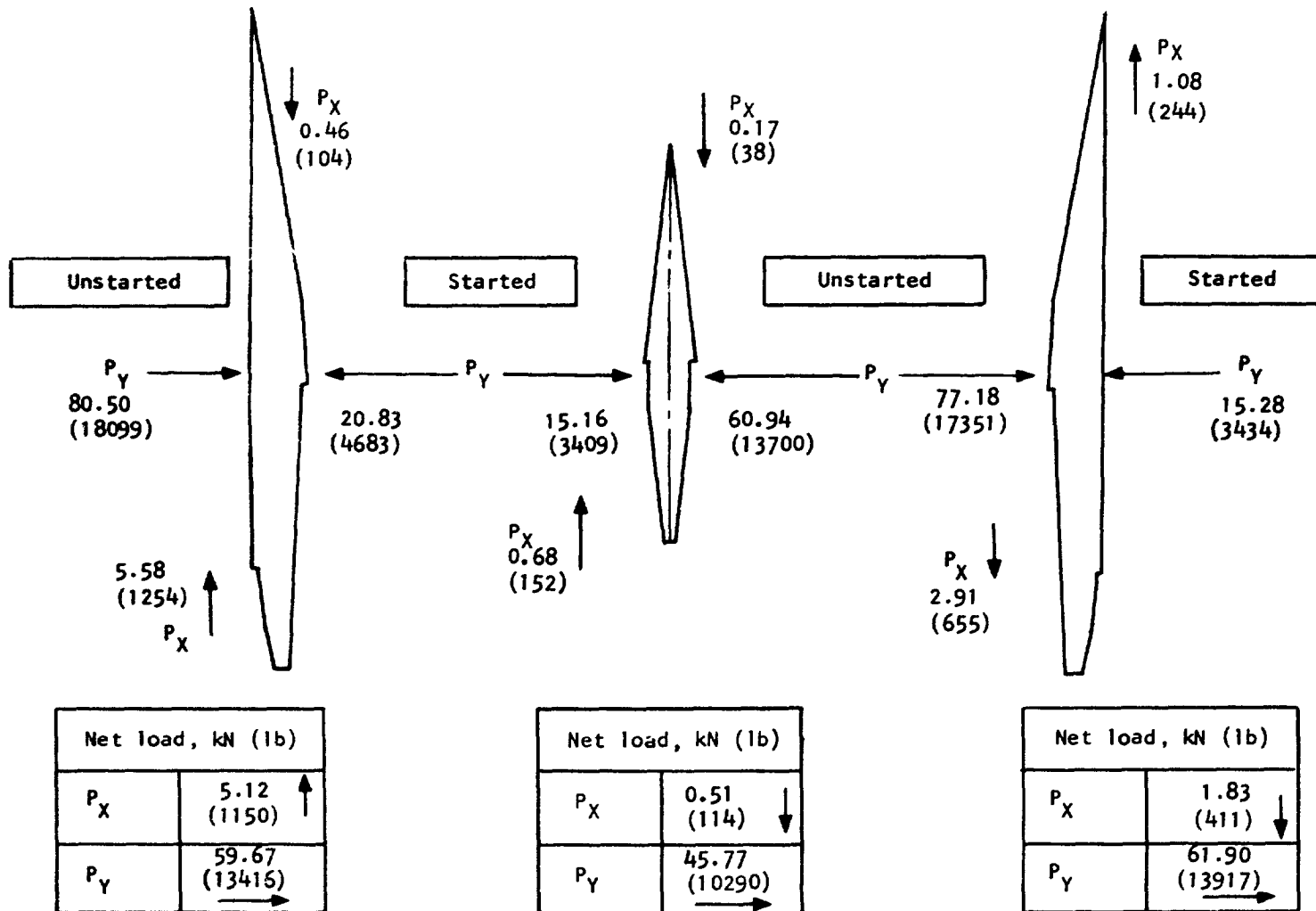


Figure 9.--Comparison of Laminar and Turbulent Heating in a Corner; Sharp Leading Edge (ref. 9).



5-24838

Figure 10.--Strut Loads, Transient Unstart Conditions.



## DESIGN APPROACH

### Cooling System

The thermal protection system was treated as a compact heat exchanger and analyzed using the methods presented in ref. 10. Heat transferred by radiation is considered negligible and the aerodynamic heat transferred to the structure is balanced by the heat removed by the coolant. All fluid properties were evaluated at the hydrogen bulk temperature as recommended (ref. 10) for offset-fin heat exchangers.

The topwall, sidewall and cowl, and the struts are each considered to be an independent cooling circuit; for maximum coolant utilization the coolant is allowed to reach the maximum allowable temperature, 890°K (1600°R). The basic flow path is to introduce cryogenic coolant at the leading and trailing edges where the panel heat flux is low and withdraw it at the engine throat where the heat flux is highest. Variations on this basic flow routing were examined to (1) match temperature gradients along the engine (minimum  $\Delta T$  between panels); (2) minimize coolant pressure drop by providing optimum flow width and length; and (3) minimize local heat input by controlling surface temperature profiles. These studies result in specification of coolant flows and manifold location in each flow route.

Cooling requirements throughout the flight envelope were determined and compared with the available cooling capacity as dictated by the fuel flow. Heat load split between engine sections, inlet, combustor, nozzle, and struts was computed to provide a basis for coolant flow control design.

Material requirements were examined and selections made based on HRE experience and the current state of the art. These selections were used for all subsequent structural analyses.

The thermal protection system (TPS) heat exchanger was examined in detail. Experience with the rectangular, offset, plate-fin coolant passages on the HRE TPS indicated that, although adequate for research purposes, the thermal fatigue life of such structures is limited. The required Scramjet engine life, 100 hours and 1,000 cycles, is an order of magnitude greater than specified for the HRE.

The maximum thermal load case, Condition H, was used as the TPS design basis. The TPS response is fast (the time constant is a few seconds) and it will reach a steady-state condition even though Condition H is a transient operating point. Consequently, the TPS passage geometry and flow routing must be sized and located to meet the maximum thermal load problem conditions. If the TPS passage geometry were optimized for cruise conditions, then it may be impossible to achieve the required Condition H coolant flow because of excessive pressure drop in the coolant passages.

The TPS hot skin temperature is dependent on the heat flux, and hence, peak temperature will occur at Condition H. It is presumed that this condition will occur at least once during every mission.

Two flow passage geometries, machined channels and pin fin, are selected as candidate surfaces because they have a potential for increased cyclic life. Heat transfer and pressure drop performance of the candidate heat exchanger flow geometries and structural materials are examined using the methods in ref. 10 and compared on the basis of in-depth temperature gradient and pressure drop. Thermal stress and, hence, the cyclic life, are directly related to the  $\Delta T$  across the TPS. Thus, the basic objective is to obtain the minimum  $\Delta T$  within the coolant pressure drop limitations.

A parallel structural analysis of the TPS is performed to predict low-cycle fatigue life of the candidate TPS structures. Two different techniques are used: linear interaction using Miner's rule, and strain range partitioning. The heat transfer and structural results are then reviewed and the best TPS geometry and materials selected.

Leading edges are given special consideration because of the high heat fluxes and geometry restrictions imposed. Hydrogen coolant is introduced at the leading and trailing edges of the individual panels and the coolant inlet temperature is, therefore, at or close to the minimum supply temperature of 56°K (100°R). The design problem is similar to that for the TPS, where low-cycle fatigue was identified as the driving parameter. A design constraint is the leading edge radius, which should be minimized for aerodynamic reasons.

### Fuel Injection Struts

The struts present a major design problem. They are slender structural elements with a span-to-depth ratio of 25 to 28. The torsional and bending stiffnesses are low. The struts must simultaneously perform the following functions:

- (a) Support a large side load such as occurs during an unstart transient
- (b) Contain high-pressure hydrogen at two temperature extremes
- (c) Withstand high thermal stresses generated by asymmetric aerodynamic heating

The cross-sectional area available for flow of the hydrogen coolant and fuel is limited by the basic cross-sectional area and the need to provide structural members. Hence, flow maldistribution could occur and produce an unacceptable fuel injection pattern and local hot spots in the TPS.

Structural analyses, described in ref. 2, were continued by NASA. The primary tool was a three-dimensional finite element model analyzed using the SPAR computer code. The side strut only was modeled, as the loading was

slightly more critical than the center-strut loading, and the results would be conservative for the center strut.

Two approaches were examined to determine the best means to reduce strut deflections and stresses. First, the boundary conditions were changed to reflect revised mounting constraints. A structural tie that joins the three struts together at their midpoint--a concept originally used in the ref. 2 analysis--was retained for this first approach. The second approach was to supply additional coolant to the strut TPS to reduce the temperature gradients along the strut and thereby decrease the thermal stresses. It was believed that "overcooling" would result in a lower combined stress and this would eliminate the mid-span tie, a decided complication in coolant flow routing and strut fabrication.

Initial results of the structural analysis were used to prepare design layouts for the strut cross-sections and flow routing schemes. From this basis the available flow areas for hydrogen fuel and coolant were established. Flow distributions were then determined using a computer program for one-dimensional compressible flow with friction in a manifold with continuous withdrawal of flow.

### Engine Primary Structure

Response of the overall engine structure to the maximum thermal and pressure loading conditions was determined using ANSYS, a finite element computer program (ref. 11). Although modeled relatively coarsely, the three-dimensional model had 4146 to 4794 degrees of freedom depending on the type of structure analyzed. The model was made up primarily of triangular and quadrilateral plate elements with both membrane and bending stiffness. Equivalent stiffness of the honeycomb, including the hot and cold face sheets, beams and clips, coolant manifolds, and the leading and trailing edge structures, was represented in the computer program. The beams were permitted to slip along the clips to represent a differential thermal expansion provision.

Three basic structures were examined: (1) seven swept beams reinforcing 9.5-mm (3/8-in.) constant thickness honeycomb, (2) seven vertical beams reinforcing 9.5-mm (3/8-in.) constant thickness honeycomb, and (3) 6.4- to 50.8-mm (0.25- to 2.0-in.) variable thickness honeycomb reinforced with two vertical beams. Maximum thermal and pressure loadings were applied to each of the models and the resulting deflections and stresses determined. Results were reviewed to select the structure that produces the minimum deflection for the least weight. Stress levels were checked to verify that the primary structure is within the elastic range. Deformations were checked against the allowable aerodynamic line distortions. Panel-to-panel deflections were examined to establish the seal problem statement.

## Transient Behavior

Maximum stresses in the primary structure are likely to occur during a transient condition, e.g., engine startup. To more clearly show the magnitude of this problem, a model of a typical engine cross-section was constructed and the transient temperature profiles determined using a finite difference thermal analyzer program. From these profiles, the thermal stresses were determined and compared with material allowables.

## Engine-Aircraft Interface

Deflection and load data from the engine finite element program were used to derive guidelines for engine mounting, including differential thermal expansion provisions and engine compartment sealing.

## Fuel System

A complete fuel system schematic was developed including the turbopump and all control valves. No detail designs were formulated. Rather, existing equipment, especially valve designs used on the HRE program, was used as the basis to obtain an estimate of size and weight.

## Layout Design

Drawings of engine panels and the struts were prepared to define the selected designs and to show manufacturing feasibility. An installation drawing was prepared to aid the aircraft designer. These drawings were used to establish a detail weight estimate for the Scramjet engine.

## DESIGN AND PERFORMANCE

### Material Selection

The study is based on the premise that existing materials and known manufacturing materials will be used. Hastelloy X is the reference material because of its extensive data base and its successful application in the Hypersonic Research Engine (HRE) program.

Since the initiation of the HRE program, several wrought superalloys with improved properties compared to Hastelloy X have been developed, e.g., Haynes 188 and Inconel 617. Refractory alloys may also be considered. Molybdenum exhibits a more than threefold increase in creep strength/density ratio over Hastelloy X, and TZM shows a tenfold increase. In addition, both materials have much better thermal properties and a higher modulus. Another approach, as proven on HRE, is to use Nickel-200 (commercially pure nickel) and balance the improved thermal properties and ductility against a lower creep strength when compared with Hastelloy X.

Thermal protection system (TPS).--The life of the HRE was 10 hours and 100 cycles compared with 100 hours and 1000 cycles for the Scramjet. The necessary increases in creep and low-cycle fatigue (LCF) life indicate that a Hastelloy X TPS could be marginal for this application and that changes in material or configuration may be required. A comparison of the material properties of the candidate alloys at two different maximum temperatures is shown in Table 4. Thin sheet properties are cited because they are more realistic for the TPS structure.

Two parameters are used to rank (in a preliminary fashion) the material resistance to LCF. The parameter

$$K_D = \sigma_y (RA)$$

where  $\sigma_y$  = yield stress

RA = reduction in area

is a measure of the ability of the material to absorb plastic strain, which is related to fatigue life. The highest value of  $\sigma_y RA$  is best for sustaining a given thermal stress without cracking.

For comparison of the materials in a high-temperature environment, a thermal stress parameter can be developed:

$$K = \frac{E\alpha}{k}$$

where E = Young's modulus

$\alpha$  = Coefficient of thermal expansion

k = Thermal conductivity

TABLE 4.--MATERIAL PROPERTIES FOR TPS CANDIDATE ALLOYS (SI UNITS)

Alloy	Nickel 200		Hastelloy X		Inconel 617		Haynes 188		TZM	
	788	871	788	871	788	871	788	871	788	871
Temperature, °C	788	871	788	871	788	871	788	871	788	871
Yield strength, $\sigma_y$ , MPa	48	31	214	186	186	186	220	186	420	400
Reduction of area, RA	0.97	0.99	0.36	0.40	0.60	0.80	0.43	0.75	0.05	0.05
Young's modulus, E, $\text{MPa} \times 10^{-6}$	0.14	0.12	0.14	0.13	0.14	0.12	0.17	0.16	0.21	0.20
Thermal expansion, $\alpha$ , cm/cm °C $\times 10^6$	16.2	16.4	16.2	16.4	15.3	15.7	16.4	16.9	5.6	5.6
Thermal conductivity, k, watts/cm °C	0.64	0.66	0.25	0.26	0.25	0.27	0.25	0.25	1.09	1.07
100-hr stress to rupture, MPa	22.7	13.7	110	62	172	97	165	90	310	296
Thermal stress parameter, $E\alpha/k$	3.5	2.9	9.1	8.2	8.3	6.9	11.0	10.7	1.1	1.1
Ductility parameter, $\sigma_y \times \text{RA}$	46.6	30.7	77.0	74.4	111.6	148.8	94.6	139.5	21.0	20.0

Estimate of the most likely value for 0.38-mm-thick section without effects of brazing, coatings, or long-term exposure.

TABLE 4 (Continued)--MATERIAL PROPERTIES FOR TPS CANDIDATE ALLOYS (U.S. Customary Units)

Alloy	Nickel 200		Hastelloy X		Inconel 617		Haynes 188		TZM	
	1450	1600	1450	1600	1450	1600	1450	1600	1450	1600
Temperature, °F										
Yield strength, $\sigma_y$ , ksi	7.0	4.5	31	27	27	27	32	27	61	58
Reduction of area, RA	0.97	0.99	0.36	0.40	0.60	0.80	0.43	0.76	0.05	0.05
Young's modulus, E, psi x 10 <sup>-5</sup>	20	17	20	19	20	17	24	23	31	29
Thermal expansion, $\alpha$ , in./in. °F x 10 <sup>6</sup>	9.0	9.1	9.0	9.1	8.5	8.7	9.1	9.4	3.1	3.1
Thermal conductivity, k Btu/ft hr °F	37	38	14.2	15.2	14.7	15.4	14.2	14.5	63	62
100-hr stress to rupture, ksi	3.3	2.0	16	9	25	14	24	13	45	43
Thermal stress parameter, E $\alpha$ /k	4.9	4.1	12.7	11.4	11.6	9.6	15.4	14.9	1.5	1.5
Ductility parameter, $\sigma_y$ x RA	6800	4500	11 200	10 800	16 200	21 600	13 800	20 300	3100	2900

32

Estimate of the most likely value for 0.015-in.-thick section without effects of brazing coatings, or long-term exposure.

The lowest value of this parameter will yield the lowest thermal stress for a given temperature distribution. These parameters for the candidate alloys are also shown in Table 4.

Among the nickel- or cobalt-base wrought superalloys there is no clear-cut superiority, although the parameters do indicate an advantage for Inconel 617. The data base for Hastelloy X, especially for direct measurements of LCF life, is more extensive than for the other alloys.

Nickel-200 is an attractive alternate for the TPS because of its exceptionally high ductility. Its creep strength is low and, hence, the maximum operating temperature must be limited to 790°C (1450°F) or less. Directly applicable low-cycle fatigue data and high-temperature creep data are lacking.

The TZM refractory alloy is attractive because its thermal stress parameter is low; however, in the unprotected condition, refractory alloys have no oxidation resistance at the Scramjet operating conditions. Applicable coating technology has not advanced significantly beyond that available in the 1960-1965 period. Without further coating development, refractory alloys cannot be considered for Scramjet.

Primary structure.--In this case, the maximum operating temperature is 650°C (1200°F). At this level, Inconel 718 is generally regarded as optimum because of its superior yield strength compared with Hastelloy X or Inconel 617. There is difficulty in fabricating Inconel 718 because the welded material distorts during the complex heat treatment cycle, and, for this reason, Hastelloy X is preferred. Where its strength is required, Inconel 718 is specified.

Final selections.--The materials selected for design are shown in Table 5.

TABLE 5.--MATERIALS SELECTED FOR DESIGN

Structural Element	Selected Material	Alternate Material
TPS	Hastelloy X	Nickel-200
Honeycomb	Hastelloy X	Inconel 718
Beams and clips	Inconel 718	Hastelloy X
Leading edge support structure	Hastelloy X	Inconel 718
Strut primary structure	Inconel 718	-
Mounts, mounting frame	Inconel 718	-



Data are lacking in the critical area of low-cycle fatigue especially for the specialized TPS structures and materials under consideration. Thermal fatigue will no doubt be the limiting factor in engine life. NASA has initiated a program to develop the required data (ref. 12). The plan is to obtain fatigue and creep data for the candidate materials including a determination of environmental effects. Fabrication techniques are to be developed and prototype panels are to be tested to measure creep-rupture strength and cyclic life. Data from this program will be used to verify or modify the above material selections.

### Coolant Flow Routing

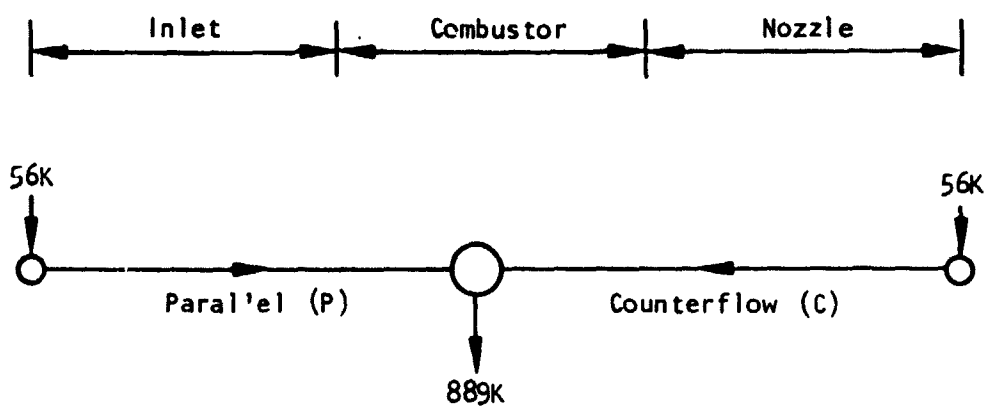
Design conditions.--Coolant inlet and outlet temperatures are 56° and 890°K (100° and 1600°R), respectively. Coolant inlet pressure is 6.9 MPa (1000 psia) and the pressure drop in any one circuit is limited to 1.4 MPa (200 psi). The reference design TPS was used in this analysis, viz., a Hastelloy X plate-fin surface, 11 fins per cm, (28 fins per in.), 1.3 mm (0.050 in.) high, 2.5 mm (0.100 in.) offset, and 0.15 mm (0.006 in. thick), with a 0.38-mm (0.015-in.)-thick hot face sheet.

Optimization was conducted at the maximum thermal loading case, Condition H. This condition involves a 2g maneuver and is short term relative to a cruise condition where design optimization is usually performed. Heating rates vary between flight conditions, but the coolant temperature profiles and the primary structure temperature tend to be similar for all operating conditions with combustion. This is because the heat flux distribution is similar for each condition and the coolant inlet and outlet temperatures are maintained constant. The coolant flow is adjusted in response to the overall heat load. Since Condition H is used for TPS design, it was retained for the flow routing optimization because of temperature profile similarity and because maximum coolant flow is required at Condition H and this controls manifold design.

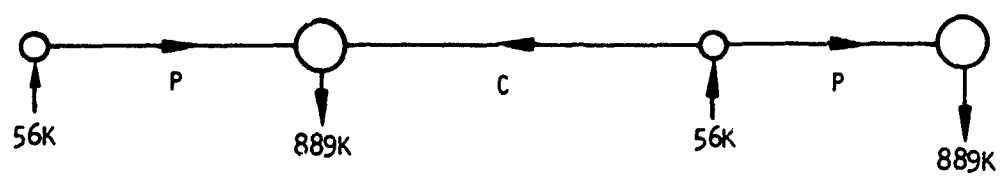
Design goals.--The coolant pressure drop across the TPS should not exceed 0.83 MPa (120 psi) to allow 0.55 MPa (80 psi) for manifolds and ducts. The local in-depth TPS temperature gradient should be less than 260°C (500°F) to meet cyclic life requirements. The 260°C (500°F) limit is an approximation and is used only for screening purposes. No specific limits are placed on the temperature difference between adjacent panels that are cooled by separate flow routes, although the  $\Delta T$  should be small to minimize axial differential thermal growth.

Manifold orientation.--The hot gas flow properties are constant along an engine sweep line, and hence all sidewall manifolds were oriented parallel to the engine 48-deg sweep line to achieve maximum coolant utilization. This arrangement also yields uniform temperature profiles along the sweep lines.

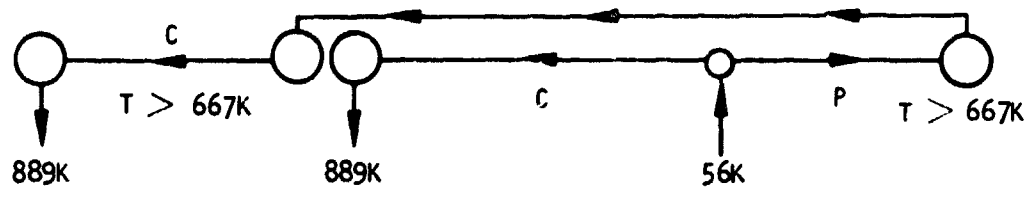
Component flow arrangement.--Possible routes through a typical component (top, sidewall, or cowl) are shown in Figure 11. The routes are designated as "P" or "C" to indicate a coolant path that is either parallel (P) or counter (C) to the hot gas flow. Heat transfer and pressure drop performance was



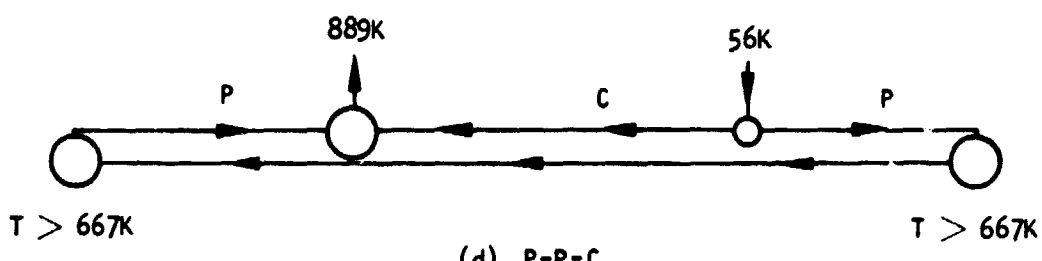
(a) P-C Configuration (Reference Design)



(b) P-C-P Configuration



(c) P-C-C



(d) P-P-C

S-15713-A

Figure 11.--Panel Flow Routing Schemes.

determined for each panel using each of the flow route options. Most of the possible routes produced an excessive pressure drop, excessive temperature gradient, or a sudden step change in skin temperature of greater than 220°K (400°R). The reference design flow route, a P-C configuration, met all the design criteria. Moreover, this scheme requires a minimum number of manifolds and the flow is easy to meter because of an adequate pressure drop in each panel. The P-C configuration was selected for final optimization.

Outlet manifold position optimization.--Initial calculations were performed on the basis of achieving minimum coolant flow and a minimum TPS in-depth  $\Delta T$  for each route. Based on these criteria, the optimum manifold locations were:

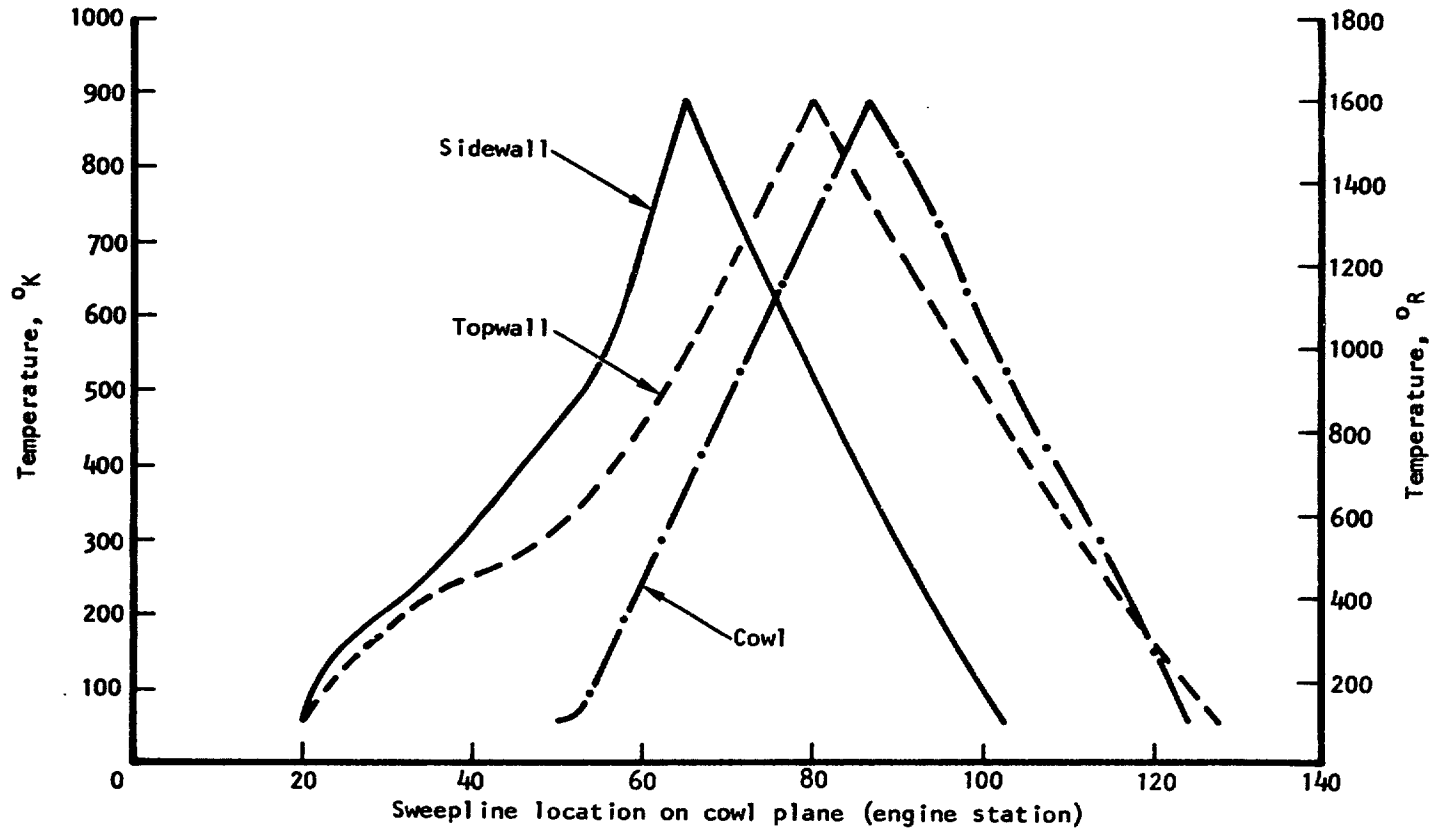
<u>Component</u>	<u>Engine Station (sweep line intersection at cowl plane)</u>
Topwall	80
Sidewall	65
Cowl	87

The primary structure temperature profiles are shown in fig. 12(a). This is the temperature at the hot face sheet of the honeycomb structure. This arrangement produces an unacceptable temperature mismatch between intersecting panels, e.g., a 528°C (950°F)  $\Delta T$  between the sidewall and cowl (sweep line located at engine station 87). Large temperature gradients adversely affect the panel-to-panel seals and complicate the provisions for accommodating differential thermal growth. A viable method of controlling interpanel gradients must provide approximately equal coolant temperatures in any two intersecting panels at all points along the axial coolant traverse.

Therefore, to alleviate the temperature mismatch, it was stipulated that the four panel outlet manifolds would be coplanar with the swept sidewall manifolds. A tradeoff analysis was conducted using coolant pressure drop and the TPS in-depth temperature gradient as parameters.

The best attainable combination of TPS metal  $\Delta T$  and pressure drop balance is achieved with the cowl segment of the exhaust manifold at Station 77.5. For this configuration, approximate internal surface temperature profiles are plotted in fig. 12(b). The structure temperature referred to in fig. 12 is the hot face temperature of the primary structure, which corresponds to the TPS cold side surface. Excessive (250° to 350°C) interpanel gradients exist between sidewall and cowl at the leading edge of the cowl (Station 51), and between sidewall and top at the trailing edge of the sidewall (cowl Station 103). The basic problem is in the relative orientation of the panels; this arrangement results in large interpanel coolant temperature disparity along the axis of the engine.

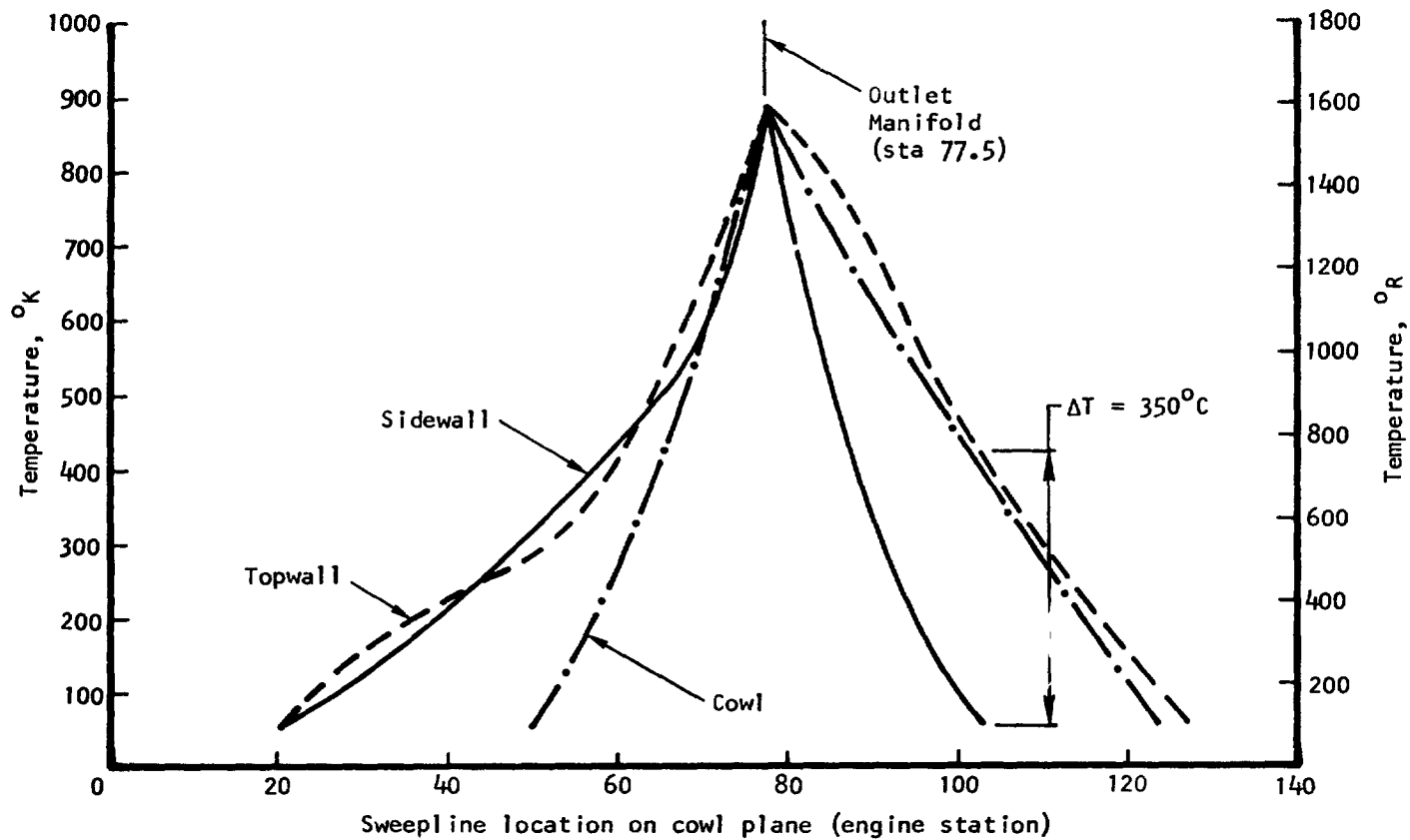
A modified flow routing scheme (fig. 13) was devised to reduce the large interpanel temperature differences noted above. With this scheme, coolant for the entire aft end of the engine is fed through the trailing edges of the cowl and top surface. Redistribution shunt manifolds are located on the top



S-24830

(a) Minimum Coolant Flow and TPS ΔT.

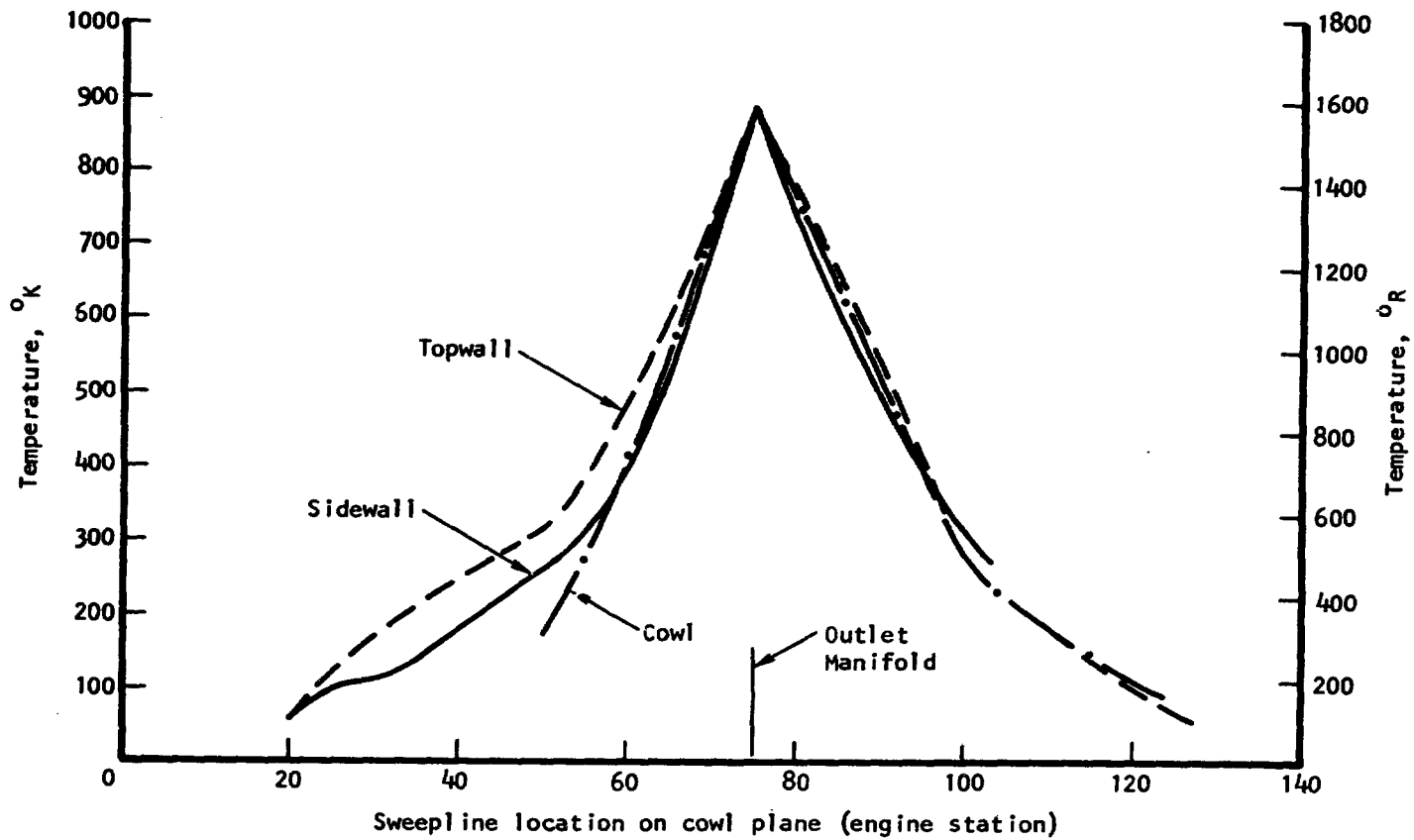
Figure 12.--Primary Structure Temperature Profiles.



S-24829

(b) Coplanar Outlet Manifolds.

Figure 12.--Continued.



S-24831

(c) Coplanar Outlet Manifolds and Shunt Flow Routing.

Figure 12.--Concluded.

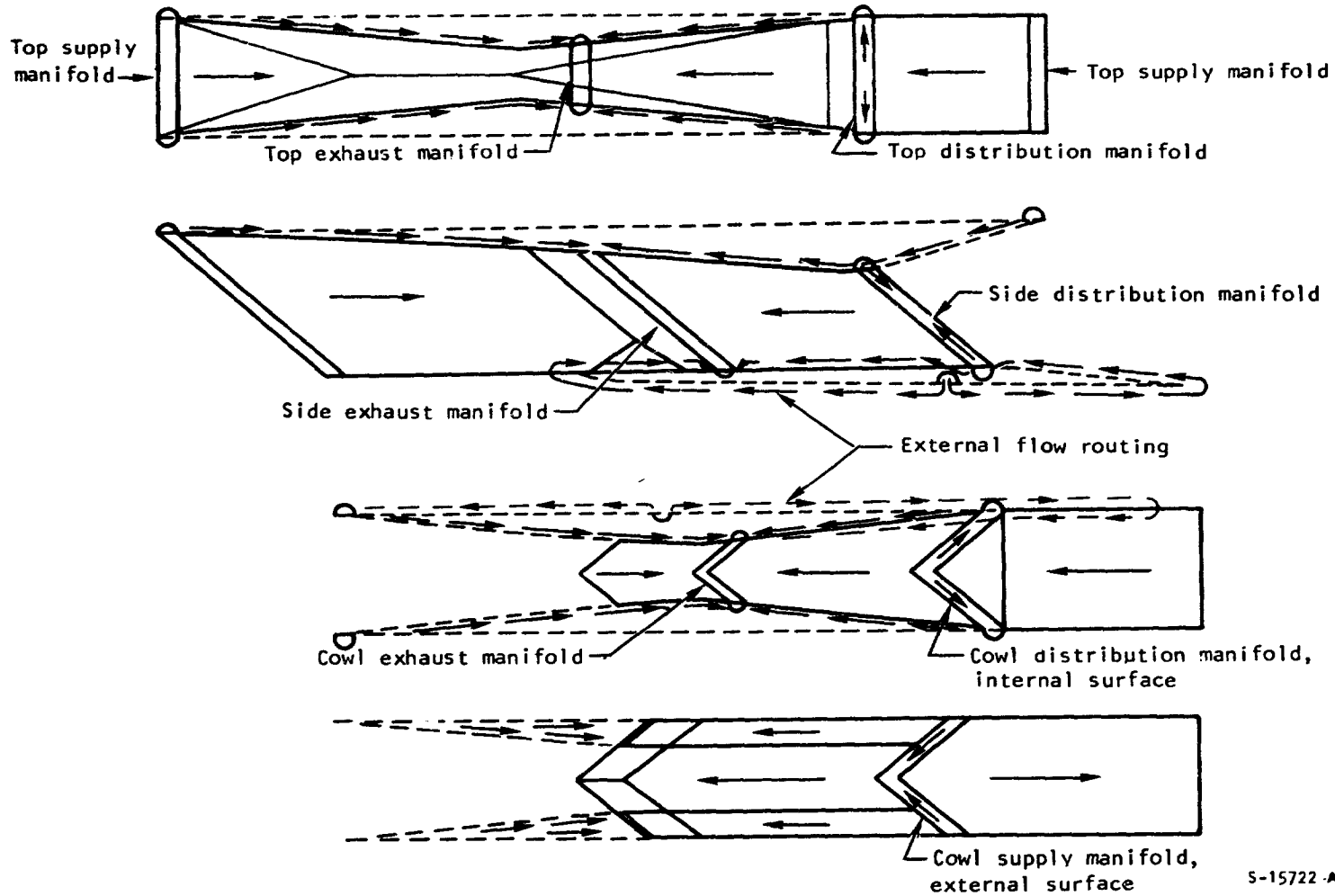


Figure 13.--Sidewall Shunt Coolant Distribution Concept.

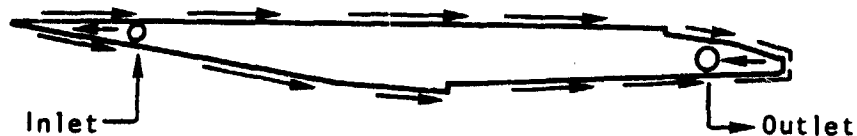
surface and internal cowl surface in line with the trailing edge of the sidewall. At this point a portion of the coolant flow is split from the aft top surface and aft internal cowl cooling circuits and is directed to an intermediate manifold. Flow is directed from this manifold to the aft portion of the sidewall circuits.

The pressure drop and TPS  $\Delta \bar{i}$  tradeoff analysis was repeated and the optimum outlet manifold position was determined to be located at Station 75 (at the cowl plane). The four outlet manifolds are on the same sweep line with the topwall outlet manifold at Station 59. The individual outlet manifolds are not necessarily interconnected.

The shunted flow route concept yields acceptable primary structure temperature profiles (honeycomb hot face sheet) as shown in fig. 12 (c). The maximum interpanel temperature difference at any sweepline position is 120°C, which is believed acceptable.

Coolant flows and conditions in each circuit are defined in fig. 14. Coolant pressure drop in each circuit was reasonable, but the TPS gradient exceeded the design goal in several instances. Thus, further studies were conducted to improve TPS performance, i.e., to reduce in-depth temperature gradient with acceptable coolant pressure drop. The shunt flow routing scheme and coolant flow noted above were retained.

Strut flow routing.--Two strut flow routing schemes were examined: (1) coolant flow parallel to hot gas flow; and (2) coolant flow along the 48-deg sweep line. The second scheme did not offer any significant advantages and the resulting flow paths created significant temperature discontinuities. The selected flow path is with the hydrogen coolant parallel to hot gas flow, as shown below. Coolant conditions for strut flow are noted on fig. 14.



S-15708



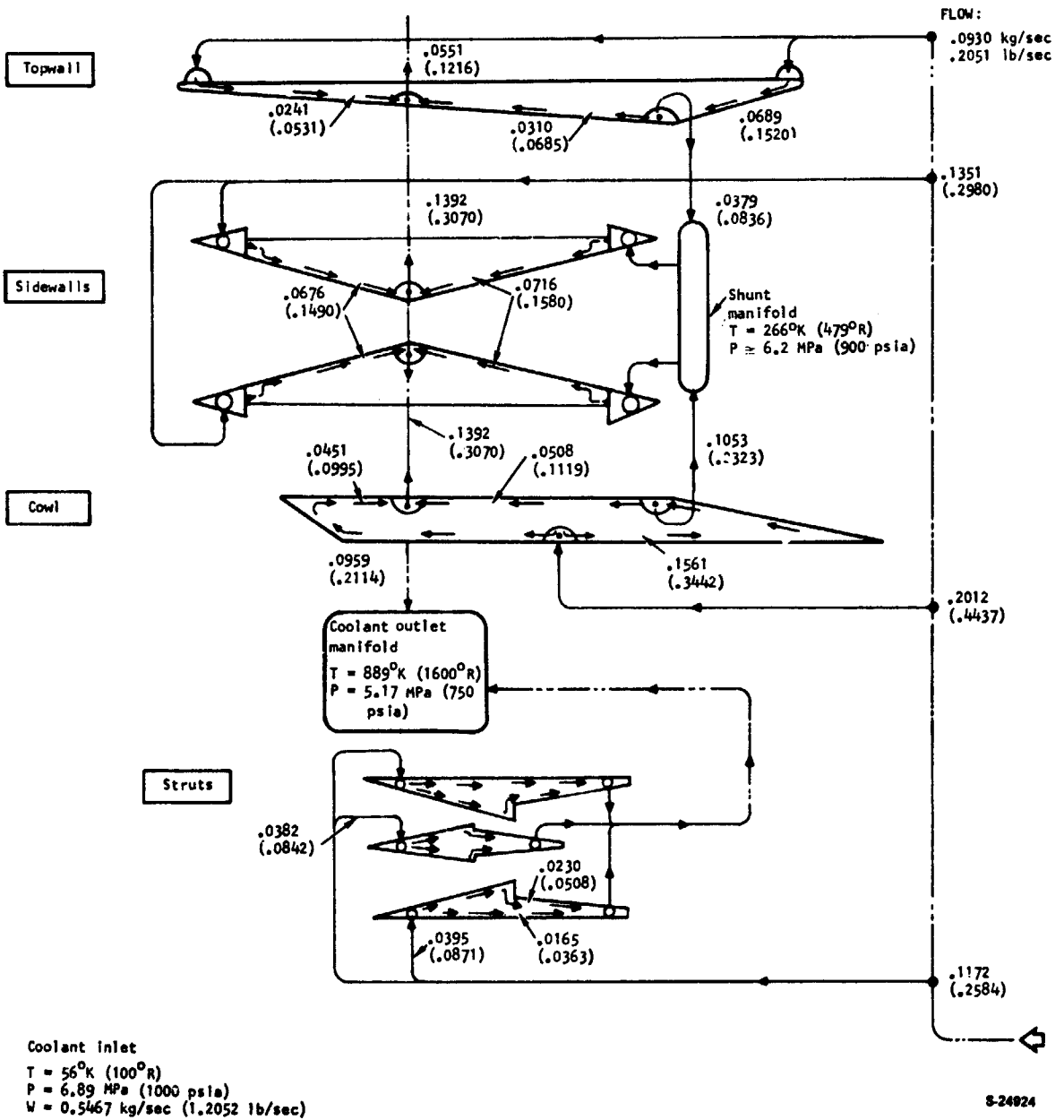


Figure 14.--Coolant Flow Conditions.

## Flight Envelope Cooling Requirements

To determine engine heat loads at conditions throughout the operating envelope (see fig. 4), the engine was divided into four regions: inlet, combustor, nozzle, and external surfaces (see fig. 5). Condition H heat loads were then scaled according to the particular heat transfer mechanism in each of these regions. The inlet has mostly laminar flow with constant total enthalpy (inlet air); the combustor has turbulent flow with increasing total enthalpy (inlet air to combustion products); the nozzle has turbulent flow with constant total enthalpy (combustion products); and the external surfaces have mostly turbulent flow with constant total enthalpy (inlet air). The calculations included the average effect of mass velocity, wall temperature, and hot gas fluid properties in each region.

Results are presented in Table 6 for an inboard module, an outboard module, and a six-module cluster (four inboard and two outboard modules). Minimum hydrogen coolant rates were established assuming that the coolant is heated from 56°K (100°R) to 890°K (1600°R) except for Condition A'. For this condition the coolant inlet temperature was increased until the entire coolant flow is heated to the 890°K (1600°R) maximum fluid outlet temperature and the cooling equivalence ratio,  $\phi_c$ , is equal to 1.0. For this cruise condition, the coolant supply temperature may be increased to 420°K (756°R), which indicates that 44 percent of the coolant heat capacity is available for airframe cooling. These coolant rates are considered minimum because of inherent inefficiencies in the cooling system.

The coolant equivalence ratio,  $\phi_c$ , is less than 1.0 throughout the engine operating envelope, and thus, the basic engine design goal of excess cooling capacity is realized. The maximum and minimum  $\phi_c$ , which occur at Conditions B and C, respectively, reflect their extreme position on the altitude-Mach number envelope, fig. 4.

An estimated  $\phi_c$  for stoichiometric combustion at all operating conditions is also indicated in Table 6. It was assumed that the heat loads are unaffected even though the fuel flow rate is reduced by one-third at Conditions B, F, and H. The resulting coolant equivalence ratio,  $\phi_c$ , remains below 1.0 except at Condition B, where the  $\phi_c$  increases to 1.239. Thus, for maximum altitude and Mach number cruise, stoichiometric combustion requires the use of additional fuel for cooling. If the objective is to maintain  $\phi_f = 1.0$ , this additional fuel can be dumped via the fuel dump valve (see section on Hydrogen Flow Control).

A breakdown of heat load by engine section is presented in fig. 15. The inlet section is composed of all internal surfaces up to the fuel injectors; the combustor section extends to the internal sweep line from station 80.755 on the top surface to 94.649 on the cowl, and the nozzle section extends to the end of the engine (see fig. 5). Included is the small fraction of external heat loads. The major portion of the heating occurs in the combustor section. There is no fixed relationship in the heating rates between sections.

TABLE 6.—FLIGHT ENVELOPE COOLANT REQUIREMENTS

Flight Condition (Fig. 4)	Flight Mode	Nach No.	Dynamic Velocity, kPa (psi)	Altitude, m (ft)	Angle of Attack, degrees	Fuel Equiv. Ratio, $\phi_f$	Inboard Module Heat Load, MW (Btu/sec)	Outboard Module Heat Load, MW (Btu/sec)	Six Module Heat Load, MW (Btu/sec)	Inboard Module Coolant Flow, kg/sec (lbm/sec)	Outboard Module Coolant Flow, kg/sec (lbm/sec)	Six Module Coolant Flow, kg/sec (lbm/sec)	Inboard/Outboard Fuel Flow, kg/sec (lbm/sec)	Six Module Fuel Flow, kg/sec (lbm/sec)	Inboard Module Cooling Equiv. Ratio, $\phi_c$	Outboard Module Cooling Equiv. Ratio, $\phi_c$	Six Module Cooling Equiv. Ratio, $\phi_c$	Six Module $\phi_c$ at $\phi_f = 1$
A	1g cruise	6	23.9 (500)	31,711 (104,040)	9.4	1.0	1.48 (1407)	1.73 (1640)	9.39 (8908)	.118 (.261)	.138 (.304)	.748 (1.650)	.245 (.540)	1.470 (3.240)	.483	.563	.509	.509
A'	1g	6	23.9 (500)	31,711 (104,040)	9.4	1.0	1.48 (1407)	1.73 (1640)	9.39 (8908)	.245 (.540) $T_{in} = 876^\circ R$	.249 (.540) $T_{in} = 756^\circ R$	1.47 (3.240) $T_{in} = 836^\circ R$	.245 (.540)	1.470 (3.240)	1.000	1.000	1.000	1.000
B	1g cruise	10	23.9 (500)	38,845 (127,446)	11.0	1.5	3.58 (3399)	4.04 (3835)	22.42 (21266)	.285 (.629)	.322 (.710)	1.79 (3.936)	.365 (.804)	2.188 (4.824)	.782	.883	.826	1.239
C	1g cruise	4	71.8 (1500)	19,050 (62,500)	5.3	1.0	1.13 (1075)	1.44 (1366)	7.41 (7032)	.090 (.199)	.115 (.253)	.591 (1.302)	.584 (1.287)	3.503 (7.722)	.155	.137	.169	.169
D	1g Cruise	6	71.8 (1500)	24,267 (79,617)	5.8	1.0	2.87 (2719)	3.31 (3135)	18.08 (17146)	.229 (.504)	.264 (.581)	1.44 (3.175)	.607 (1.339)	3.644 (8.034)	.376	.434	.395	.355
E	1g Cruise	8	71.8 (1500)	28,047 (92,019)	6.2	1.0	4.06 (3855)	4.60 (4361)	25.45 (24142)	.324 (.714)	.367 (.808)	2.03 (4.471)	.581 (1.280)	3.484 (7.680)	.558	.631	.582	.582
F	1g Cruise	10	71.8 (1500)	31,137 (102,156)	6.5	1.5	5.75 (5454)	6.41 (6076)	35.81 (33968)	.458 (1.010)	.510 (1.125)	2.85 (6.290)	.828 (1.826)	4.970 (10.956)	.553	.616	.574	.861
G	2g Turn, Unstart	5.1	71.8 (1500)	22,161 (72,707)	7.3	1.0	2.70 (2562)	3.16 (2993)	17.12 (16234)	.215 (.474)	.251 (.554)	1.36 (3.006)	.667 (1.471)	4.003 (8.826)	.332	.377	.341	.341
H	2g Turn	10	71.8 (1500)	31,137 (102,156)	8.9	1.5	5.85 (5500)	7.72 (7319)	42.85 (40638)	.546 (1.204)	.615 (1.355)	3.41 (7.526)	1.007 (2.220)	6.042 (13.320)	.542	.610	.565	.848
I	2g Turn	10	71.8 (1500)	31,137 (102,156)	8.9	0.0	3.25 (3078)	3.88 (3680)	20.74 (19672)	.259 (.570)	.309 (.681)	1.65 (3.643)	0.0	0.0	-	-	-	.410

Another breakdown of engine heating is presented in fig. 16, where the heating on the forward engine section is presented as a percentage of total engine load. The forward section includes the inlet section plus the forward external surfaces. The aft section (the complement of the forward section on a percentage basis) includes the combustor, nozzle, and aft external surfaces. This heating breakdown corresponds to the loading on forward and aft coolant flow routes on the engine. Again, there is no fixed relationship in the heating rates between sections.

Thus, for efficient utilization of coolant throughout the operating envelope, active controls must be used to vary the coolant flow split between the forward and aft portions of the engine. Flow control by means of fixed orifices would not suffice.

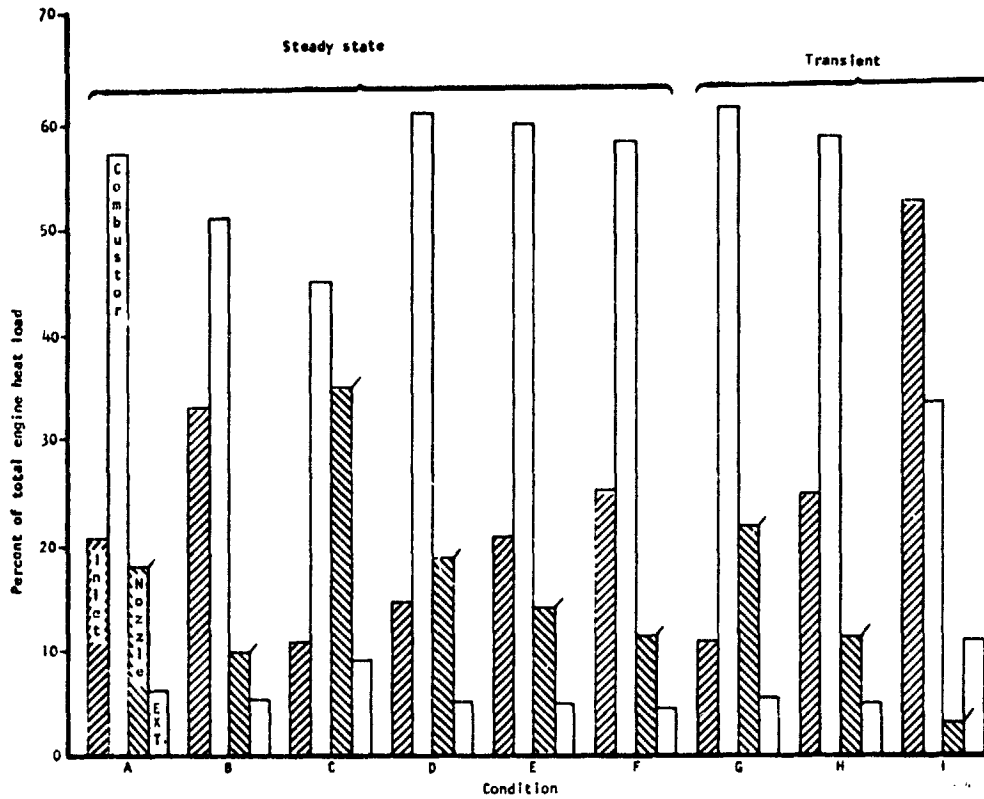


Figure 15.--Heat Load Split Between Engine Sections.

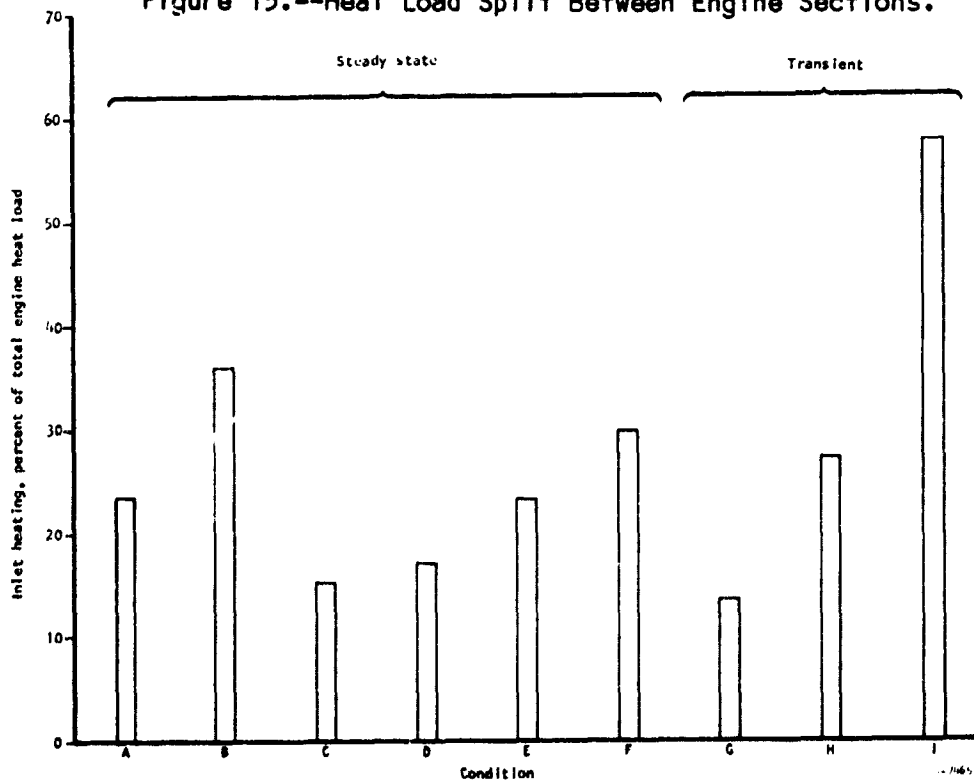


Figure 16.--Inlet Heating Fraction.

## Thermal Protection System (TPS)

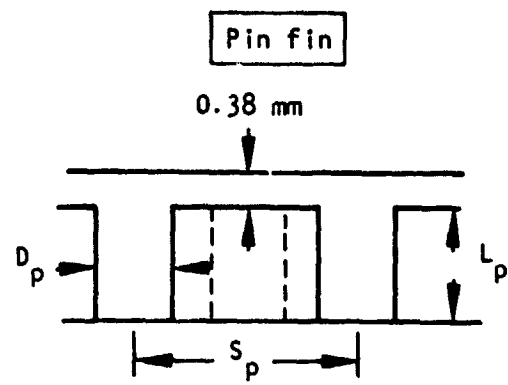
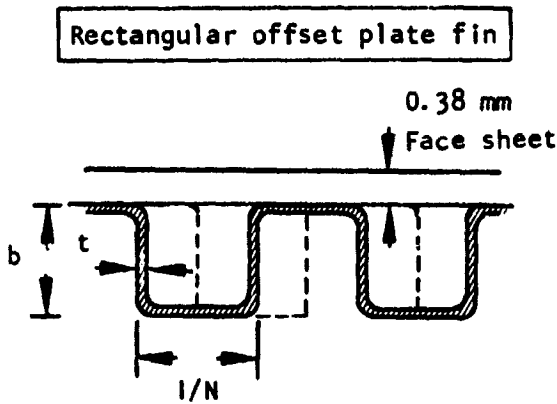
Heat exchanger design.--Three types of TPS configurations were considered: (1) rectangular offset plate-fin, (2) rectangular plain machined channel, and (3) equally spaced (equilateral triangle) circular pin fin. Fig. 17 presents a sketch of these surfaces and the dimensional ranges.

The 11-fin-per-cm rectangular offset fin is the reference design and is the basis of comparison. The 14-fin-per-cm fin is half the above passage height and is considered for high heat flux areas to minimize in-depth temperature differences ( $\Delta T$ 's). For the machined fins, the 2.0-mm (0.080-in.) fin spacing and 0.51-mm (0.020-in.) fin thickness are reasonable manufacturing limits. The pin fin was considered because it can provide the interrupted coolant passage characteristics of an offset plate-fin. Spacing-to-pin diameter ratios ( $S_p/D_p$ ) of 2 and 2.7 were selected herein to provide adequate coolant pressure containment. In all configurations, a 0.38-mm (0.015-in.) face sheet was used.

Coolant flowrates and passage lengths in each circuit were defined by the flow routing studies and are fixed. The coolant pressure drop in each circuit is limited to approximately 0.83 MPa (120 psi) (0.55 MPa for manifolds and ducting); each circuit should expend as much as possible of this allotment. The struts have shorter flow lengths than the panels and hence, the unit pressure drop can be higher.

Heat transfer performance curves were developed for each surface; typical examples are shown in fig. 18. It is possible to trade off reductions in the TPS in-depth temperature gradient with increases in coolant pressure drop or in TPS material (thermal conductivity).

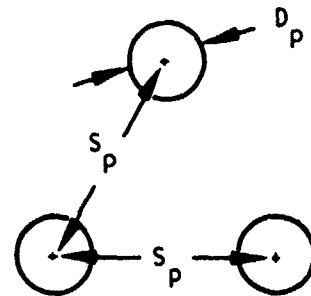
The performance in each flow route was determined for each candidate surface at average hydrogen flow conditions. Coolant pressure drop was estimated for the entire flow route; the TPS  $\Delta T$  was determined only at the peak heat flux condition. Results for the sidewall are shown in Table 7. Here the 0.64-mm (0.025-in.)-deep channel provides the lowest  $\Delta T$  within the pressure drop guidelines.



$N = \text{fins per cm of flow width}$

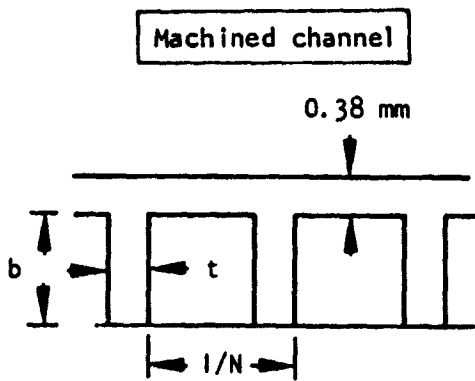
Fins considered:

- (1)  $N = 11, b = 1.3 \text{ mm}, t = 0.15 \text{ mm}$
- (2)  $N = 14, b = 0.64 \text{ mm}, t = 0.05 \text{ mm}$



Dimensions considered:

- $S_p = 2.0 \text{ mm}$
- $D_p = 0.76 \text{ and } 1.02 \text{ mm}$
- $L_p = 0.64, 1.27, 1.91 \text{ mm}$

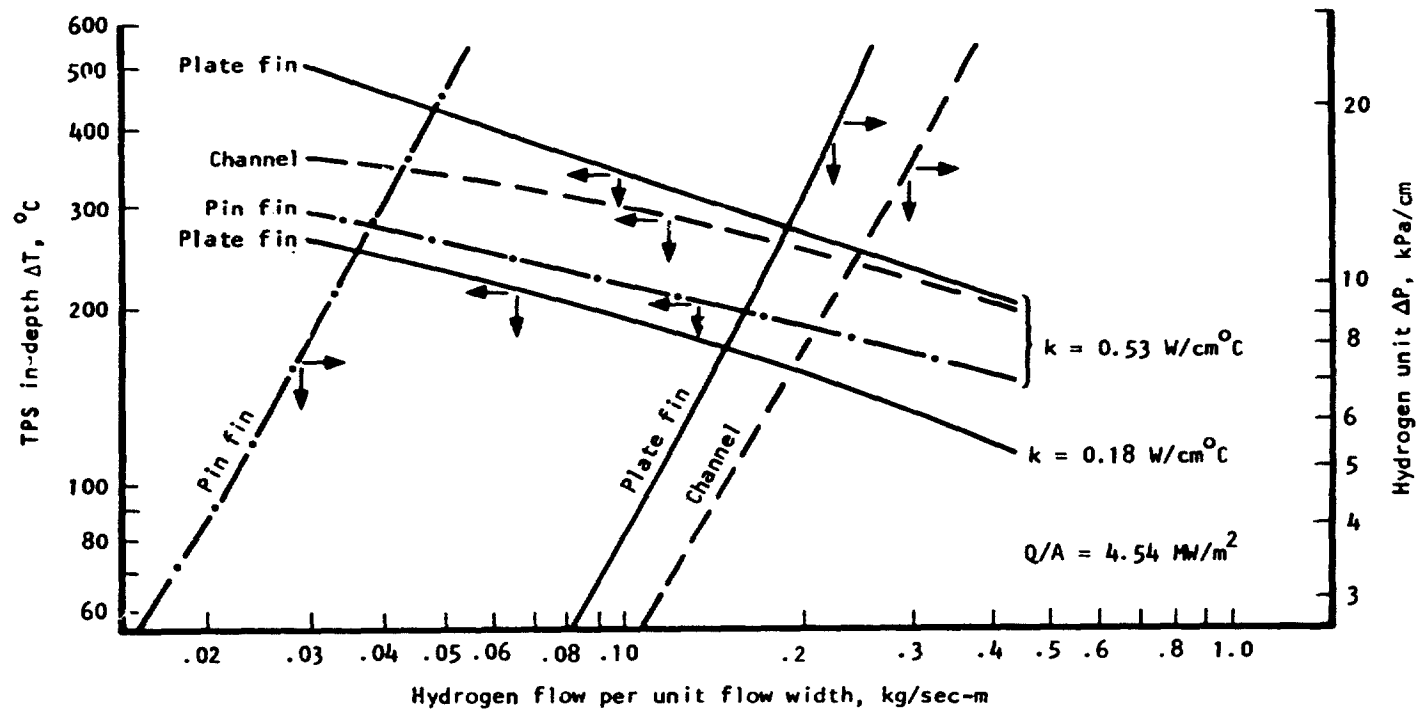


Dimensions considered:

- $1/N = 2.0 \text{ mm}$
- $t = 0.5 \text{ mm}$
- $b = 0.64 \text{ and } 1.27 \text{ mm}$

S-15719-A

Figure 17...TPS Heat Exchanger Configurations.



#### Flow passage geometries

Plate fin: 11 fins/cm

Channel: 0.64 mm depth

Pin fin: 0.64 mm depth, 1.0 mm pin diameter

#### Hydrogen flow conditions

$P = 6.2 \text{ MPa}$

$T = 556 \text{ }^\circ\text{K}$

Figure 18.--TPS Heat Exchanger Performance.



TABLE 7.--SIDEWALL TPS TEMPERATURE GRADIENT AND PRESSURE DROP (SI Units)

Material: Hastelloy X,  $k = 0.18$  watts/cm°C  
 Hydrogen Conditions:  $T = 556^\circ\text{K}$ ,  $P = 6.20$  MPa

Surface Description	Forward Flow Route(1)		Aft Flow Route(2)	
	$\Delta T$ , °C	$\Delta P$ , MPa	$\Delta T$ , °C	$\Delta P$ , MPa
Plate fin 11 fins/cm 14.2 fins/cm	256	1.14	189	0.94
	206	5.10	152	4.03
Channel 1.27 mm deep 0.64 mm deep	357	0.12	266	0.09
	234	0.70	178	0.52
Pin fin 1.02 mm dia x 0.64 mm deep 1.02 mm dia x 1.27 mm deep 1.02 mm dia x 1.91 mm deep 0.76 mm dia x 1.27 mm deep	172	24.06	131	19.03
	220	7.10	162	5.64
	254	3.15	188	2.44
	232	3.34	172	2.54

- (1) Flow = 0.0631 kg/sec, average flow width = 0.419 m, flow length = 1.40 m, heat flux = 4.02 MW/m<sup>2</sup>.
- (2) Flow = 0.0692 kg/sec, average flow width = 0.349 m, flow length = 0.63 m, heat flux = 3.27 MW/m<sup>2</sup>.

TABLE 7 (Continued).--SIDEWALL TPS TEMPERATURE GRADIENT AND PRESSURE DROP  
(U.S. CUSTOMARY UNITS)

Material: Hastelloy X,  $k = 10 \text{ Btu/hr ft}^\circ\text{F}$   
 Hydrogen Conditions:  $T = 1000^\circ\text{R}$ ,  $P = 900 \text{ psia}$

Surface Description	Forward Flow Route <sup>(1)</sup>		Aft Flow Route <sup>(2)</sup>	
	$\Delta T$ , $^\circ\text{F}$	$\Delta P$ , psi	$\Delta T$ , $^\circ\text{F}$	$\Delta P$ , psi
Plate fin 28 fins/in.	460	165	340	136
36 fins/in.	371	740	274	585
Channel .050 deep	643	18	478	13
.025 deep	422	101	320	76
Pin fin .040 dia x .025 deep	310	3490	235	2760
.040 dia x .050 deep	396	1030	292	816
.040 dia x .075 deep	458	457	338	354
.030 dia x .050 deep	418	484	310	368

(1) Flow = .1392 lb/sec, average flow width = 1.375 ft, flow length = 55 in.,  
 heat flux = 354 Btu/sec sq ft

(2) Flow = .1527 lb/sec, average flow width = 1.144 ft, flow length = 25 in.,  
 heat flux = 288 Btu/sec sq ft

Thermal conductivity has a pronounced effect on the TPS thermal gradient.  
 The following results are for the sidewall forward flow route:

	TPS Material	
	Hastelloy X, $k = 0.18 \text{ W/cm}^\circ\text{C}$ (10 Btu/hr ft $^\circ\text{F}$ )	Nickel-200 $k = 0.53 \text{ W/cm}^\circ\text{C}$ (30 Btu/hr $^\circ\text{F}$ )
TPS hot skin temperature, $^\circ\text{K}$ ( $^\circ\text{R}$ )	784 (1412)	685 (1233)
Primary structure temperature, $^\circ\text{K}$ ( $^\circ\text{R}$ ) (honeycomb hot face sheet)	550 (990)	550 (990)
TPS temperature gradient, maximum $\Delta T$ , $^\circ\text{K}$ ( $^\circ\text{R}$ )	234 (422)	135 (243)

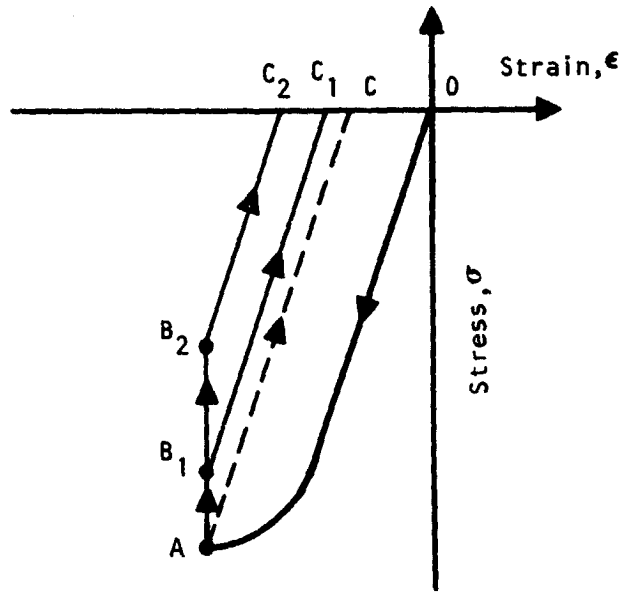
For external surface cooling, passive as well as active schemes were investigated with the following results at steady state:

Method	Metal substrate temperature, °K (°R)	Net heat input, MW/m <sup>2</sup> (Btu/sec sq ft)
Reusable surface insulation (RSI) 0.25 in. thick, k = 0.18 W/cm°C (1.0 Btu/hr ft°F)	1300 (2340)	0.054 (4.8)
Rockide Z insulation, 0.025-in. thick, k = 0.018 W/cm°C (0.1 Btu/hr ft°F)	1420 (2550)	0.093 (8.3)
Bare metal, emissivity = 0.8	1440 (2590)	0.10 (8.9)
Active cooling with hydrogen, inlet temperature = 56°K (100°R)	200 (360)	0.45 (40)

The internal structure was assumed to be at 278°K (500°R) in all cases. RSI thickness is limited by the cowl depth.

The passive schemes are all feasible in that the equilibrium temperature of the metal substrate is below the melting point of a Hastelloy X structure. The net heat input is low, but means to absorb this input are still required. The primary drawback to passive cooling is that the hot substrate must be attached to the cooler engine structure with resulting problems in heat leak and thermal stress. The selected approach is to use active cooling and accept the greater heat input.

Structural design.--In the TPS, the primary structure is relatively cold and limits the thermal expansion of the hot surface, which is less stiff. In fig. 19, curve OA represents the elastic-plastic loading produced by the temperature gradient across the TPS. Without hold time, the  $\Delta T$  gradient decreases to zero and the line AC represents the unloading; however, even a short hold time--especially if the stress at A is high--will produce stress relaxation (point B<sub>1</sub> in fig. 19). The amount of relaxation will depend on the stress, temperature, and creep properties of the material under consideration. The amount of damage incurred in one cycle increases as point B<sub>1</sub> moves to B<sub>2</sub> (more creep).



S-15709

Figure 19.-- Elastic-plastic Cycle.

Repetitive cycles around the hysteresis loop (fig. 19) result in accumulated damage and eventually a fatigue crack develops. The failure mechanism is low-cycle fatigue (LCF).

Thermal stresses are the predominant load in the TPS structure. Bending stresses induced by the hot gas flow are secondary. Thus, the life of the TPS is governed by LCF considerations. The basic analytical approach is to consider creep relaxation effects with an elastic plastic mode of behavior.

Design configurations: The two basic designs selected for analysis of relative merits are: (1) a formed plate fin, and (2) a machined fin. Dimensions of the TPS and its supporting structure are shown in fig. 20. Dimensions used here are different from those finally selected (see fig. 17). The resulting cycle life predictions, however, are valid for comparison purposes.

The machined fin is considered an attractive alternate because of (1) reduced stress concentration, and (2) elimination of a braze joint next to the hot face sheet. Brazing is known to adversely affect fatigue life.

Thermal stress analysis: Finite element models of the candidate structure were constructed and the boundary conditions defined. The plate fin model is shown in fig. 21. Hastelloy X material was first evaluated. A TPS hot face temperature of 788°C (1450°F) was specified because it is an average value of the temperature gradient across the face sheet at the maximum imposed heat flux condition. Coolant pressure was assumed to be 5.52 MPa (800 psia) and the hot gas pressure equal to 0.69 MPa (100 psia).

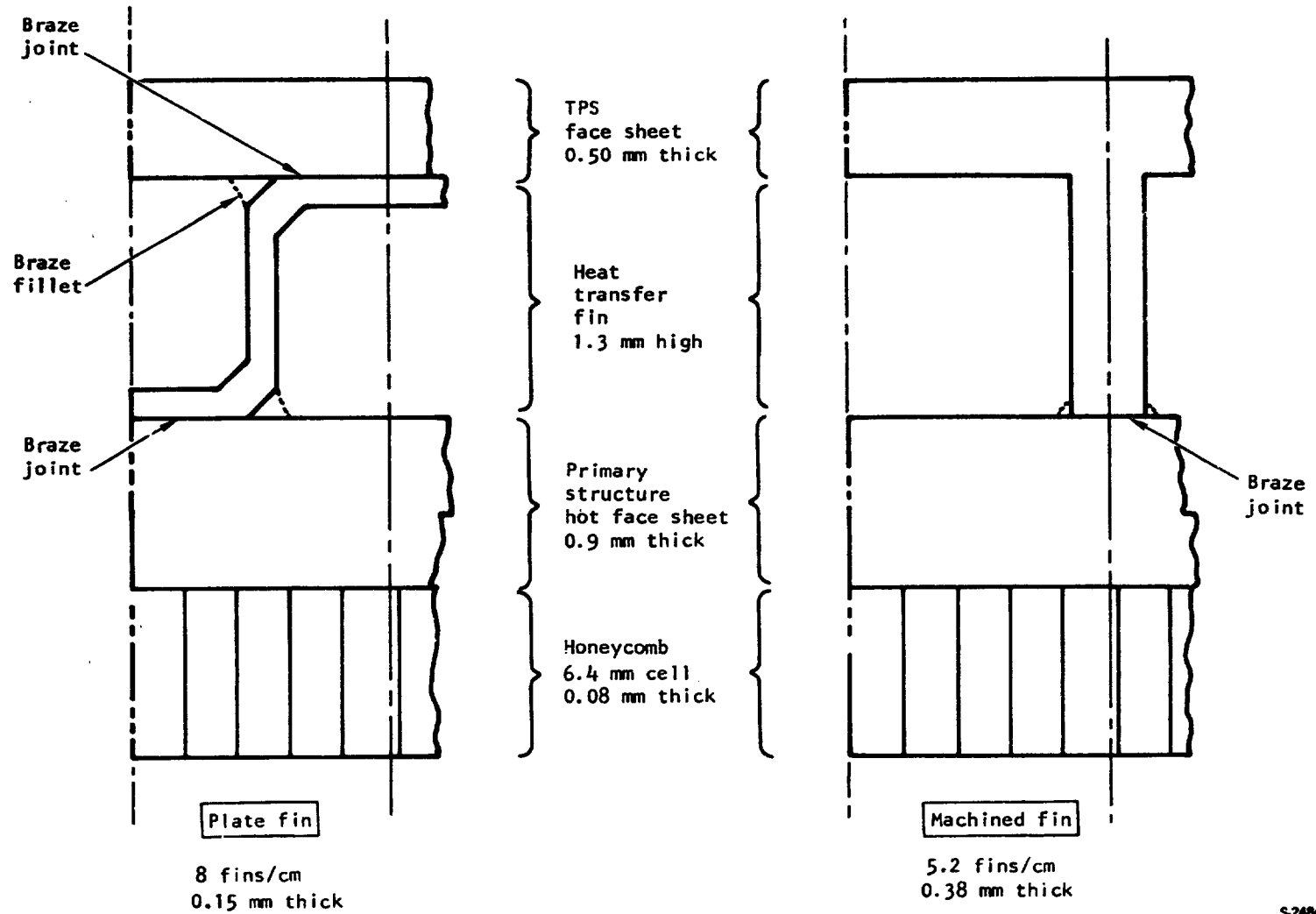
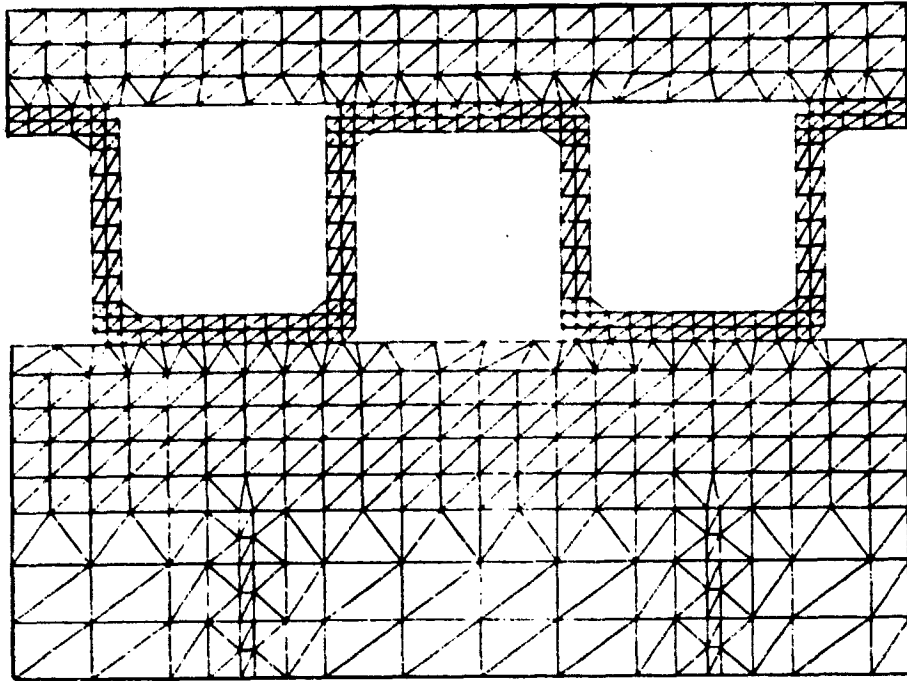


Figure 20.--TPS Structural Design Fin Configurations.

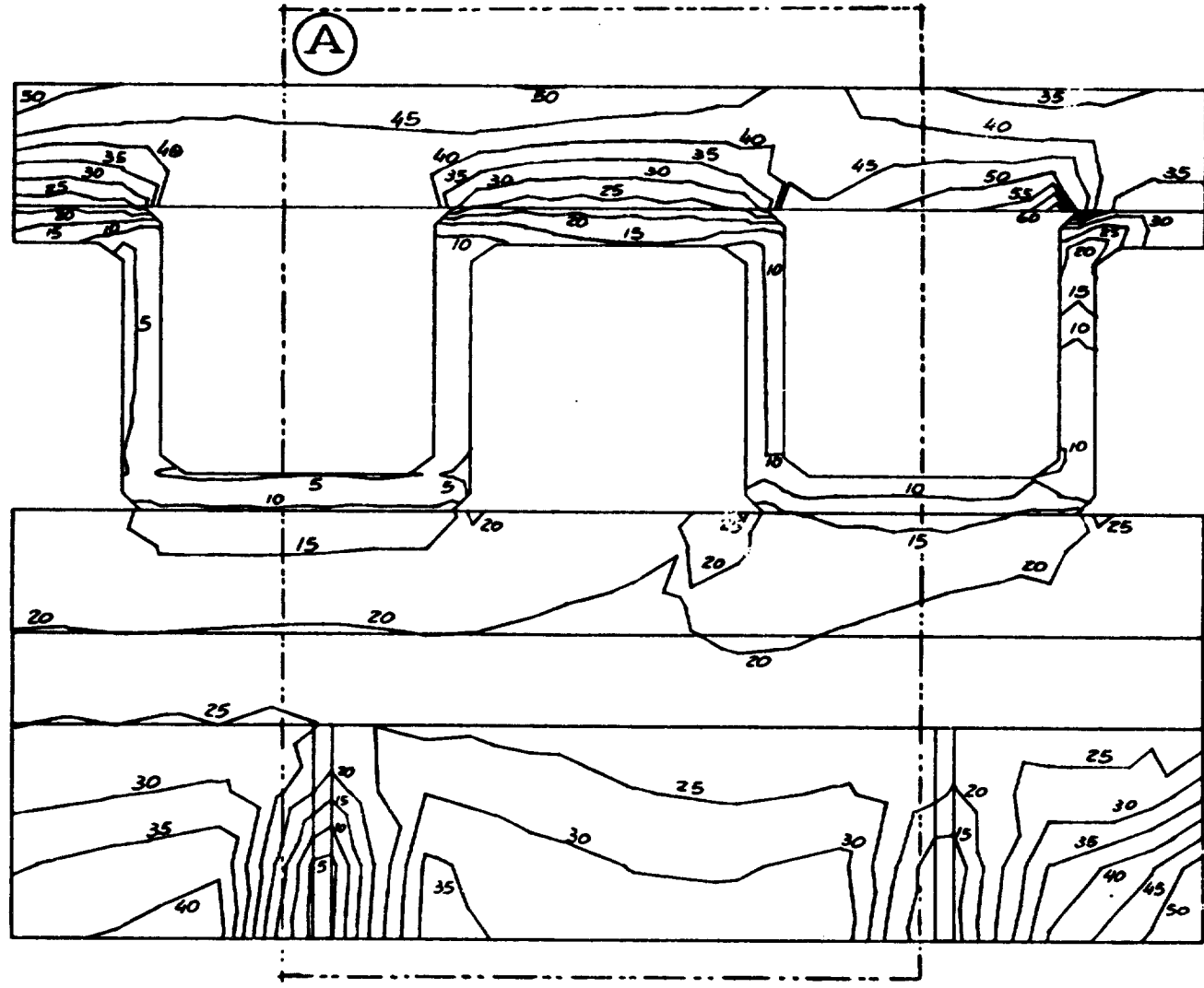


S-24839

Figure 21.--Finite Element Model.

Maximum elastic stresses and displacements were determined for a range of in-depth temperature gradients. A typical result for the plate fin design is shown in fig. 22. For the high gradient cases, the resultant stresses are sufficient to cause plastic deformation plus creep. The elastic analysis indicated that the plastic region (that area where the stress exceeds the material yield strength) would be extensive, and hence, a full elastic-plastic analysis including creep relaxation was performed using finite element models. Temperature differences of 193°, 354°, and 499°C (379°, 670°, and 930°F) were imposed across the TPS face sheet and fins. Resulting strains were determined as a function of hold time at temperature from 4 seconds to 700 hours. Strain is the most important parameter because it defines the number of fatigue cycles the structure can withstand without cracking.

Results: Plastic plus creep strains for the plate-fin and machined-fin structures are shown in fig. 23. The particular area under examination is the TPS hot face sheet where the strains are maximum. The maximum primary structure temperature, 616°C (1140°F), was used as the baseline. The plastic flow region is well developed within the first minute. The stress relaxation is greater for the larger temperature differences, but less than the direct proportion between gradients.



S-24840

Figure 22.--Effective Stresses (ksi) in Plate-Fin Structure.

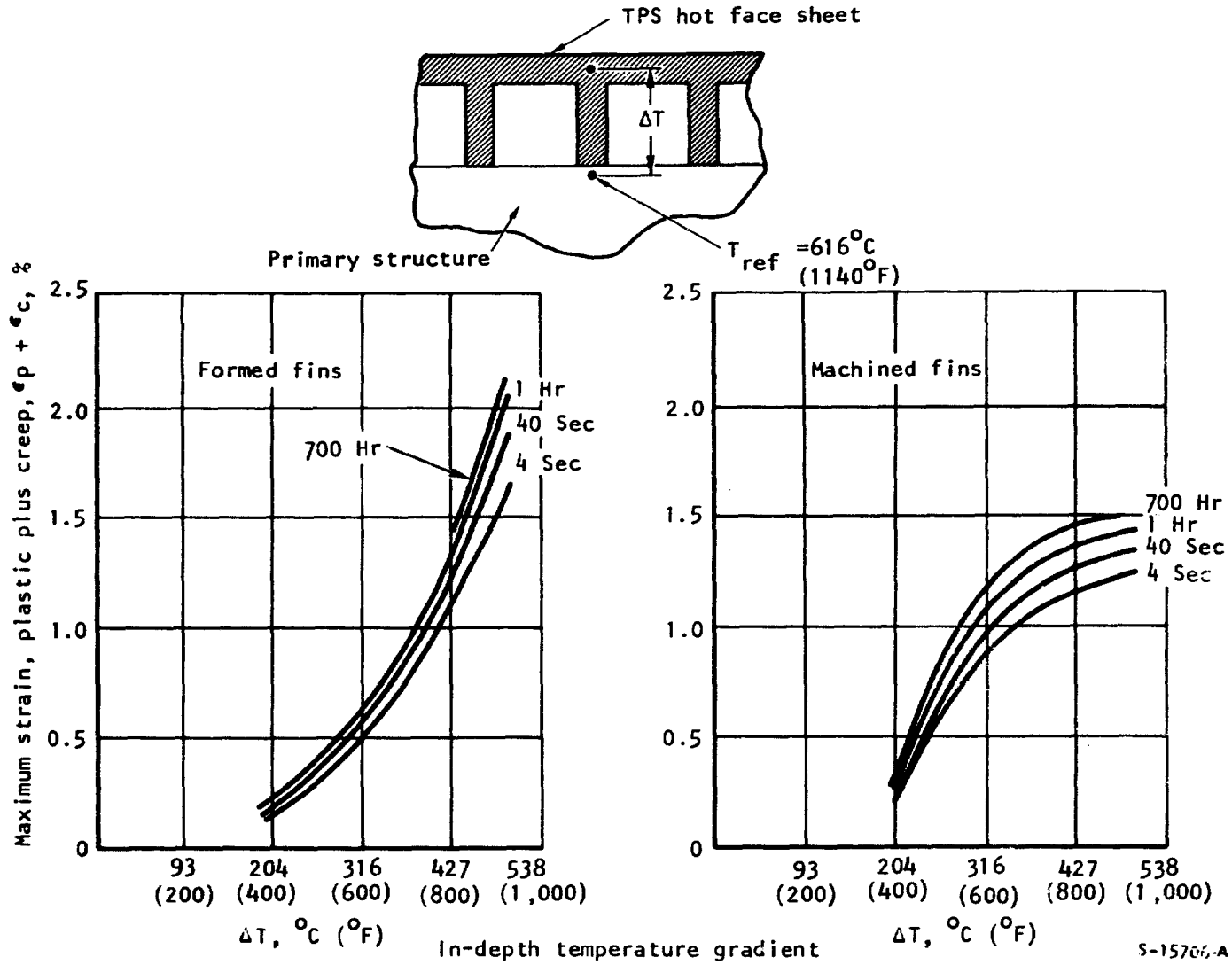


Figure 23.--TPS Response to Thermal Gradient.



The rate of strain development as  $\Delta T$  is increased differs between the two structures, primarily because of the difference in the ratio of fin-to-face sheet stiffness. With the formed fin structure, the fin is flexible relative to the face sheet and, thus, the face sheet absorbs most of the axial load. In the machined-fin structure, more of the thermally induced load is taken by the fin. In the area of interest, i.e.,  $\Delta T = 222^\circ$  to  $278^\circ\text{C}$  ( $400^\circ$  to  $500^\circ\text{F}$ ), more plastic strain is developed in the machined-fin structure; however, this does not necessarily relate to a lower cycle fatigue life. A larger radius at the root of the machined fin would reduce the plastic strain.

Low-cycle fatigue (LCF) analysis: Two techniques were used to relate creep damage to LCF: linear interaction, a technique described in refs. 13 and 14, and strain range partitioning, the most recent evolution, described in refs. 15, 16, and 17.

Strain range partitioning involves the concept that two modes of deformation may exist separately or concurrently, and that their interaction influences the fatigue behavior of the material to a significant degree. In this method, the two strain modes of plastic flow and creep are distinguished in relation to their time dependency. Plastic flow is regarded as the inelastic strain component that occurs immediately upon application of stress, while creep is regarded as the time-dependent component. This distinction allows the separation of the inelastic strain components by relatively simple experimental procedures.

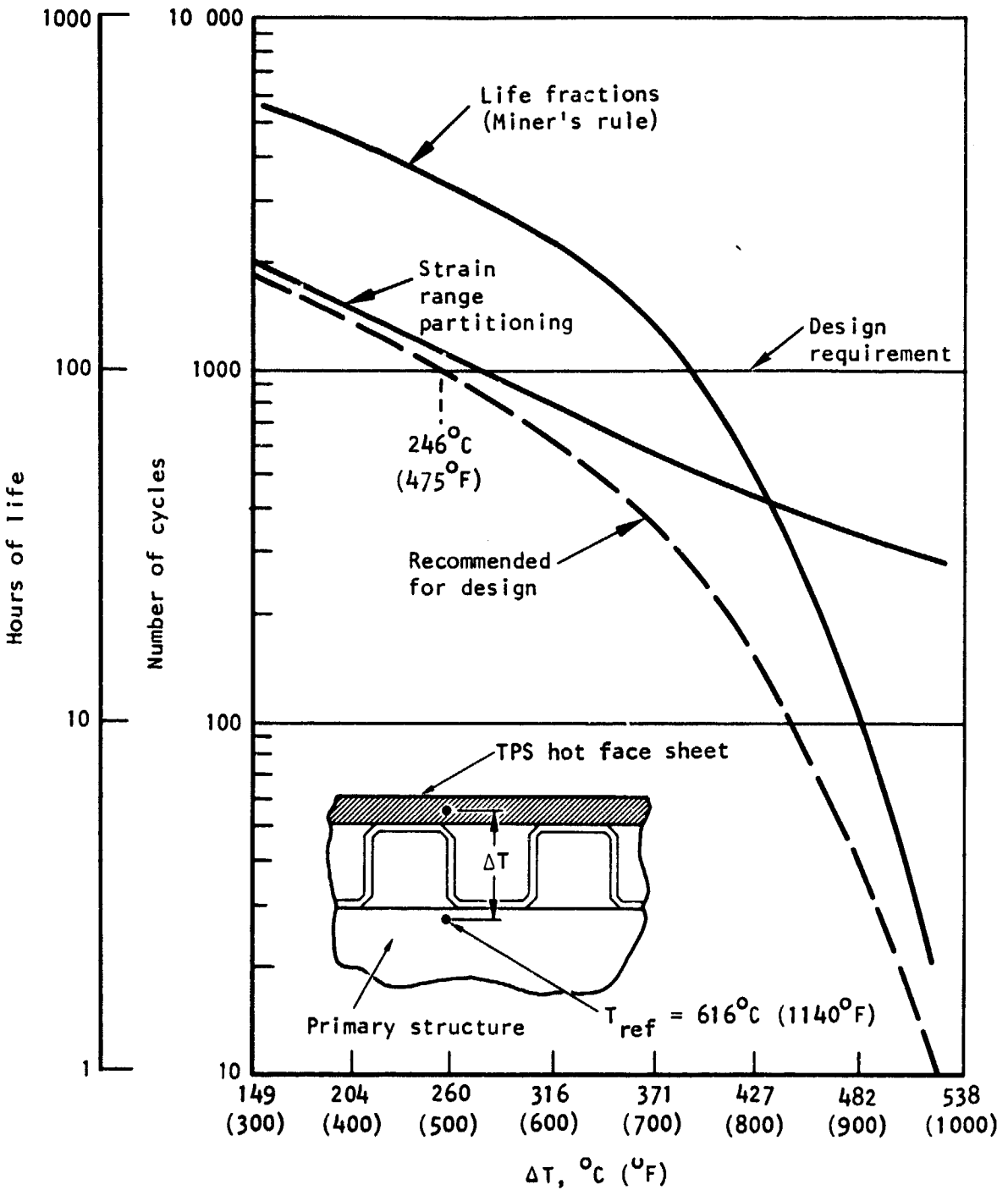
Safety factors for linear interaction were as follows:

Creep damage fraction	4 (on time)
LCF damage fraction	10 (on life)

With strain range partitioning, a 2.5 to 4.0 safety factor was assigned depending on the relative amounts of plasticity or creep in the hysteresis loop. A higher safety factor is used where creep dominates.

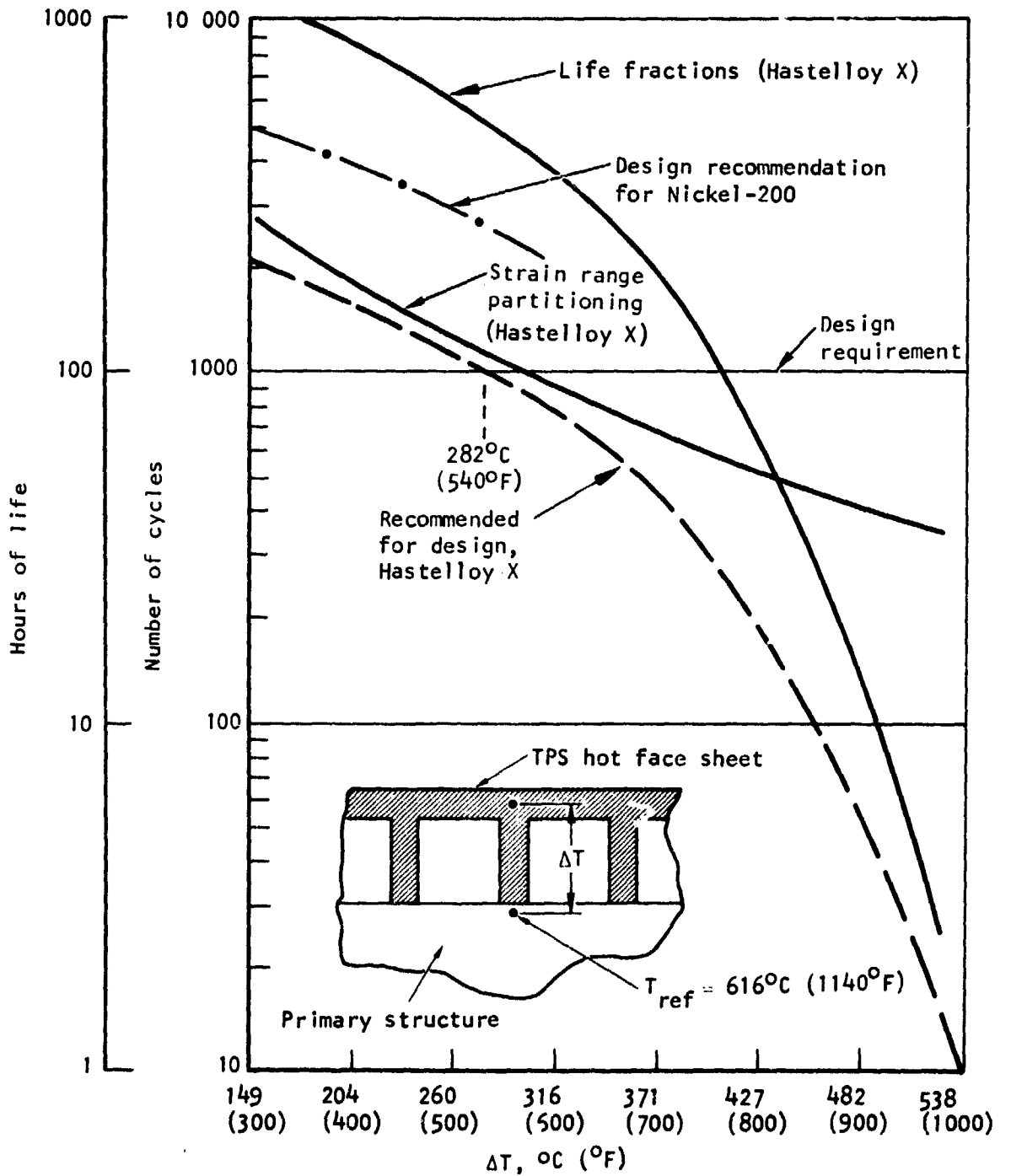
Cycle life predictions for Hastelloy X material are presented in figs. 24 and 25. Strain range partitioning gives a more conservative cycle life prediction in the range of interest, i.e., temperature gradients less than  $360^\circ\text{C}$  ( $650^\circ\text{F}$ ). At high temperature gradients, i.e., high strain levels, the life fractions method is probably more reliable. The recommended design curve was drawn to reflect the most conservative approach.

In terms of cycle life, the machined fin is superior to the formed-fin structure, even though the amount of plastic strain is greater for the machined fin at temperature differences less than  $444^\circ\text{C}$  ( $800^\circ\text{F}$ ) (see fig. 23). The formed-fin structure cycle life is degraded because of two factors. First, the ultimate tensile strength and ductility, important factors in the cycle life equation, are degraded by about 15 percent to account for brazing adjacent to the critical section (TPS hot face sheet). Second, there is a greater proportion of creep damage in the overall cycle with the formed fin. The relationship between creep and fatigue damage fractions is especially significant in the strain range partitioning analysis.



S-15715-A

Figure 24.--Cycle Life for Formed-Fin TPS.



S-15716-A

Figure 25.--Cycle Life for Machined-Fin TPS.

Fatigue life for a Nickel-200 machined-fin structure was estimated by assuming that the strain versus  $\Delta T$  behavior was similar to that predicted for Hastelloy X. The strain was adjusted, however, to reflect the difference in Young's modulus. The estimated life is shown in fig. 25 for the temperature range where the estimate is most valid.

Performance summary.--Final selections and estimated performance for the TPS are presented in Table 8 and in fig. 26. The following criteria were used: (1) overall coolant pressure drop including any shunt circuits must be less than 1.38 MPa (200 psi); (2) Hastelloy X material except where in-depth  $\Delta T$  exceeds 222°C (400°F); (3) Nickel-200 material in high heat flux areas where Hastelloy X is not suitable; and (4) maximum TPS face sheet temperature less than 1144°K (2060°R) for Hastelloy X and 1060°K (1910°R) for Nickel-201.

The cyclic life given for the channel structures is in accordance with the recommended design curves in fig. 25. For the Nickel-200 pin fin structure, as used in the strut, the cycle life was computed as follows: (1) a two-dimensional finite element model of the contoured cross-section was constructed and the strain concentration factor determined; (2) the creep strain was computed assuming that the stress would be fully relaxed during the cycle; and (3) the cycle life was determined using the strain range partitioning technique.

For external surface cooling, TPS passage geometry is not critical. Formed or machined fins, spaced circular tubes, or D-tubes are all feasible. A machined channel is recommended because of its greater structural rigidity, low temperature gradients, and compatibility with the other TPS geometries.

### Leading Edges

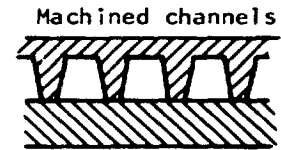
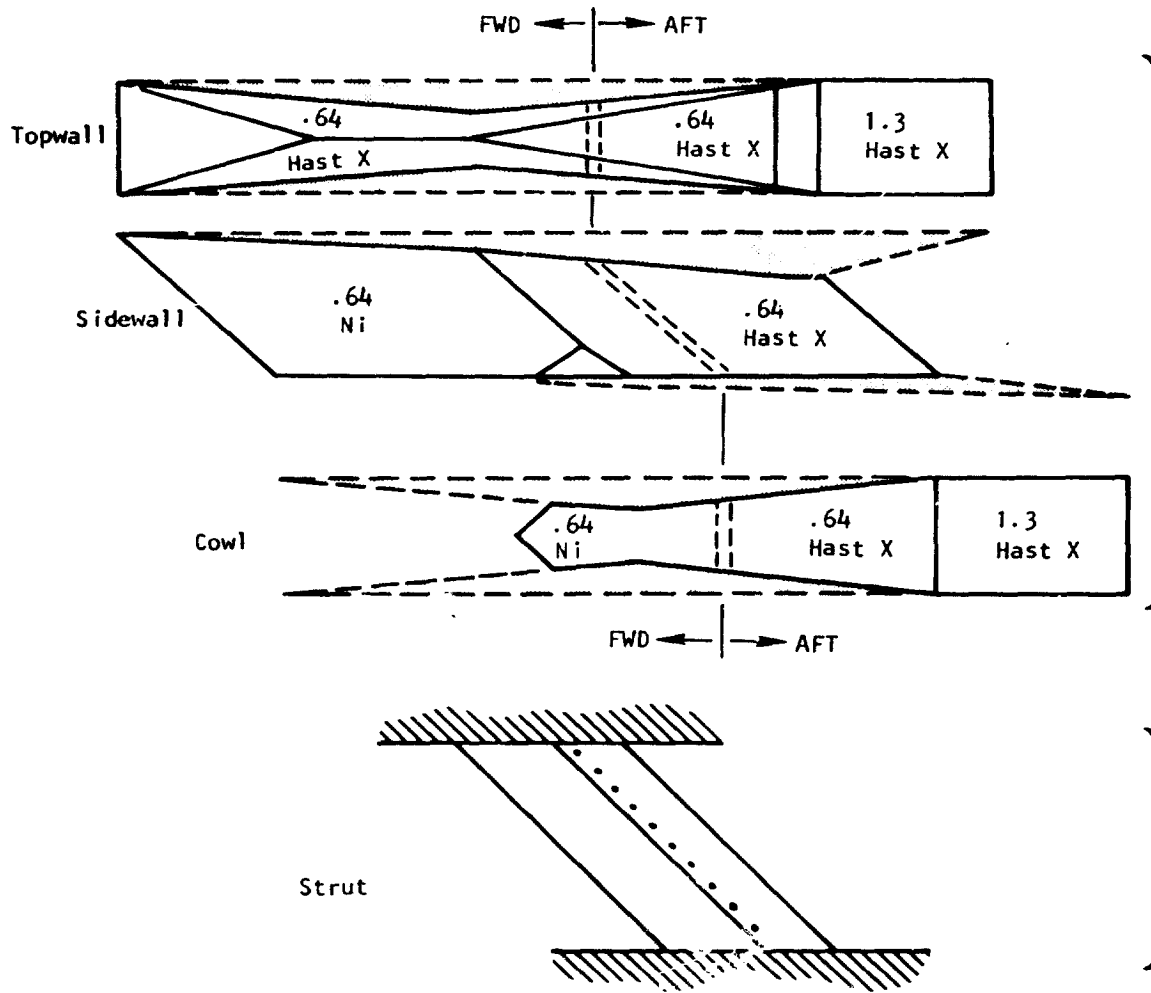
Two basic cooling options shown in fig. 27 were considered: impingement, direct and indirect; and parallel-flow concepts. Impingement can be directed parallel to the hot gas flow or normal to the sweep line. With indirect impingement, the flow turns nearly 180 deg (less the wedge angle) thus producing a near-impingement cooling effect.

In parallel-flow cooling, the coolant flows in a channel just behind and parallel to the leading edge as shown in fig. 27. The inherent disadvantage of this basic concept is that the coolant heat transfer coefficient is lower than with impingement, pressure drop is higher, and the flow routing is not compatible with the longitudinal flow routing of the engine panels.

TABLE 8.--TPS PERFORMANCE

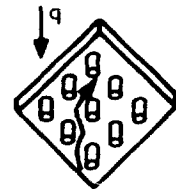
Flow circuit	Surface	Material	In-depth $\Delta T$ , °F (°R)	Maximum skin temperature, °K (°R)	Total $\Delta P$ , MPa (psi)	Cycle life
Cowl, forward	Channel, 0.64 mm deep	Nickel	169 (305)	423 (761)	0.76 (110)	5000 +
Cowl, aft*	Channel, 0.64 mm deep	Hastelloy X	202 (363)	1102 (1983)	1.07 (155)	1450
Side, forward	Channel, 0.64 mm deep	Nickel	135 (243)	685 (1233)	0.70 (101)	10,000 +
Side, aft	Channel, 0.64 mm deep	Hastelloy X	178 (320)	1078 (1940)	1.24 (180)	1820
Top, forward	Channel, 0.64 mm deep	Hastelloy X	146 (263)	608 (1094)	0.35 (51)	5000 +
Top, aft	Channel, 0.64 mm deep	Hastelloy X	119 (215)	1019 (1835)	0.65 (94)	5000 +
Strut, center	Pin fin, 1.0 mm dia by 0.64 mm deep	Nickel	167 (300)	1011 (1820)	0.33 (48)	2500 +
Strut, side	Pin fin, 1.0 mm dia by 0.64 mm deep	Nickel	138 (249)	1038 (1869)	0.79 (114)	4000 +

\*External cowl and nozzle portions of the top wall and internal cowl utilize a 1.27-mm-deep channel surface.



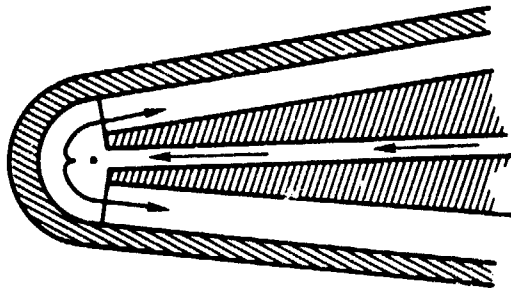
Note: TPS thickness is given in mm

Staggered pin pins

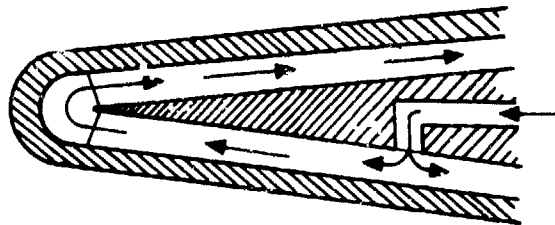


S-24834

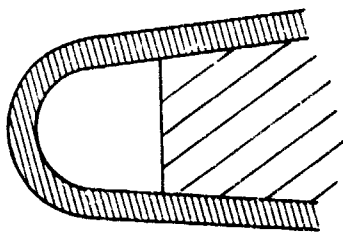
Figure 26.--TPS Configuration.



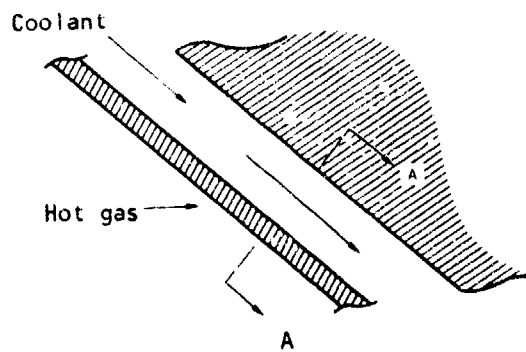
a. Direct impingement



b. Indirect impingement



Section AA



c. Parallel flow

5-15981-A

Figure 27.--Cooling Options.

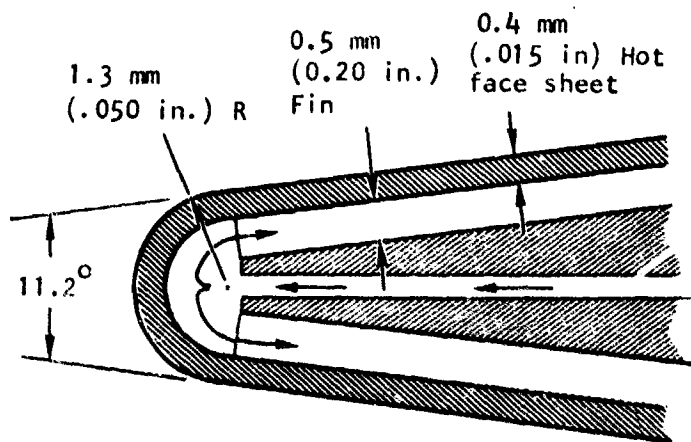
Flow route options.--Inlet coolant flow can be split with only a portion of the flow directed to the leading edge. The leading edge flow is subsequently joined with the main flow stream. This scheme is sometimes necessary because of pressure drop considerations. It was verified that the total coolant flow for a particular route could be flowed through the leading edge with reasonable pressure drop. This route is preferred to obtain maximum possible cooling.

Flow routing and control considerations favor a common leading edge assembly for adjacent sidewall panels. This concept is best for leading edge life and was used for this analysis.

For the sidewalls and struts, direct impingement cooling is inherently better because the coolant flow is about twice that available with indirect impingement cooling. For the cowl, ducting simplicity in the basic flow route, wherein the flow is first through the external surface, favors indirect impingement.

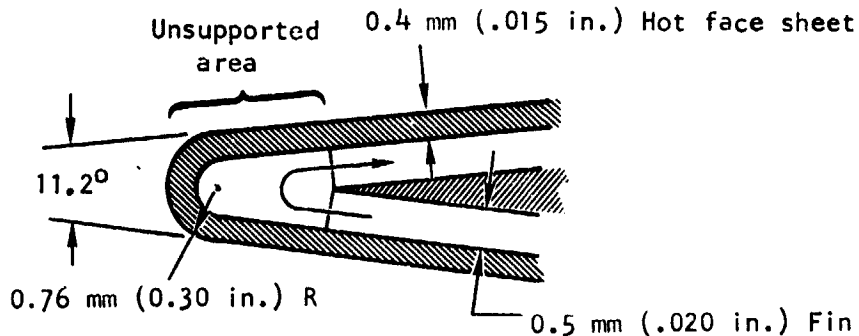
The cowl apex is a unique cooling point because it is the intersection of two swept leading edges. As noted in Design Conditions, the local heat flux can be especially high at the apex. Direct or indirect impingement cooling of the cowl with the flow parallel to the hot gas flow is feasible. The apex cooling rate can be augmented by using a separate tube to flow coolant directly at the apex.

Geometric constraints.--To accommodate direct impingement concepts, a minimum leading edge radius of 1.3 to 1.5 mm (0.050 to 0.060 in.) is required. This limitation is illustrated below using the sidewall common leading edge as an example (cross-section parallel to gas flow).





A sharper leading edge radius is possible with indirect impingement as illustrated below for the sidewall common leading edge (cross section parallel to hot gas flow).



S 24836

Because of the small wedge angle, a large unsupported area results and this configuration is not structurally tenable. Hence, a 1.3 mm (0.050-in.) leading edge radius was used for evaluation of all cooling concepts. The larger radius also reduces the heat flux although there is an increase in drag.

Heat transfer performance.--Typical temperature gradients around the sidewall and side strut leading edges are shown in fig. 28. Metal temperatures are for 0.38-mm (0.015-in.)-thick Hastelloy X material. Performance with direct or indirect impingement cooling is similar except for the first 2.5 mm (0.1 in.) of length. Results are summarized in Table 9.

The temperature difference across the leading edge is not directly proportional to the heat flux. This results because: (1) two-dimensional heat transfer conduction paths are dependent on the hydrogen flow path, and (2) the resulting difference in temperature level around the structure affects the material thermal conductivity and, hence, the temperature gradient.

Direct impingement normal to the sweep line gives the lowest temperatures except for the cowl and cowl apex, where indirect impingement is best. The sidewall, cowl, and side strut leading edge temperatures appear to be acceptable, although temperature differences are high. Performance at the cowl apex is unacceptable with Hastelloy X. Nickel-200 was therefore considered for use here and to increase the cycle life of other leading edges.

The parallel flow concept was checked for the sidewall leading edge with a 1.3-mm (0.050-in.)-radius leading edge. With a flow of 0.90 g/sec (0.002 lb/sec) (total flow for the sidewall route is 36.3 g/sec (0.080 lb/sec)), the outer surface reached 1389°K (2500°R) and the flow choked before the outlet was reached. It was concluded that parallel flow concepts are unacceptable for this application.

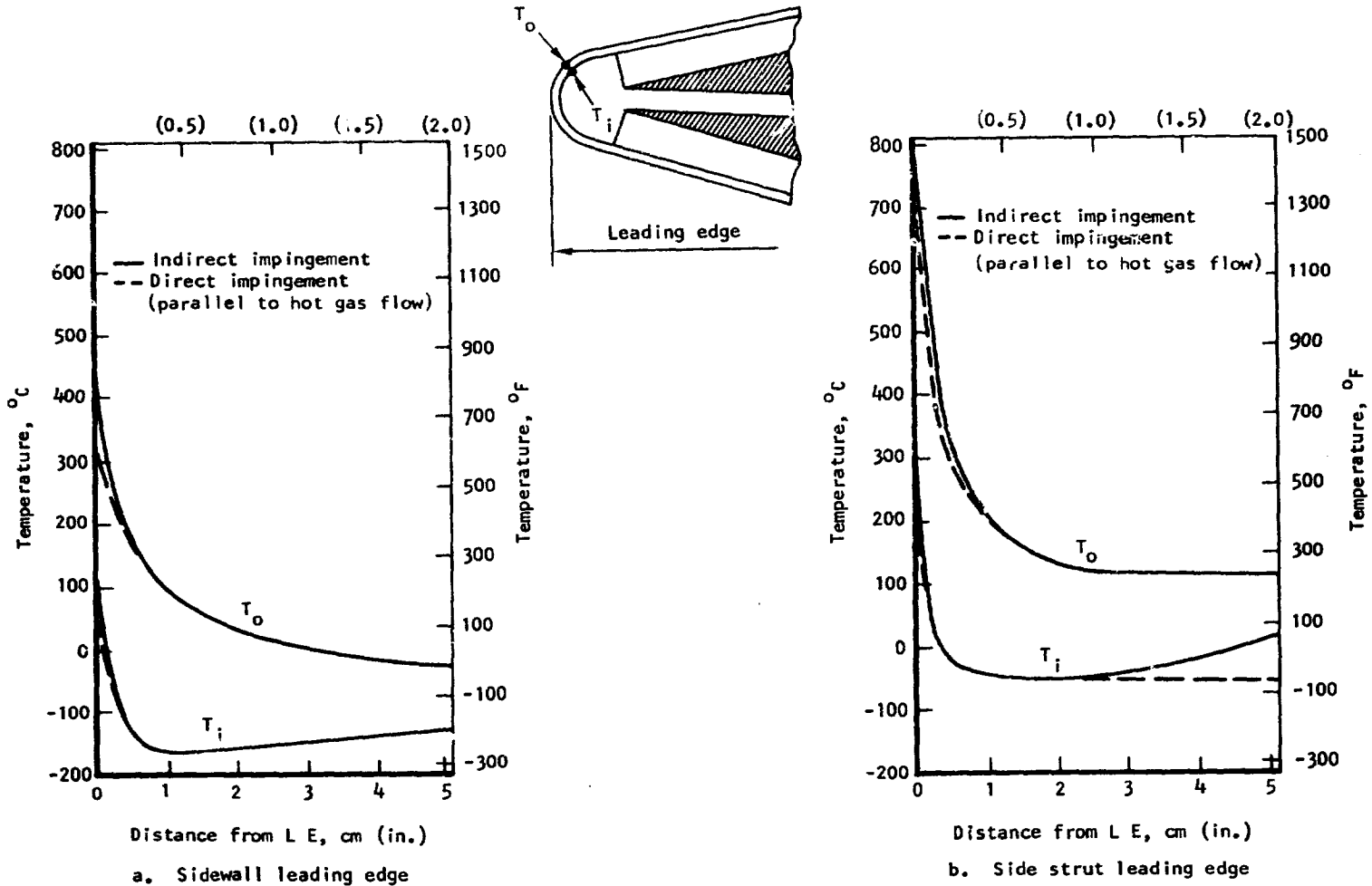


Figure 28.--Typical Temperature Gradients Around Sidewall and Side Strut Leading Edges.

TABLE 9.--LEADING EDGE THERMAL PERFORMANCE  
HASTELLOY X MATERIAL

Leading edge	Heat flux, MW/m <sup>2</sup> (Btu/sec sq ft)	Indirect impingement			Direct impingement					
					Parallel to hot gas flow			Normal to sweep line		
		T <sub>wo</sub> , °K (°R)	T <sub>wi</sub> , °K (°R)	ΔT <sub>w</sub> , °K (°R)	T <sub>wo</sub> , °K (°R)	T <sub>wi</sub> , °K (°R)	ΔT <sub>w</sub> , °K (°R)	T <sub>wo</sub> , °K (°R)	T <sub>wi</sub> , °K (°R)	ΔT <sub>w</sub> , °K (°R)
Sidewall	10.61 (935)	758 (1365)	464 (835)	294 (530)	587 (1057)	313 (564)	274 (493)	560 (1008)	286 (515)	274 (493)
Cowl	14.36 (1266)	582 (1048)	211 (380)	371 (668)	681 (1226)	310 (558)	371 (668)	-	-	-
Cowl apex	45.84 (4042)	1364 (2456)	440 (792)	924 (1664)	-	-	-	1494 (2690)	639 (1150)	855 (1540)
Center strut	1.68 (1792)	1261 (2270)	835 (1503)	426 (767)	1125 (2025)	599 (1079)	526 (946)	1052 (1893)	527 (948)	525 (945)
Side strut	4.14 (1331)	1037 (1867)	647 (1165)	390 (702)	901 (1621)	511 (919)	390 (702)	840 (1512)	394 (710)	446 (802)

Note: Temperatures are for conditions at the stagnation line. Heat fluxes are shown for T<sub>wo</sub> = 833°K (1500°R)

Cycle life analysis.--The estimated leading edge cycle life is shown in Table 10. The analysis used the strain range partitioning technique with a safety factor of 4. Typical material properties and a strain concentration factor of 2.0 were specified. For Hastelloy X material, the temperature data presented in Table 9 were used directly. For Nickel-200 material, the data in Table 9 were ratioed by the thermal conductivities to estimate the operating temperatures.

TABLE 10.--LEADING EDGE CYCLE LIFE

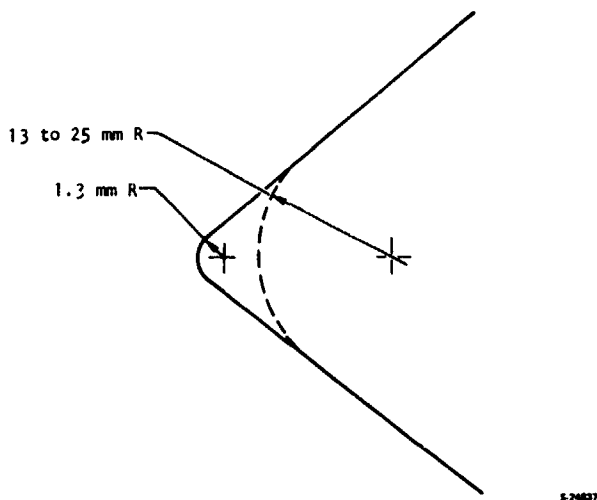
Location	Impingement cooling mode	Cycle life with candidate materials	
		Hastelloy X	Nickel 200
Sidewall	Direct	2800	10 000
	Indirect	500	-
Cowl	Indirect	1000	16 000
Cowl apex	Indirect	40	1400
Side strut	Direct	400	2600
	Indirect	300	-
Center strut	Direct	-	-
	Indirect	150	1700

These results lead to the following conclusions:

- (a) Cycle life requirements can be met by using Nickel-200 material for all leading edges including the cowl apex.
- (b) Direct impingement cooling should be used for the sidewalls and struts because it produces superior cycle life.

Although Nickel-200 is the recommended material, its creep strength is low and a detail analysis of the long-term behavior of the leading edge structure is required. Consideration must also be given to the adverse effects on material properties in the braze-affected zone.

Cycle life at the cowl apex is marginal. A supplementary cooling circuit can be utilized to impinge a jet of cold hydrogen directly on the apex. Another option is to blunt the apex in the cowl plane as shown below.



Blunting eliminates the 1.3-mm (0.050-in.) hemispherical radius, thereby reducing the stagnation heating from three-dimensional to two-dimensional with a corresponding 25 percent reduction in heat input. By blunting the radius to 13 to 25 mm (0.5 to 1.0 in.) and without any supplementary cooling, the cowl apex cycle life can be increased to greater than 5000 cycles.

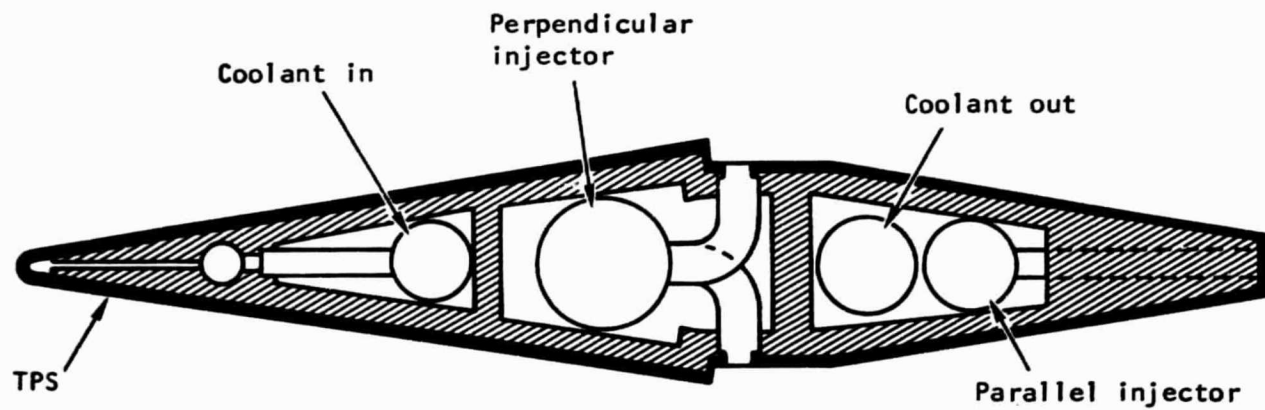
Because of the uncertainty of the inlet shock structure and the heat flux intensity, the recommended approach is to blunt the apex and to use supplementary cooling.

### Fuel Injection Struts

Hydrogen manifolding and flow distribution.--The fuel and coolant can be routed through the strut either by separate lines within the strut structure or by using the strut structure itself to contain the hydrogen. The two concepts are shown in fig. 29.

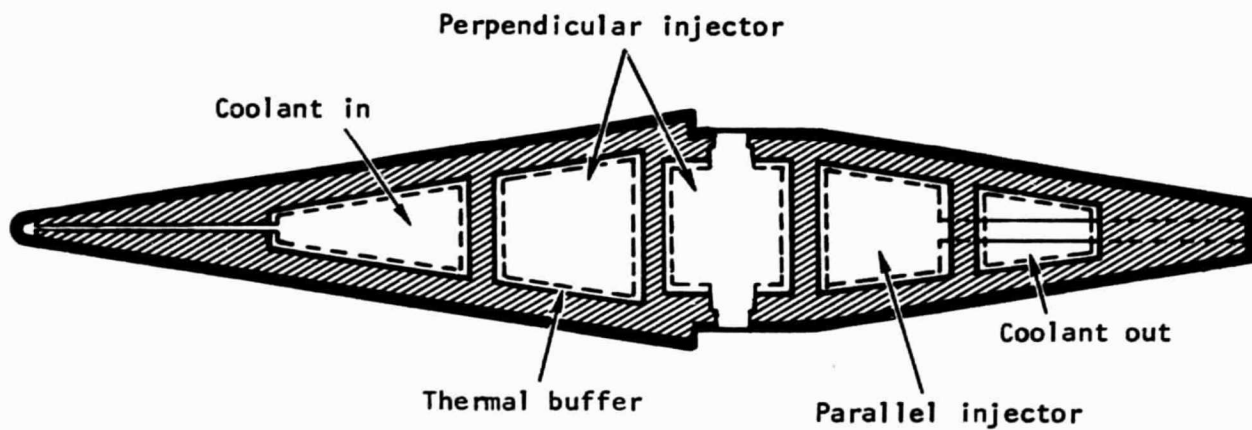
The integral manifold approach was evaluated in ref. 2 and was found to be effective. The key feature in the design was the use of a thermal buffer (a layer of stagnant hydrogen) that reduces the internal convection heating from the hot hydrogen in the manifolds. The resulting thermal stresses were reasonable.

An alternate approach with tubular manifolds was also considered for this study. It was believed that by using separate lines to contain the fuel and coolant, the overall plumbing arrangement would be simplified and the thermal stresses minimized.



a. Tubular Manifold

71



b. Integral Manifold

S-7511-B

Figure 29.--Center Strut Fuel/Coolant Passages.

Coolant design conditions: Maximum flow conditions are shown in fig. 14. The inlet and outlet temperatures shown for Condition H in fig. 14 are assumed to be identical for all flight conditions.

Fuel design conditions: For the perpendicular injectors, maximum fuel flow occurs at the Mach 10 maximum thermal loading condition and is 1.01 kg/sec (2.22 lb/sec). This flow is equally divided between the three struts. This is a transient operating condition with a fuel equivalence ratio of 1.5. Fuel flows at steady-state cruise condition are less. Moreover, it is at cruise condition that ideal flow distribution is most essential. The maximum flow condition was selected for preliminary design, however, to ensure that reasonable flow distribution could be achieved at all operating conditions.

The estimated internal module aerodynamic heat load at Condition H is about 6.85 MW (6500 Btu/sec). Assuming no airframe cooling requirements for the 1.01 kg/sec hydrogen flow, the mixed mean temperature of the coolant outlet hydrogen (889°K, 1600°R) and the hydrogen directly from the tank is 507°K (913°R). This was increased to 611°K (1100°R) to account for a 20-percent uncertainty in the aerodynamic heating. The minimum fuel manifold pressure is 4.82 MPa (700 psia).

For the parallel (supersonic) fuel injectors, the maximum flow occurs at the Mach 5.1 Condition G and is 0.445 kg/sec (0.981 lb/sec). Fuel flow per strut is 0.148 kg/sec (0.327 lb/sec). Hydrogen fuel inlet conditions of 4.82 MPa (700 psia) and 611°K (1100°R) were selected.

Results with tubular manifolds: Initial estimates of the required flow area compared with the available strut cross section indicated some severe conflicts. To reduce the flow velocity head at the fuel manifold inlets to a value consistent with acceptable flow distribution, it was necessary to flow hydrogen from both ends of the strut. A summary of manifold sizes and performance is presented in Table 11.








Manifold routing within the limited space available in the cowl was found to be a complex, difficult design problem. It was concluded that the tubular approach did not offer any design advantages.

Integral manifold design.--Design activity is in process.

Midspan tie.--Structural analyses conducted by NASA (ref. 2) indicated an excessive stress level within the side strut when subjected to an unsymmetrical unstart condition. A possible solution is to tie the struts together at their mid-point, thereby decreasing the bending stresses due to the external side load by a factor of 2.

This concept was investigated in greater detail. For evaluation, a symmetrical diamond airfoil, 1.52 cm thick by 7.62 cm chord, was specified (fig. 30). The tie is placed with an angle of attack of 10 deg, which corresponds with the flow direction through the struts at Condition D.

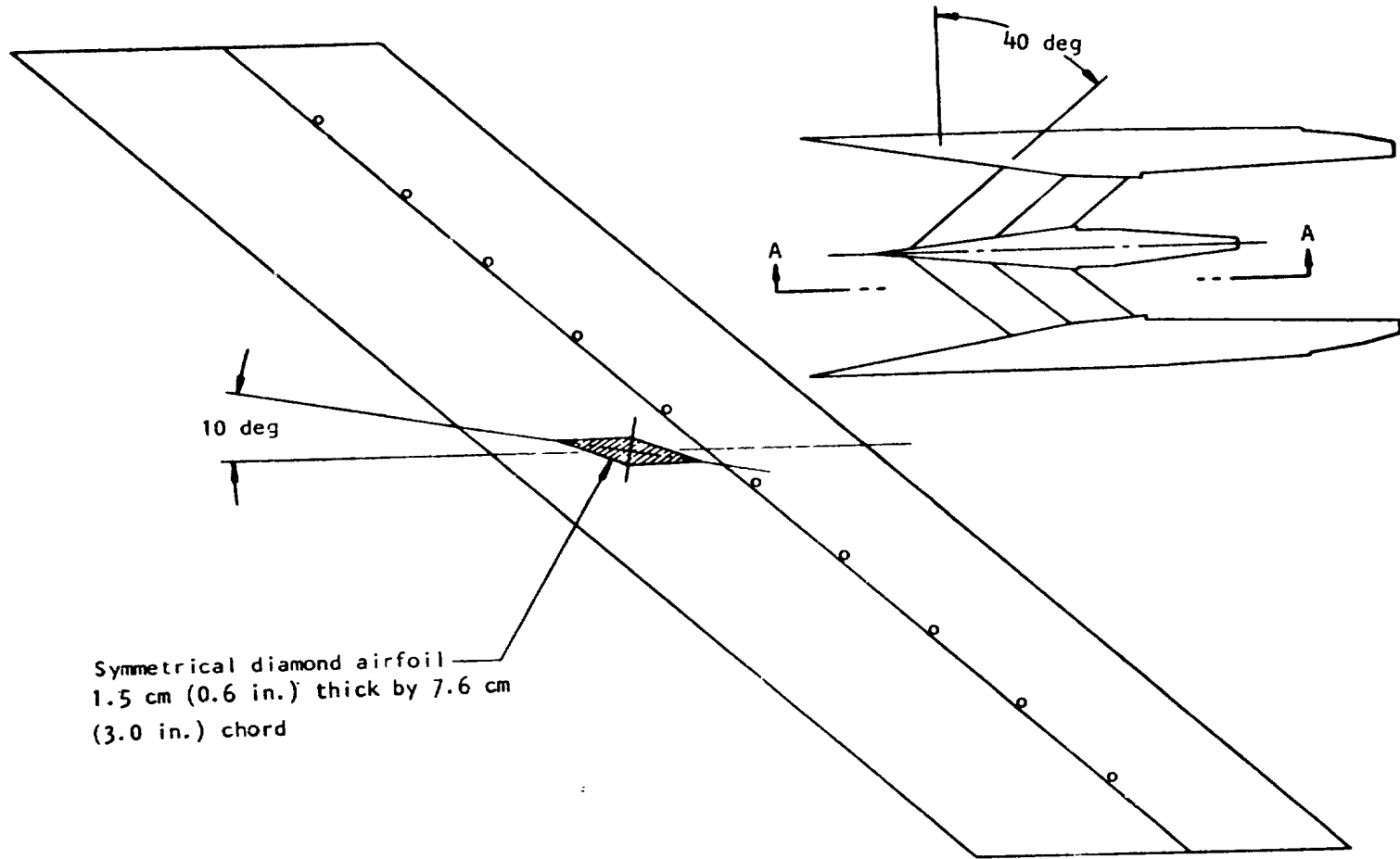
TABLE 11.--TUBULAR MANIFOLD PERFORMANCE

	Coolant inlet	Perpendicular Injectors	Parallel Injectors	Coolant outlet
Tube pattern at topwall surface				
Tube pattern at cowl surface				
Tube sizes	1 at 8 mm OD X 0.25 mm wall	4 at 13 mm OD X 0.5 mm wall	2 at 13 mm OD X 0.5 mm wall	2 at 13 mm OD X 0.5 mm wall
	(1 at 5/16 OD) (X 0.010 in.) wall	(4 at 1/2 OD) (X 0.020 in.) wall	(2 at 1/2 OD) (X 0.020 in.) wall	(2 at 1/2 OD) (X 0.020 in.) wall
Flow area, sq cm (sq in.)	0.434 (0.0672)	4.29 (0.6648)	2.14 (0.3324)	2.14 (0.3324)
H <sub>2</sub> flow rate per strut, kg/sec (lb/sec)	0.0454 (0.100)	0.336 (0.740)	0.148 (0.327)	0.0454 (0.100)
H <sub>2</sub> total pressure, MPa (psia)	6.89 (1000)	4.83 (700)	4.83 (700)	5.17 (750)
H <sub>2</sub> total temperature, °K (°R)	56 (100)	611 (1100)	611 (1100)	889 (1600)
Mach number	0.061	0.220	0.196	0.067
Velocity head, kPa (psi)	17.9 (2.6)	158 (22.9)	126 (18.3)	15.9 (2.3)

Σ Flow area through strut top = 4.88 sq cm (0.757 sq in.)



74



Symmetrical diamond airfoil  
1.5 cm (0.6 in.) thick by 7.6 cm  
(3.0 in.) chord

S-15738

Figure 30.--Midspan Tie Design.

A finite element model of the three-strut assembly was constructed as shown in fig. 31. The ends of the strut were assumed at first to be simply supported at the bottom and guided at the top, restraining rotation in all three axes but allowing axial movement. Space limitations at the cowl limit the amount of fixity that can be achieved. This is considered to be a coarse model and was used as a first approximation.

A uniform net pressure load of 0.69 MPa (100 psi) was applied to the side strut simulating the unstart condition. This load is approximate and was used only to gain an insight to the strut behavior. The strut will deflect 8 mm (0.32 in.) or 13 mm (0.5 in.) depending on end fixity conditions if no midspan tie is used. Since the normal distance between struts is about 25 mm (1.0 in.), the deflection is significant. The deflection with a midspan tie was reduced to 4 to 6 mm (0.15 to 0.22 in.).

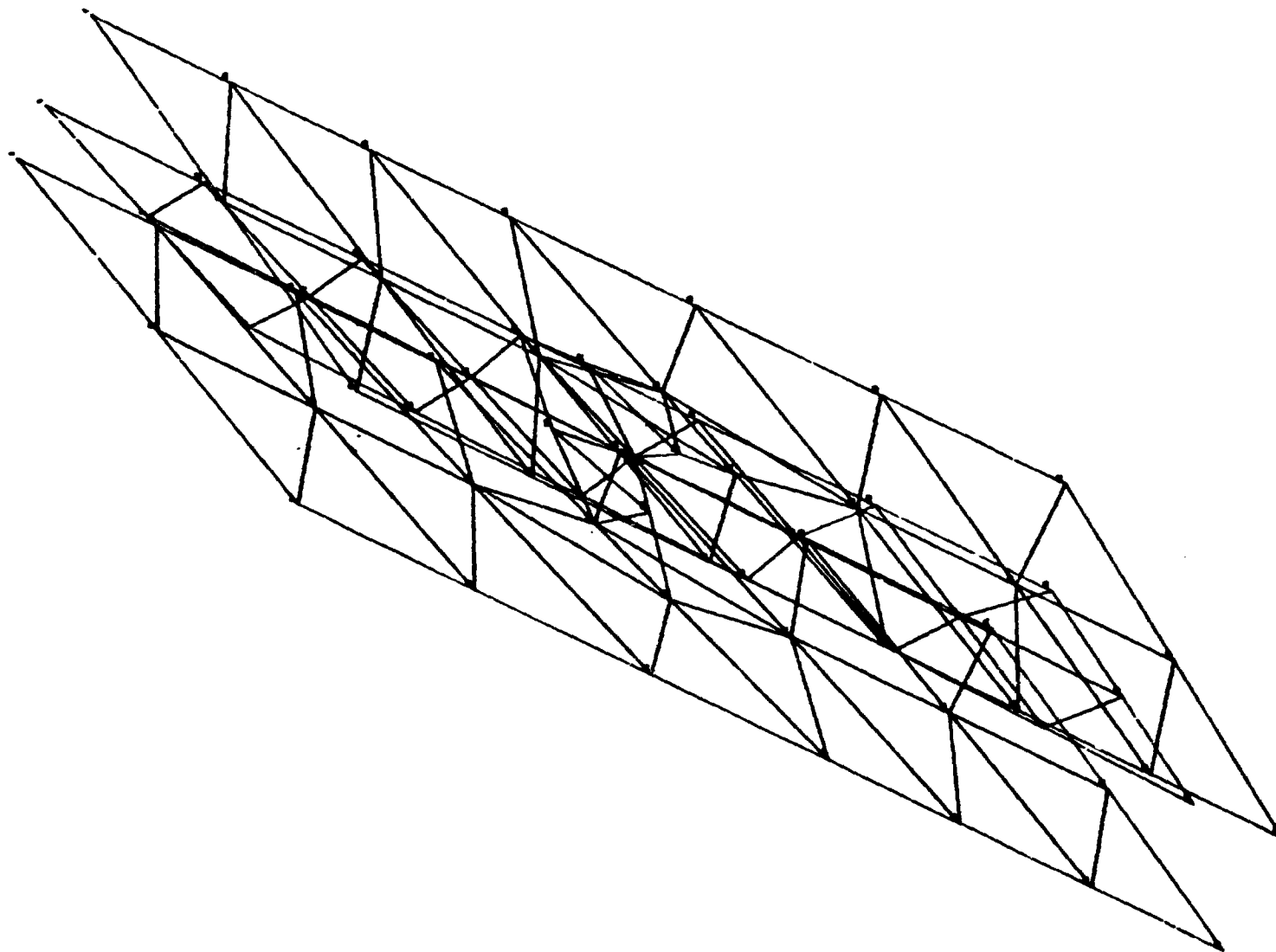
The capability of the midspan tie to stiffen the struts against lateral pressures such as the unsymmetric unstart is clearly demonstrated, even with a tie connecting only the struts, without attachment to the engine side walls.

Unstart condition dynamic response: Transient data obtained from a 3.8-cm-high model of the Scramjet (ref. 4) indicate that the unstart shock propagation velocity is on the order of 30.5 m/sec (100 ft/sec). For the 31.8-cm (12.5-in.)-long chord side strut, the period of the unstart disturbance is about 100 Hz. The period is in the range of the strut natural frequency, indicating a potential for load amplification. To explore this possibility the finite element model (fig. 31) was subjected to a natural frequency vibration analysis with the following results:

Strut midspan tie	Natural frequency, Hz	Strut
No	274 (first mode)	Side
No	323 (first mode)	Center
Yes	380 (first mode)	Side
Yes	567 (second mode)	Side
Yes	792 (third mode)	Side

The midspan tie can increase the natural frequency of the struts by 38 percent (side strut) to over 150 percent (central strut). By moving the tie along the strut height, the strut structural vibration response can be conveniently tuned (or detuned).

For a side strut without a tie, the ratio of pulse period to strut period is 0.37, which yields a loading factor of 1.3 (half sine wave shock profile). By adding a midspan tie, the loading factor is decreased to 0.9. These calculations must be considered to be approximate, but they do show the load reduction provided by a midspan tie.



S-15739

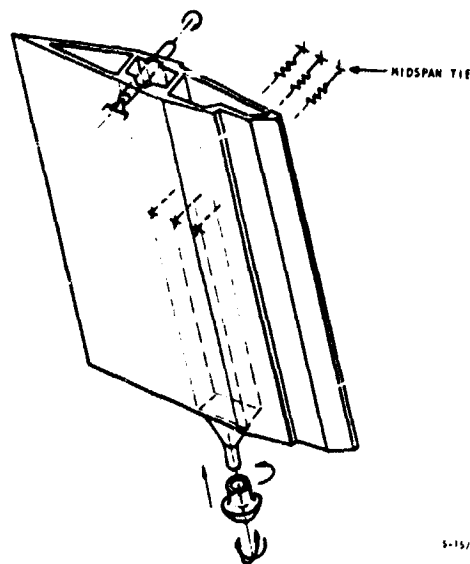
Figure 31.--Finite Element Model of Three-Strut Assembly.

Conclusions: A midspan tie can provide several benefits and is structurally and aerodynamically feasible; however, the resultant complications in coolant flow routing and strut fabrication are substantial. It is also recognized that the data used in establishing the loading condition are uncertain. Means for reducing the thermal loading are being considered as an alternate approach to reduce the combined loading without resorting to a midspan tie.

Side strut structural analysis.--A large 3-dimensional finite element model of the side strut was constructed by NASA using the SPAR computer code. Only the side strut was modeled, as its loading was slightly more critical than the center strut loading and the results would be conservatively representative for the center strut. The model was comprised primarily of triangular and quadrilateral plate elements with both membrane and bending stiffness, and had 2600 unrestrained degrees of freedom.

Initial results, described in ref. 2, are based on the following strut mounting scheme: at the top, a three-point suspension is used in which the leading edge is fixed and the other two points have two degrees of freedom each. The strut is permitted to move chordwise from the leading edge and laterally from one side. At the cowl, the strut is fitted to a slot that permits longitudinal expansion but provides support for side loads. Local stresses developed with this scheme were found to be excessive.

Performance with revised mounting scheme: Boundary conditions were adjusted to permit thermal growth and rotation along the strut main plane; a set of springs was used to represent the midspan tie. These conditions are shown schematically in the sketch below.



9-15/25

The finite element model was constructed on the basis of the following: (1) two main longitudinal webs, 2.79 mm (0.11-in.) thick; (2) uniform thickness sidewalls, 2.03 mm (0.080-in.) thick; and (3) 6.60 mm (0.26 in.) by 28.45 mm (1.12 in.) leading and trailing edge sections.

Pressure loads defined for an unsymmetrical unstart (at Condition G) were applied along with the Condition H thermal loading. It is presumed that the coolant flow is modulated to maintain the coolant outlet temperature at 889°K (1600°R). Hence, the coolant temperature distribution, the primary structure temperature distribution, and the resulting thermal stresses are similar for all operating conditions even through the overall heat input varies.

Results of the computer runs for the pressure loads alone and for the pressure loads combined with the temperature distributions were reviewed and the following conclusions were reached:

- (1) High stresses are mainly due to the pressure loads and are basically local stresses.
- (2) Most of the high stresses are on the outside wall (side facing the sidewall), with some high stresses on the inside wall.
- (3) Use of a midspan tie is essential for the specified loading conditions.

Fig. 32 shows the high stress areas for the pressure only and for the pressure plus temperature cases. The effective (von Mises) stresses are not excessive compared with an allowable stress of 900 MPa (130 ksi) for Inconel 718 material. Design margins may become minimal, however, when dynamic effects such as impulse loading and combustion-induced vibrations are considered.

Figs. 33 and 34 depict deformation maps for several representative locations (leading and trailing edge, top, bottom, and mid-distance) along the strut due to pressure loading. These results indicate that:

- (1) The trailing edge displaces significantly more than the leading edge.
- (2) The overall strut rotates along the axis defined by the two end constraints.
- (3) Although the midspan tie somewhat restrains bowing, there are large local deformations along the strut trailing edge due to bending in a spanwise direction about the midspan tie.
- (4) Strut deformation is not excessive in that it is a transient condition and the strut will not contact the adjacent strut or sidewall.

Bending of the strut in the  $x_1 - x_2$  plane (transverse bending) can be observed by subtracting the strut rotation from the absolute deformation as shown in fig. 34. A straight line connecting the leading and trailing edge nodes represents pure rotation; any deviation from this straight line indicates strut bending in the flow direction.

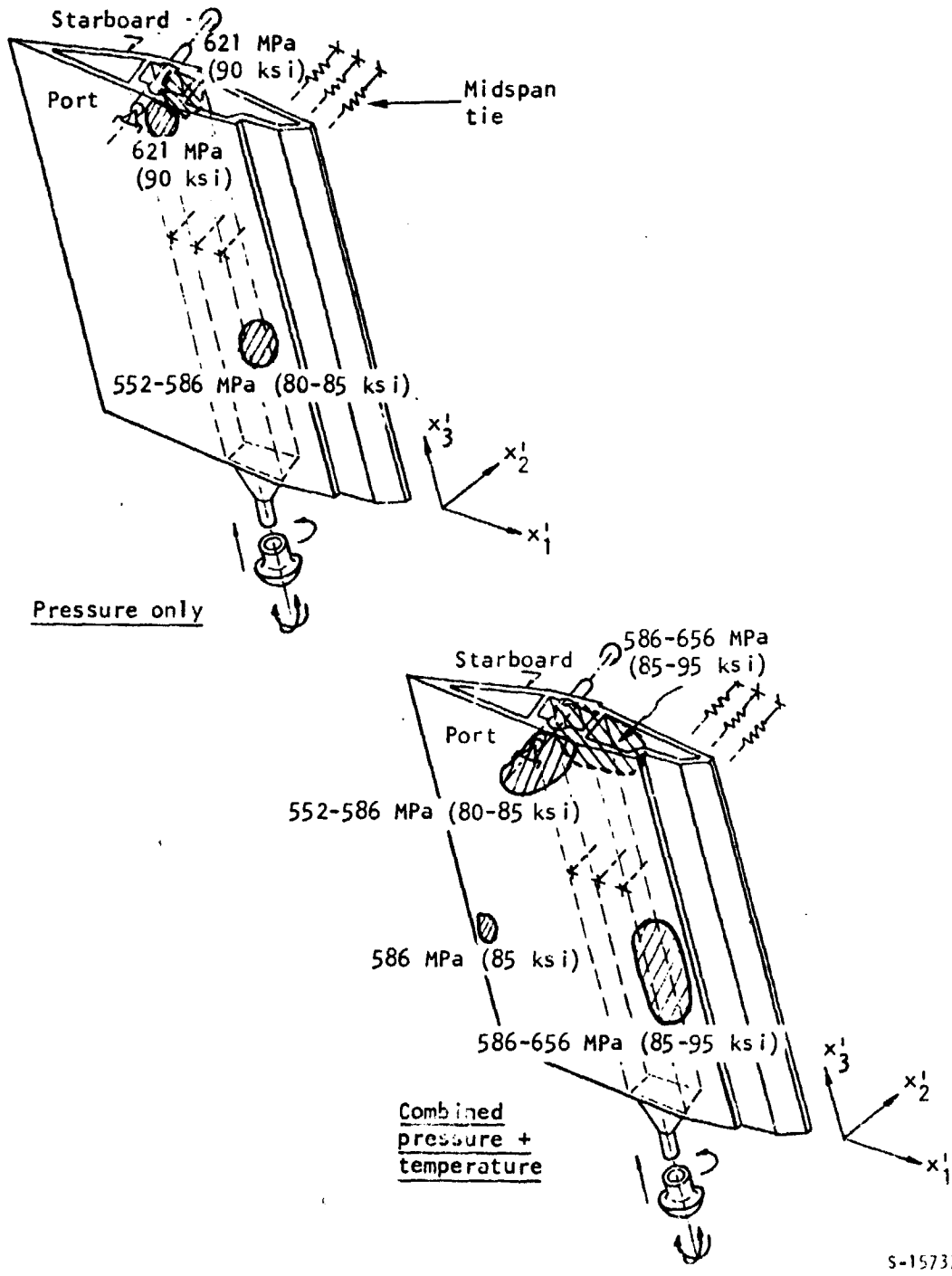


Figure 32.--Effective (von Mises) Stresses--Highly Stressed Areas with Midspan Tie.

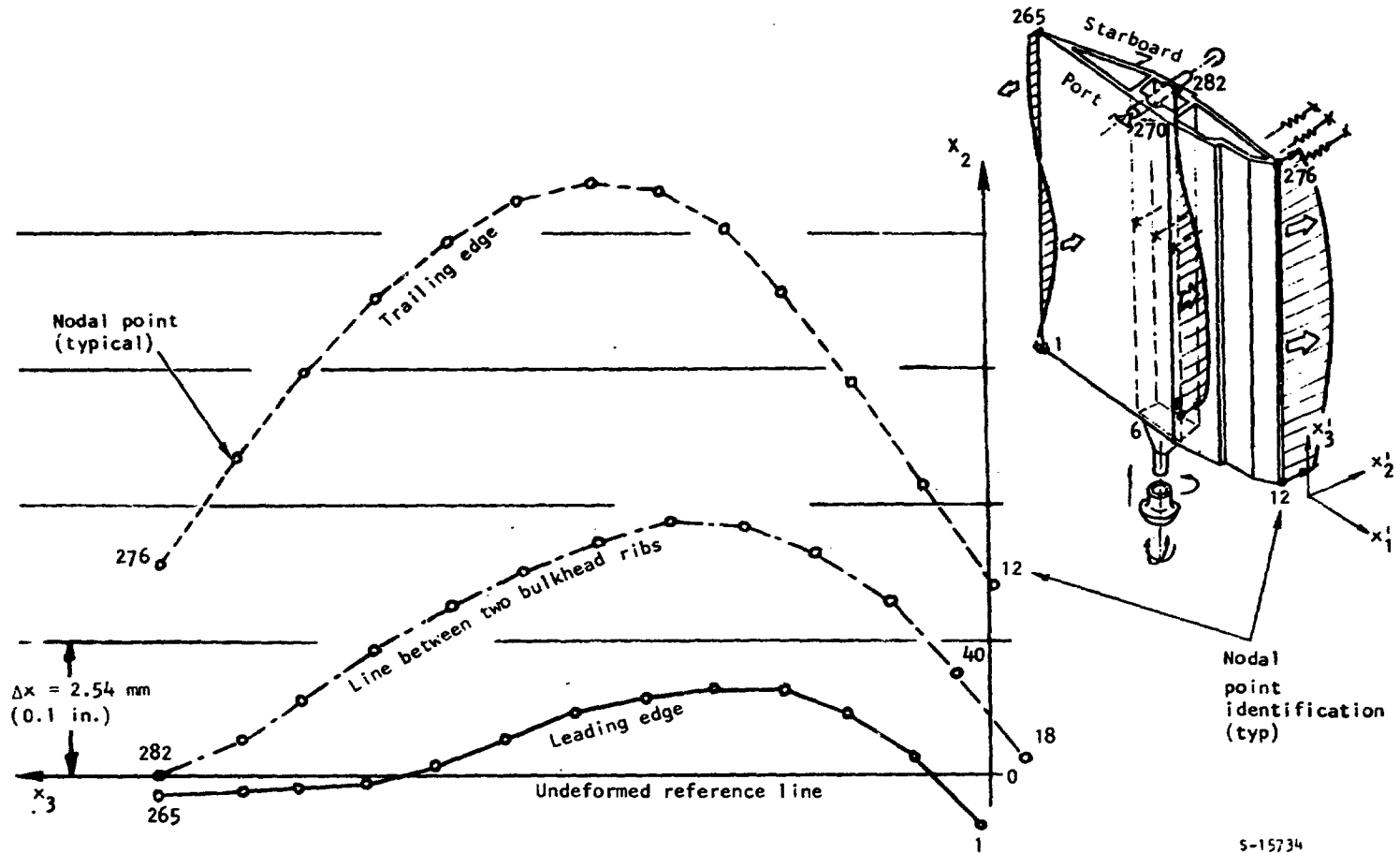
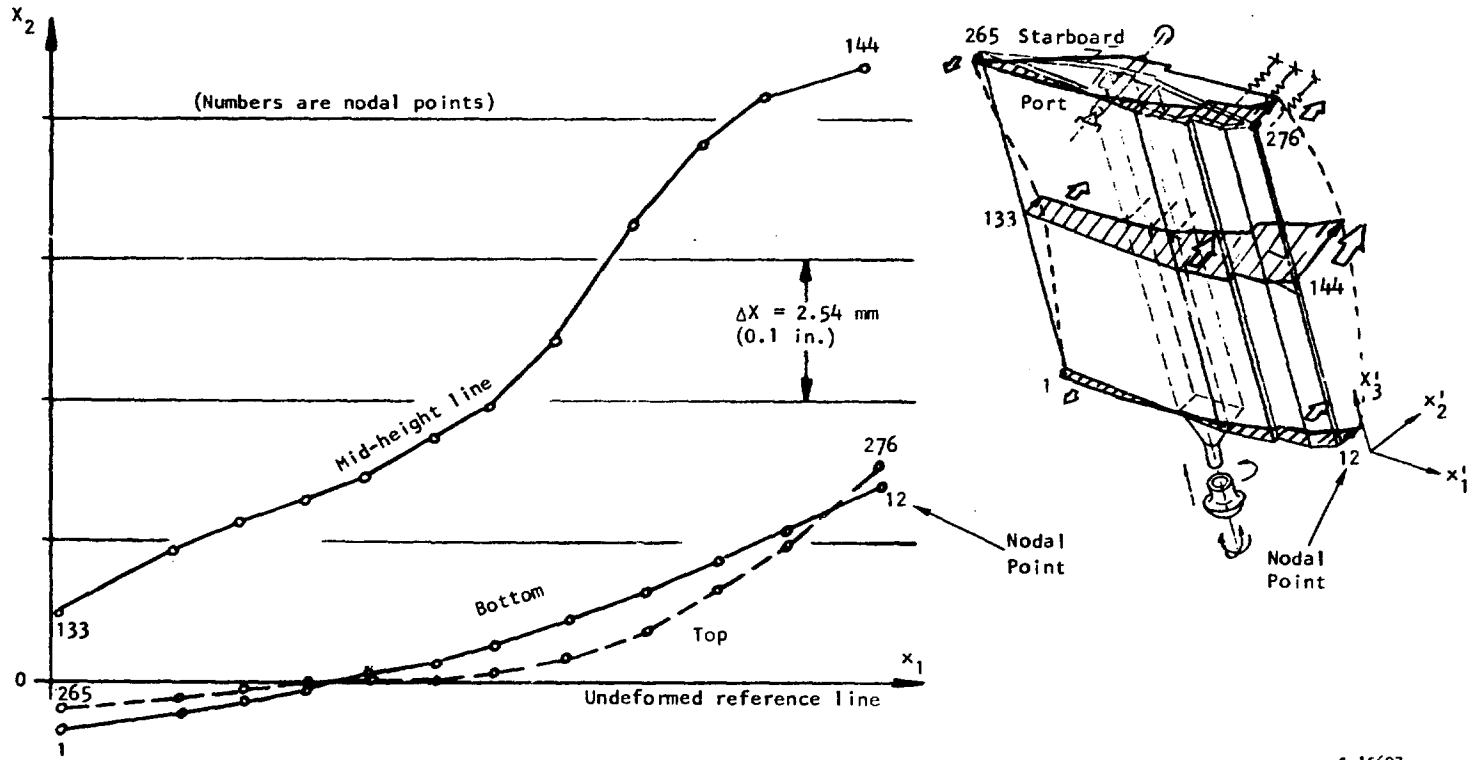


Figure 33.--Absolute Deformation with Midspan Tie, Perpendicular to Flow, Due to Pressure Only.



S-15697

Figure 34.--Absolute Deformation with Midspan Tie, Parallel to Flow, Due to Pressure Only.



Various modifications were considered to limit strut deflection and achieve a corresponding reduction in the primary structure stress level. As a general guideline, it was stipulated that if additional constraints are to be used, they should control pressure-produced displacements without interfering with the temperature displacements.

Fig. 35 illustrates a modified configuration. Two pins are placed on the end plates near the trailing edge. These pins will engage slots or holes on the supporting structure, which will limit the overall strut rotation without adding restraints to the thermal deformation. Four additional longitudinal ribs, 3 to 3.6 mm (0.12 to 0.14 in.) thick, are specified to control spanwise bowing. Transverse bending would be controlled by adding three transverse ribs, 3 to 3.8 mm (0.12 to 0.15 in.) thick. This configuration will reduce the absolute deformations below 3 to 3.3 mm (0.12 to 0.13 in.) and reduce the maximum effective stresses by 103 to 207 MPa (15 to 30 ksi). The primary structure stress level is then well within the capabilities of Inconel 718 material, including an allowance for dynamic loading.

Performance with increased cooling: The coolant outlet temperature was reduced to 417°K (750°R) from 889°K (1600°R), which results in increasing the TPS coolant flow by a factor of 2. The increased flow at Condition G is then about equal to the maximum coolant flow at Condition H with a 889°K (1600°R) coolant outlet temperature. The overall engine coolant  $\phi$  at Condition G is increased by about 20 percent. This is considered a reasonable trade if the strut midspan tie can be eliminated.

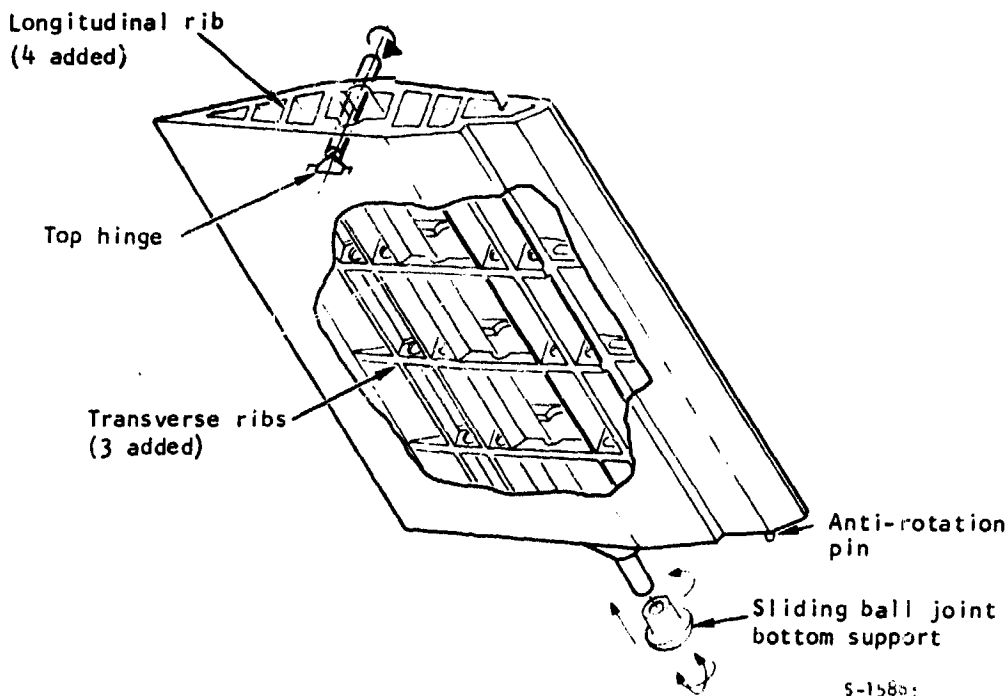


Figure 35.--Modified Strut Structural Design with Midspan Tie.

The primary structure was modified to the configuration shown in fig. 36. The primary structure included three spanwise ribs, 2.5 mm (0.100 in.) thick, to resist bending. These ribs also act as bulkheads between the coolant and fuel flow passages. Seven thin ribs, 0.3 mm (0.012 in.) thick, take tensile loads only and are used to react the internal hydrogen pressure. The thin ribs can be perforated to facilitate communication between compartments. (Analysis of this configuration is continuing and results will be presented in the final report.)

### Primary Structure

Three-dimensional finite element models.--The original reference design primary structure used a combination of beam and honeycomb to contain the high-pressure airflow. The concept, shown in fig. 37, included seven beams located parallel to the engine sweep line. Details shown in fig. 37 include the clip concept used to secure the beams to the honeycomb (the clip concept is discussed in ref. 6).

Two other structural concepts were considered in this study. The first is similar to the reference design except that the beams are oriented vertically (normal to the airflow). The second is an all-honeycomb design in which the beams were eliminated in favor of a thicker honeycomb structure.

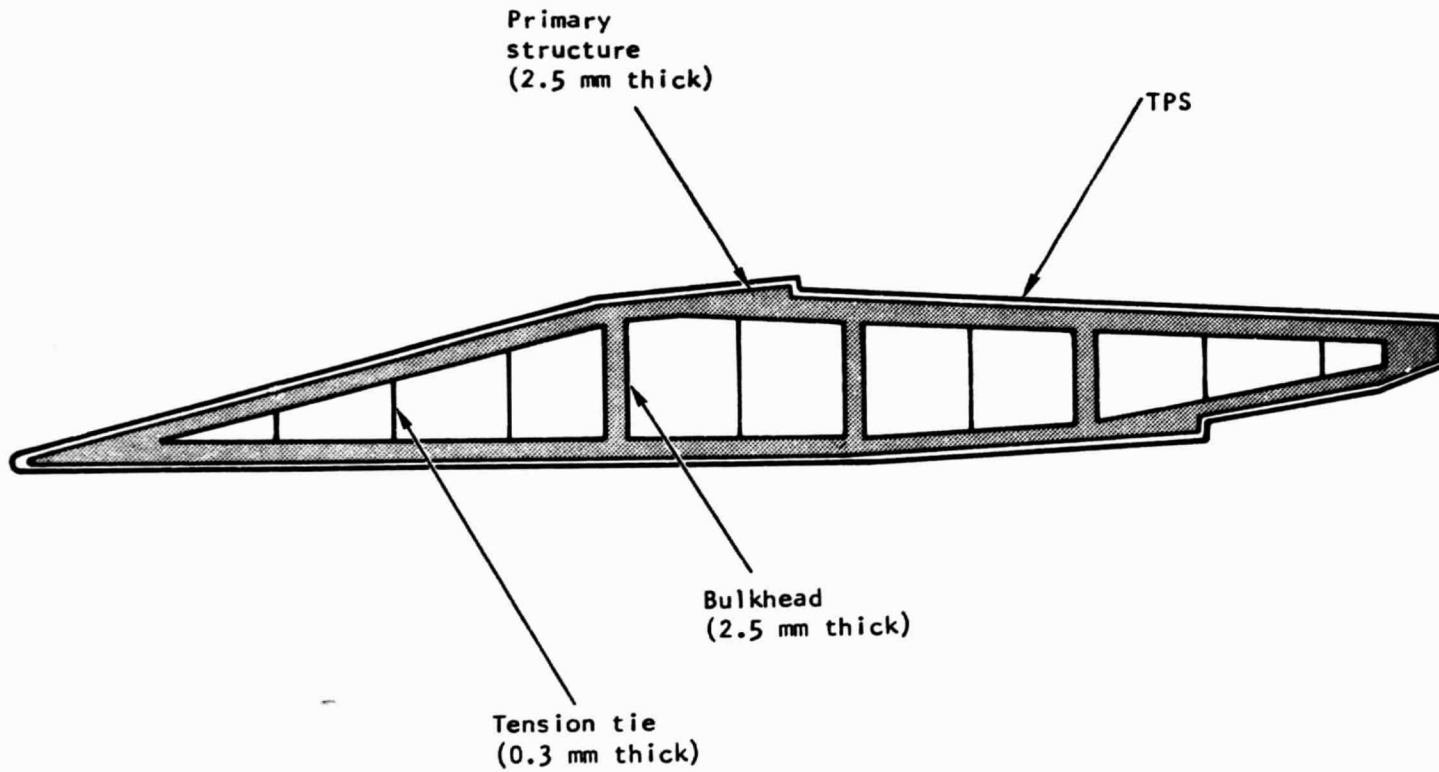
Each of the three structures was analyzed using a large finite element model. Primary structure elements, which include the honeycomb, facesheets, clips, beams, and manifolds, are represented in the finite element models. The contribution of the TPS was neglected. The following elements are typical for all structures:

Honeycomb hot face sheet	1.5 mm (0.060 in.) thick
Honeycomb cold face sheet	1.3 mm (0.050 in.) thick
Honeycomb cell	6.4 mm (0.25 in.) hexagon, 0.08 mm (0.003 in.) gauge

Panel support beams are I-shaped and are mechanically joined to the attachment clips. Two vertical beams, located at the module mount locations, are retained in the all-honeycomb concept to help distribute the inertial loads. The beam-to-beam connections are rigidly joined and, in the combustor area, the beams form a continuous frame. In the swept and vertical beam models, the panels are permitted to move with respect to the adjacent panel. Thus, gaps or interferences can occur at the sidewall-to-topwall or sidewall-to-cowl intersections. The panels may also deflect with respect to the adjacent panel in the axial direction.

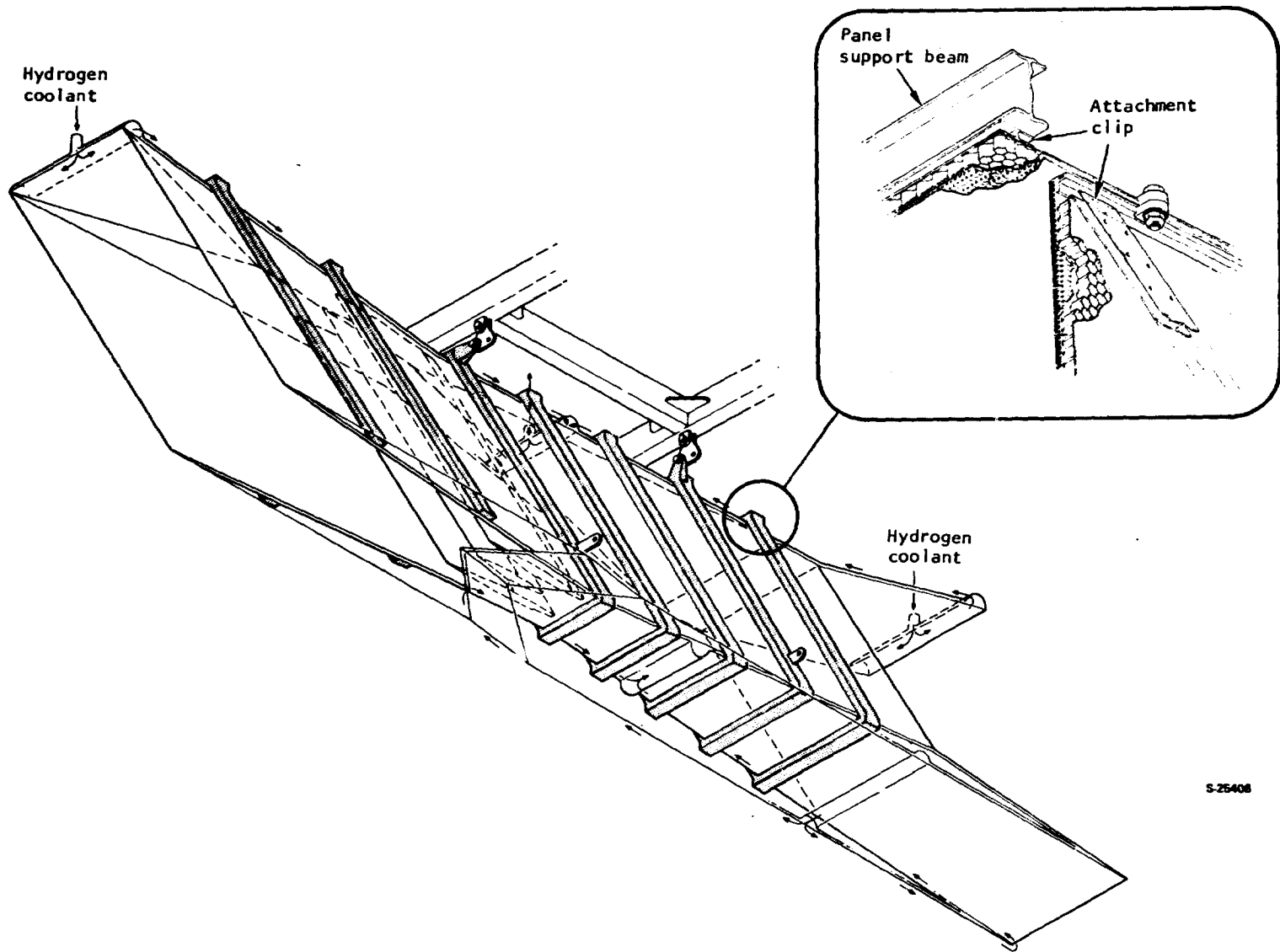
In addition to the panel support beams, other structural elements that act as stiffening members are as follows:

- (a) Coolant inlet and outlet manifolds



S-25062

Figure 36.--Side Strut Structure for Increased-Cooling Analysis.



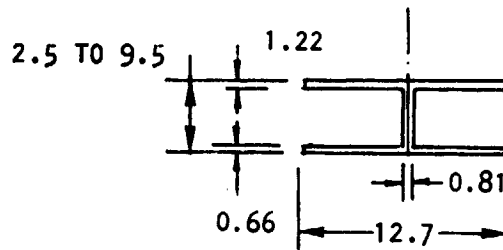
S-25408

Figure 37.--Primary Support Structure for Swept Beam Model.

- (b) Leading and trailing edge structures that also incorporate coolant manifolds
- (c) Bottom surface of the cantilevered sidewalls (engine inlet)
- (d) Sidewall panel edges--panel-to-panel seal support structure in the swept and vertical beam models
- (e) Struts

Each of these elements was represented in the model as an equivalent cross-sectional area and moment of inertia.

The attachment clips are wide flanged beams brazed either to the TPS or to the sandwich panel that supports the TPS. Structural width of each particular clip is constant, but the depth varies from 2.5 to 9.5 mm (0.1 to 0.375 in.) depending on the location. The clips transmit pressure loads to the support beams and frames. Elongated bolt holes are provided in the clip flange to accommodate relative motion between the clip and beam to reduce thermal stresses. Clip geometry used in the analysis is shown below.



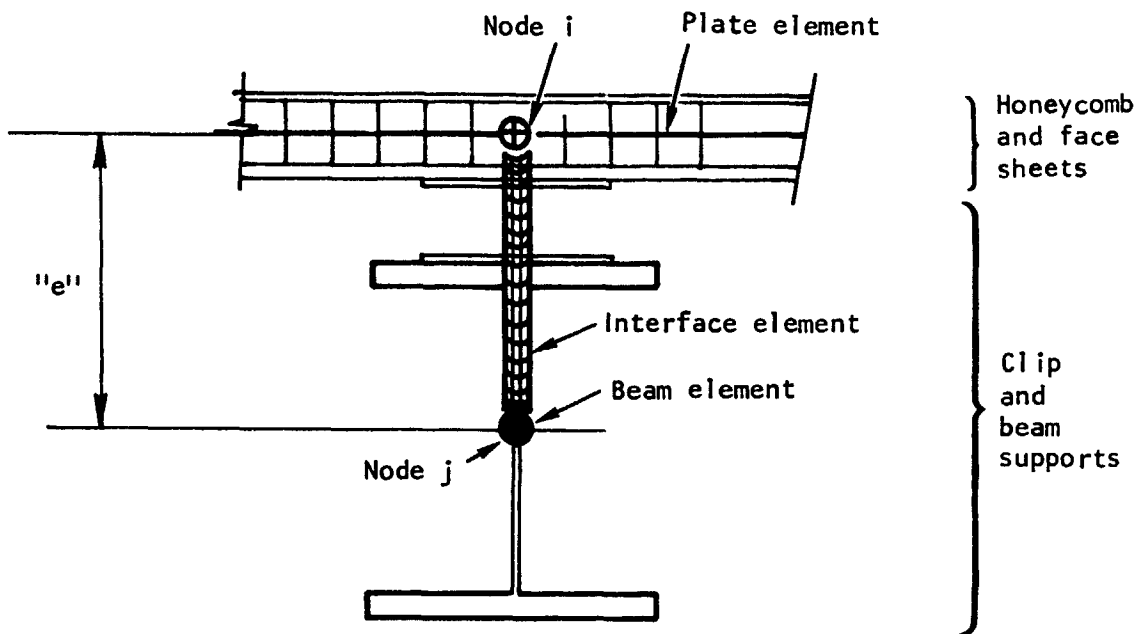
S-15803

(DIMENSIONS IN MM)

Slip between the beam and clip and the eccentricity between the beam and honeycomb structure centroids are represented by an interface element as shown in fig. 38. Slip is represented by stipulating a low coefficient of friction in the interface element along the longitudinal beam axis.

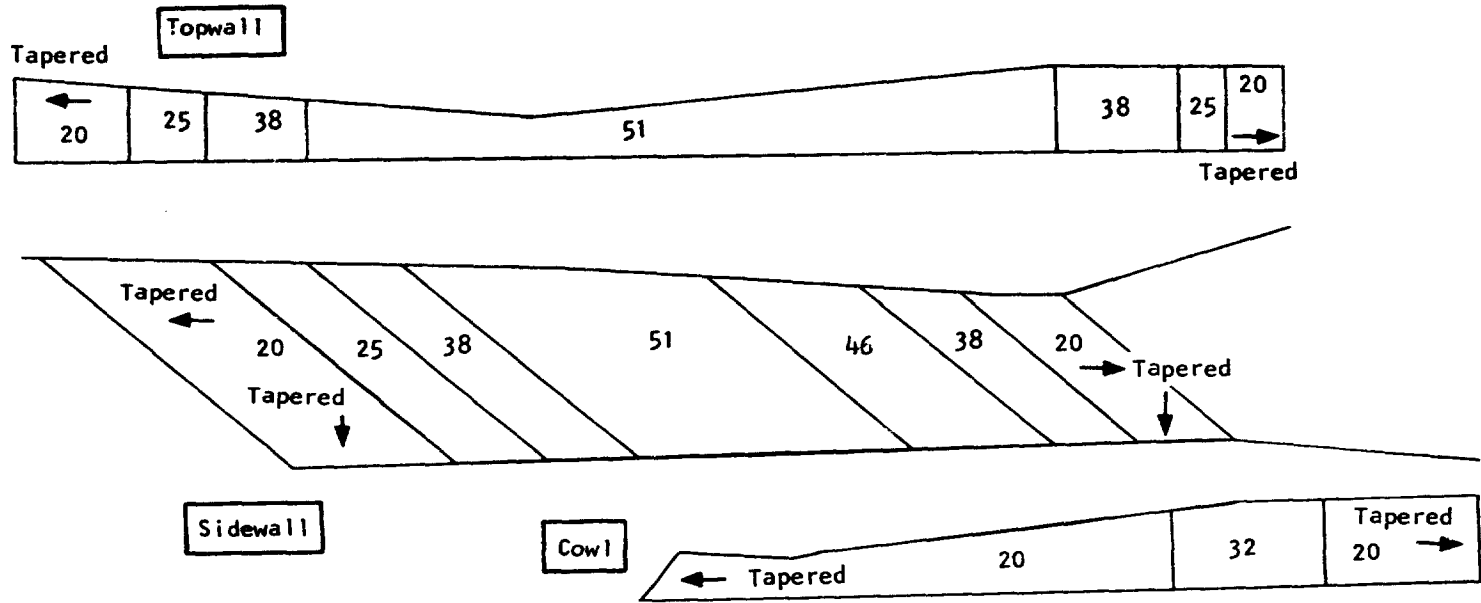
A constant 9.5-mm (3/8-in.)-thickness honeycomb is used for all panels in the swept and vertical beam model except for the external cowl and sidewall panel, which are 6.4-mm (1/4-in.) thick. Distribution of honeycomb thickness for the all-honeycomb model is defined in fig. 39. For the all-honeycomb model, it was assumed that the panel-to-panel intersections are rigidly connected and that there is a continuous honeycomb structure around the corner.

Initial computer runs indicated an excessive deflection in the nozzle area, and hence, additional beams oriented along the main engine axis were placed along the topwall edges for reinforcement.



S-15805

Figure 38.--Plate-Beam Element Sliding Connection Simulation.



(dimensions in mm)

S-24833

Figure 39.--Honeycomb Thickness Variation (All-Honeycomb Model).

Each fuel injection strut was represented by a single sheet of elements of equivalent stiffness. A midspan tie was included.

Two materials were used throughout the structure: Inconel 718 for the panel support beams and Hastelloy X for all other engine structure. The honeycomb panel weight for inertial load calculations was approximated by using an equivalent density. The modulus of elasticity and thermal expansion coefficient were used as functions of temperature. Other mechanical properties such as Poisson's ratio and density were assumed constant because their influence is minor. The friction coefficient was held constant because reliable data describing this as a function of temperature are not available.

Model geometry: Finite element models for the three structural concepts are shown in fig. 40. One-half of an engine module is represented; the plane of symmetry is vertical and passes through the center strut and cowl apex. Model statistics are as follows:

	Swept Beam	Vertical Beam	Honeycomb
Three-dimensional beam elements	416	398	155
Flat elastic shell elements	424	424	424
Total elements	840	822	579
Degrees of freedom	4146	4794	4710

The panel support beams are readily apparent because they are separate elements and an interface element exists between the clip and beam.

Loads: Maximum thermal (Condition H) and maximum pressure (unstart at Condition G) loads were applied to the structural models. The Condition H isotherms were used in both cases. The cumulative heat load does change between the G and H conditions but the general heat flux distribution remains constant as do the coolant inlet and outlet temperatures. Hence, the temperature gradients remain similar.

Panel performance: Computer results are summarized for the sidewall, top-wall, and cowl in figs. 41, 42, and 43, respectively. Plots of displacements and isostress lines are shown for the honeycomb structure at the maximum pressure loading conditions. Generally, the honeycomb structure deflects less than the beam models under maximum pressure loading. The plots are similar for all structures.

The term "comparative" stress is used in the tabular data because the computer model uses a single element to represent the honeycomb primary structure. The element correctly represents the stiffness of the actual panel, and thus the computed deflections are valid while the computed stresses are somewhat fictitious. The maximum stress usually occurs in the outermost



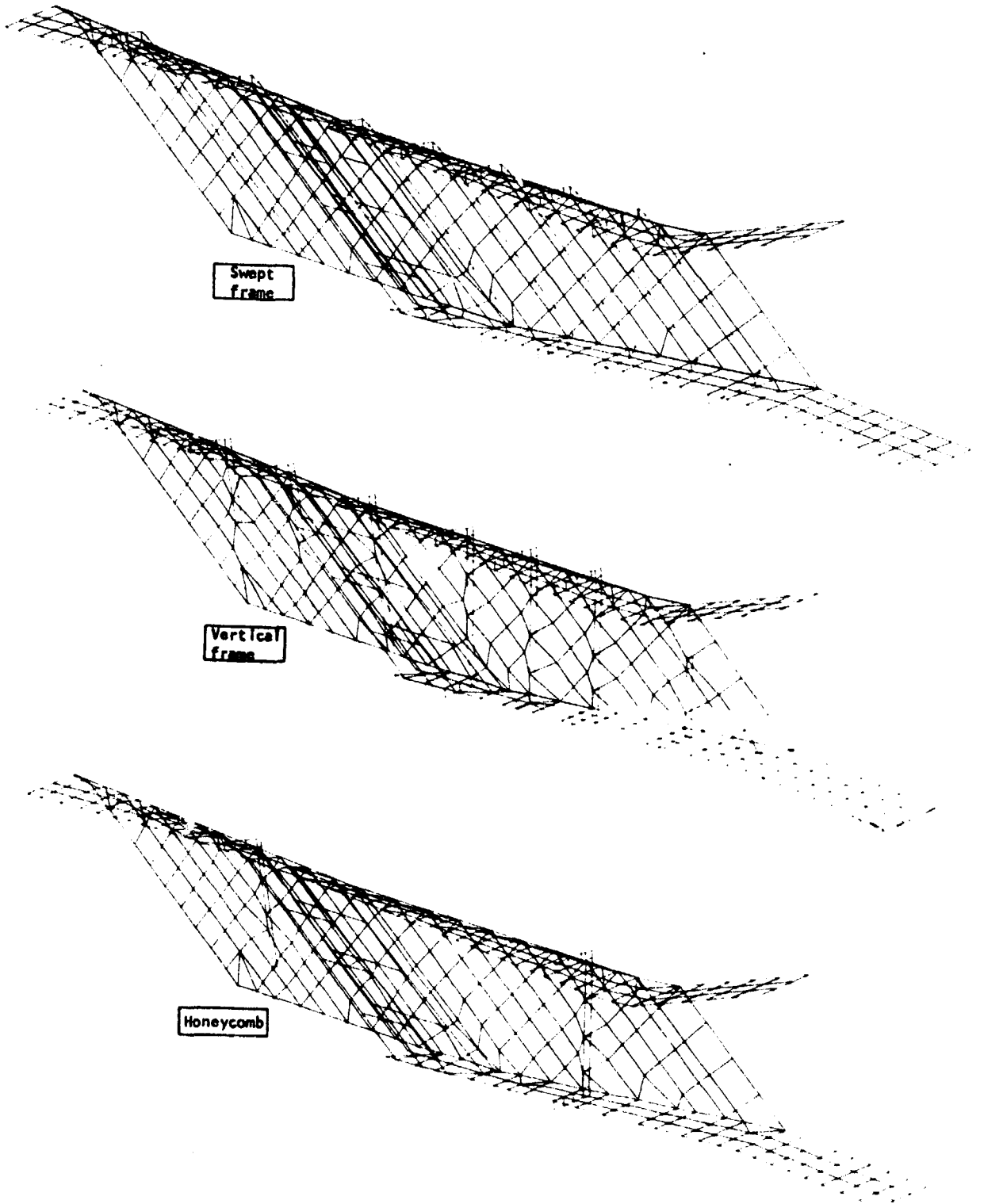
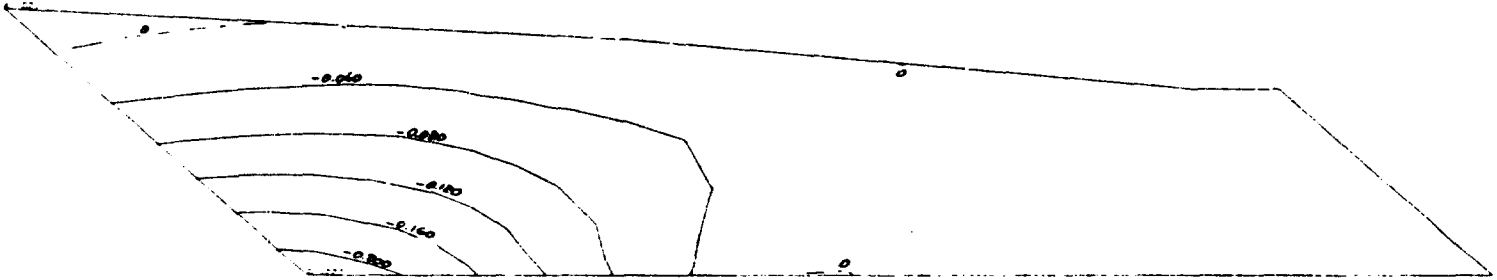


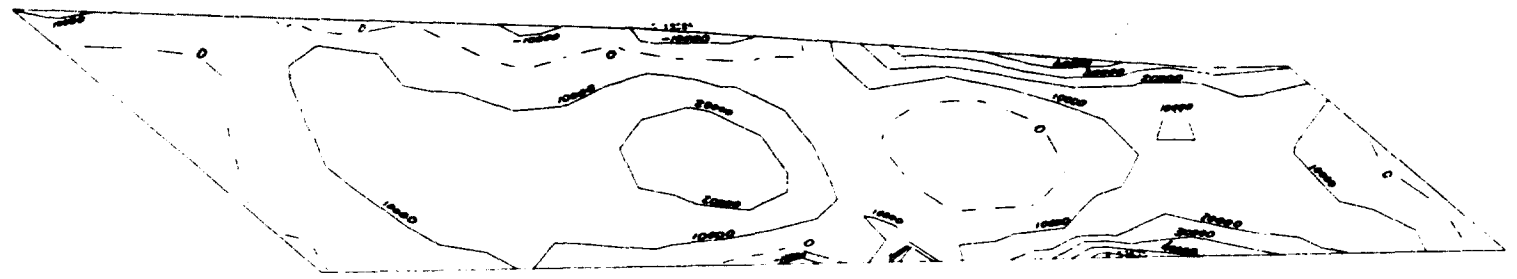
Figure 40.--Finite Element Models.

S-24844

**Displacements**



**Isostress**



16

Structure	Maximum thermal load		Maximum pressure load	
	Displacement, mm (in.)	Comparative stress MPa, (ksi)	Displacement, mm (in.)	Comparative stress MPa, (ksi)
Swept beam	5.1 (.20)	496 (72)	55 (2.29)	469 (68)
Vertical beam	3.3 (.13)	414 (60)	27 (1.08)	593 (86)
Honeycomb (shown)	0.5 (.02)	248 (36)	5.8 (0.23)	400 (58)

S-25474

Figure 41.--Sidewall Performance.

**Displacements**



**Isostress**



92

*CL*

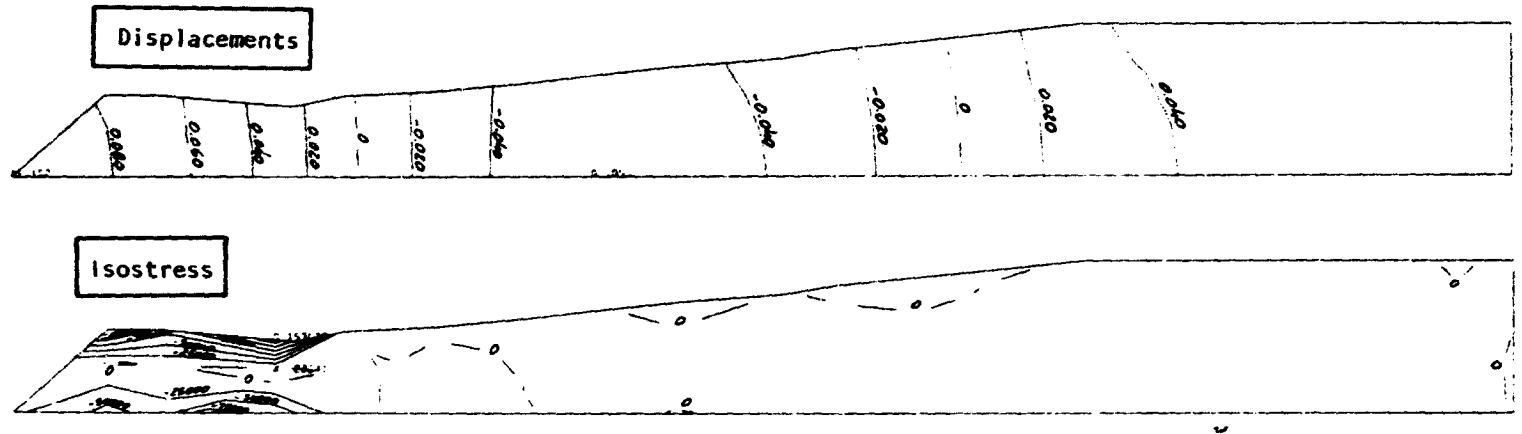
Structure	Maximum thermal load		Maximum pressure load	
	Displacement, mm (in.)	Comparative stress, MPa (ksi)	Displacement, mm (in.)	Comparative stress, MPa (ksi)
Swept beam	6.1 (.24)	207 (30)	24.4 (.96)	758 (110)
Vertical beam	2.5 (.10)	255 (37)	3.8 (.15)	979 (142)
Honeycomb (shown)	3.0 (.12)	441 (64)	4.6 (.18)	607 (88)

ORIGINAL PAGE IS  
LOW RESOLUTION COPY

100

5-25386

Figure 42.--Topwall Performance.



Structure	Maximum thermal load		Maximum pressure load	
	Displacement, mm (in.)	Comparative stress, MPa (ksi)	Displacement, mm (in.)	Comparative stress, MPa (ksi)
Swept beam	2.0 (.08)	724 (105)	2.5 (.10)	1090 (158)
Vertical beam	1.0 (.04)	634 (92)	1.0 (.04)	607 (88)
Honeycomb (shown)	1.0 (.04)	1160 (168)	1.0 (.04)	1150 (167)

S-25475

Figure 43.--Cowl Performance.

cold face-sheet. The computed stresses are representative of the structure but a detailed analysis would be required to establish the actual values.

The distorted geometry for the sidewall is shown in fig. 44. Results are shown for the honeycomb structure, which is typical. The S-shape is a direct result of the applied temperature gradient--cold leading and trailing edges with a hot central portion. The major portion of the growth, about 2.5 mm (0.1 in.), is attributed to just the thermal growth. The topwall and cowl surfaces follow the sidewall S-shape.

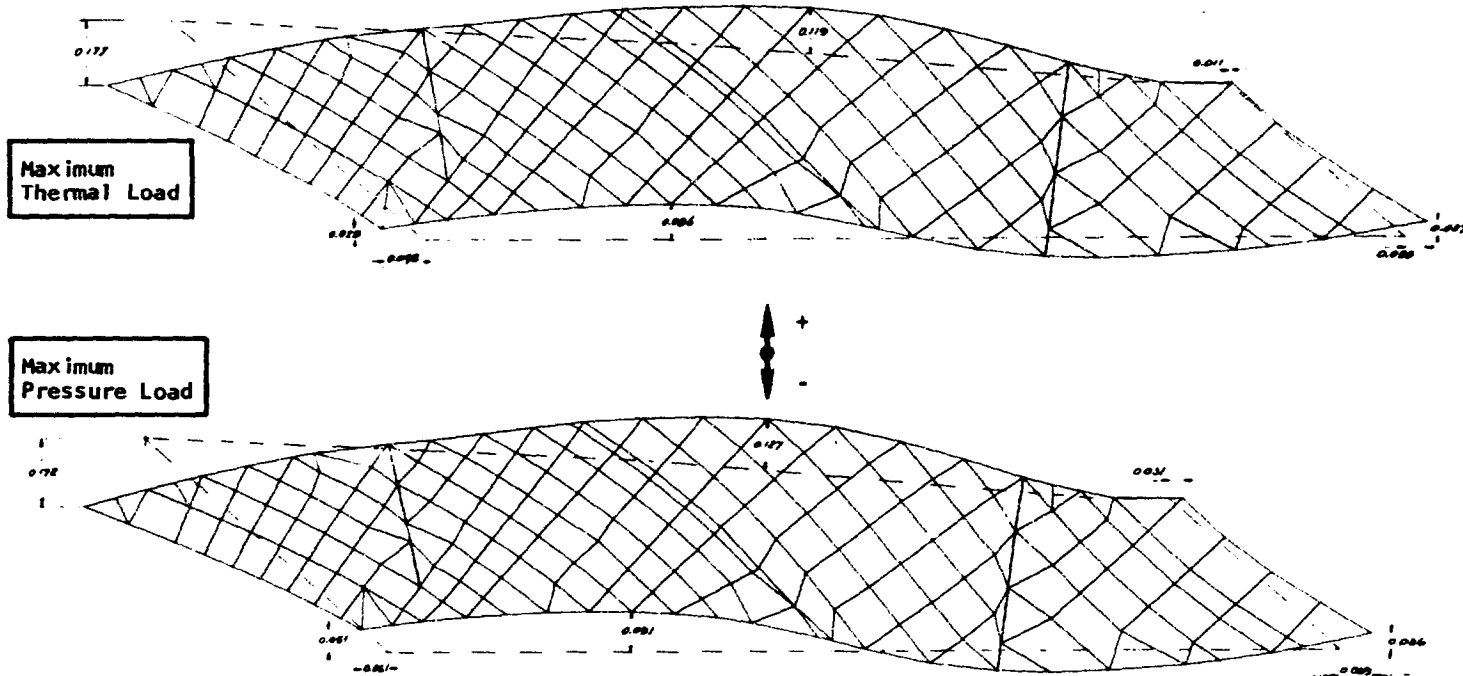
It was found that the sidewall leading edge bends forward, and in some cases exceeds the 0.4-deg angle change limit; however, an angular deviation of the leading edge is not critical. The deviation limit is of concern mainly with respect to the internal flow contours.

Nozzle performance: Data are presented in fig. 45. The displacements are reasonable and the change in flow area is within specified limits for all configurations. The displacements are strongly influenced by the sidewall distortion. In an actual aircraft application, the topwall vertical displacement would be limited by the installation. Hence, the 1.1-deg topwall angle change for the vertical beam model would be less. The honeycomb configuration is best in terms of minimum flow area change.

Corner displacements: Relative motion between panels is summarized in Table 12. Displacements are similar for both swept and vertical beam models and are generally small except for a few areas. It appears that the panel corners could also be rigidly joined in the beam models, thus permitting the use of a simple static seal or even a welded corner design. There are no gaps in the honeycomb design because the corners are modeled as a continuous joint and no gaps are permitted.

Weight comparison: Estimated weights were determined for each structural design using layout drawings as a basis. The weights are consistent with the dimensions of the individual parts used in the finite element analysis. Results are listed in Table 13 for a six-module cluster. The honeycomb design is the least weight. The weight differences are not considered especially significant at the current level of detail design.

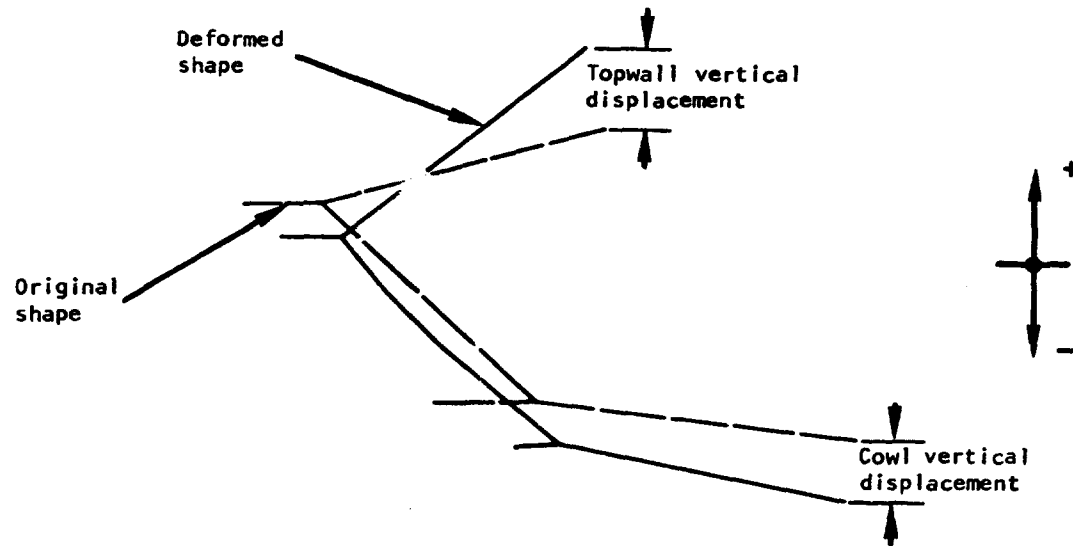
Design selection.--The honeycomb configuration is selected as the best design primarily because (1) it exhibits the least deflection in the sidewall and nozzle areas--an order of magnitude lower than the beam models; (2) it is the least complex structure--minimum beams and clips; and (3) it weighs less than the beam models. A reduced number of beams is desirable because the beams do act as a restraint to thermal growth and thereby increase thermal stresses. Layout design will be required to define means to carry loads around the corners (panel-to-panel) and across the manifold, and to alleviate locally high stresses.



Structure	Vertical displacement, mm (in.) (maximum pressure load)						
	Leading edge top	Leading edge bottom	Mid-topwall	Mid-cowl	Trailing edge top	Trailing edge bottom	Leading edge angular change, degrees
Swept beam	+0.13 (+.005)	+7.62 (+.300)	+2.79 (+.110)	0 (0)	-2.34 (-.092)	-2.74 (-.108)	0.54
Vertical beam	-3.91 (-.154)	+3.71 (+.146)	+3.81 (+.150)	+4.17 (+.164)	0 (0)	+0.13 (+.005)	0.40
Honeycomb (shown)	-4.37 (-.172)	+1.30 (+.051)	+3.22 (+.127)	+2.31 (+.091)	0 (0)	+0.91 (+.036)	0.45

S-25414

Figure 44.--Sidewall Distorted Geometry.



Structure	Maximum thermal load			Maximum pressure load		
	Topwall vertical disp, mm (in.)	Cowl vertical disp, mm (in.)	$\Delta$ flow area, %	Topwall vertical disp, mm (in.)	Cowl vertical disp, mm (in.)	$\Delta$ flow area, %
Swept beam	+7.6 (.30)	-5.8 (.23)	2.6	+1.3 (.05)	-5.1 (.20)	1.2
Vertical beam	+9.7 (.38)*	-3.6 (.14)	2.5	+4.6 (.18)	-2.5 (.10)	1.4
Honeycomb	+0.5 (.02)	-0.5 (.02)	0.2	+1.5 (.06)	+1.0 (.04)	0.1

\*Angle change =  $1.1^\circ$

S-25478

Figure 45.-- Nozzle Deformation.

TABLE 12.--CORNER DISPLACEMENTS

Panel	Station	Corner Relative Displacement, mm (in.)	
		Maximum Thermal Load (Condition H)	Maximum Pressure Load (Unstart)
Topwall	11.0	0.56 (.022)	1.30 (.051)
	17.3	0.41 (.016)	0.48 (.019)
	29.1	0.28 (.011)	0.69 (.027)
	37.0	0.48 (.019)	2.74 (.108)
	40.9	0.30 (.012)	2.34 (.092)
	49.1	1.04 (.041)	1.83 (.072)
	53.4	1.04 (.041)	1.45 (.057)
	61.7	0.20 (.008)	0.36 (.014)
	70.0	0.08 (.003)	0.18 (.007)
Cowl	80.8	0.43 (.017)	0.58 (.023)
	62.5	0.58 (.023)	0.18 (.007)
	70.0	0.28 (.011)	0.41 (.016)
	81.1	0.20 (.008)	0.58 (.023)
	92.3	0.05 (.002)	0.08 (.003)

TABLE 13.--WEIGHT COMPARISON

6-Module Engine [36.6 x 45.7 cm (14.4 x 18 in.) Capture Area]

Structure Element	Weight, kg (lb)		
	Swept Beam	Vertical Beam	Honeycomb
TPS	408 (900)	408 (900)	408 (900)
Honeycomb Core	42 ( 93)	42 ( 93)	114 (251)
Cold Face Sheet	209 (460)	209 (460)	209 (460)
Beams and Clips	146 (322)	133 (294)	27 ( 59)
Manifolds	143 (315)	143 (315)	143 (315)
Leading and Trailing Edges	85 (188)	85 (188)	85 (188)
Struts (3)	166 (366)	166 (366)	166 (366)
Braze Alloy	25 ( 56)	25 ( 56)	25 ( 56)
Weld and Misc.	95 (209)	94 (207)	93 (205)
Total Weight	1319 (2909)	1305 (2879)	1270 (2800)



External cowl panel.--The bottom (external) surface of the engine cowl is a cooled structure supported by a honeycomb primary structure, which is tied to the engine sidewalls through flexures. A V-shaped coolant inlet manifold is incorporated in the structure.

The loads acting on this component consist of external aerodynamic pressure, inertia, and thermal loads due to a temperature gradient along the assembly. The net pressure acting on the cowl surface is approximated by assuming that the pressure in the cowl cavity is equal to the freestream static pressure. The following net pressure loads were determined.

	External pressure,		Internal pressure,		Net pressure load,	
	kPa	(psia)	kPa	(psia)	kPa	(psi)
Condition G	10.8	(1.57)	3.9	(0.57)	6.9	(1.00)
Condition H	7.1	(1.04)	1.0	(0.15)	6.1	(0.89)

Thermal analysis indicates that the temperature of the airflow-exposed surfaces will vary between 222° to 389°K (400° to 700°R) and the back side will be approximately 111°K (200°R) cooler.

The inplane temperature gradients are low and thermal stresses due to either the 111°K (200°R)  $\Delta T$  between the hot and cold skin or the cowl in-plane temperature distribution will remain below the elastic limit of the material. Inertial loads were found to be negligible.

Thermal transient analysis.--During an off-design transient condition, e.g., at engine ignition, the temperature gradients developed in the structure can become controlling with regard to structural design. An analysis was performed, therefore, to assess the magnitude of the transient temperature gradients and their effect on the selected design concepts.

A typical structure, shown in fig. 46, was subjected to a two-dimensional nodal point thermal transient analysis. The beam material was Inconel 718. The honeycomb and TPS were either Hastelloy X or Nickel-200. The network forcing function was a time-varying coolant convective heat transfer coefficient and TPS metal temperature. Conditions near the coolant outlet manifold were specified because the metal temperatures reach a maximum here.

The primary source of heating is aerodynamic heating, which will almost entirely be absorbed by the TPS coolant, which in turn will dissipate to the structure during transients. The time constant of the TPS and the adjacent 1.5-mm (0.060-in.)-thick plate is a few seconds so that these parts will essentially track the coolant temperature.

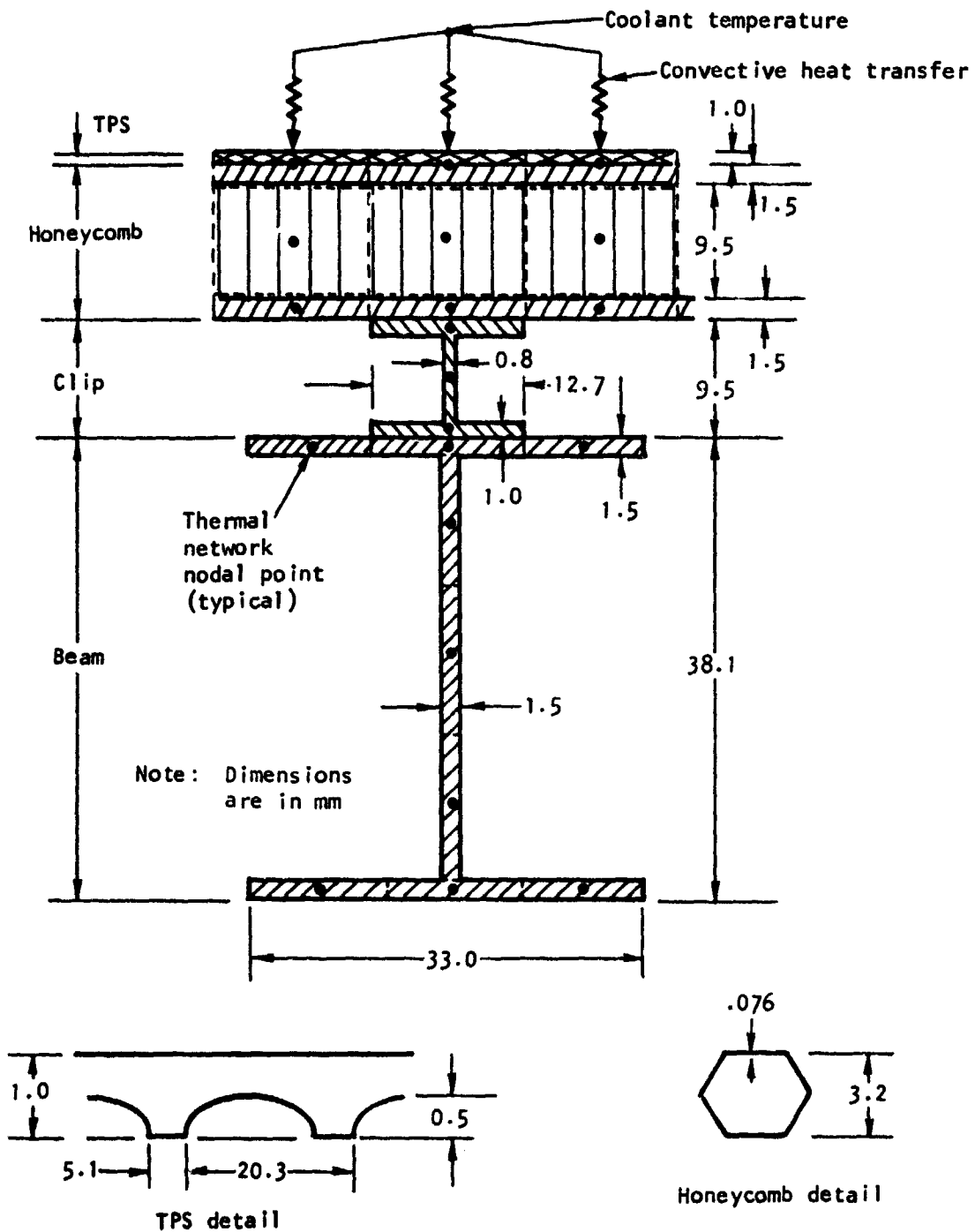


Figure 46.--Model for Transient Temperature Analysis.

A mission profile typical for a research airplane was used and is shown in fig. 47. An estimate of the coolant temperature is shown in fig. 48. The engine is uncooled below Mach 3 and the effective temperature is equal to the freestream recovery temperature. At 75 sec, the coolant flow begins and the engine is initially over-cooled. The coolant flow and temperature gradually increases as the airplane accelerates. Combustion occurs at 120 sec, at which point the coolant has reached a maximum design condition of 889°K (1600°R). At this same instant, the coolant flow is doubled because the heat load with combustion is about twice the unlit value. The inverse of these operations occurs during deceleration.

Structural temperature response is shown in fig. 49 for a Hastelloy X structure. The TPS temperature essentially tracks the local coolant temperature. At the midbeam position the response is slow compared with the TPS; the maximum temperature rise for the 300-second mission is 88°C (190°F). The maximum honeycomb  $\Delta T$  is 500°K (900°R) for Hastelloy X and 378°K (680°R) for nickel. Both of these high-temperature gradients occur just at the onset of combustion when the TPS prime structure is at 889°K (1600°R) and the honeycomb cold side is just beginning to respond.

As indicated, the midbeam temperature is unresponsive to the several operations of this mission. When accelerating to Mach 6 and maintaining a long cruise at this speed, the midbeam will take approximately 0.5 to 1 hr to reach steady state at a value near the local coolant temperature. Conversely, the opposite effect will occur on a deceleration from a long-duration Mach 6 cruise. The midbeam temperature will take approximately 0.5 to 1 hr to cool to ambient conditions.

Because the midbeam response is slow, the temperature difference from top surface midbeam to sidewall midbeam and from sidewall midbeam to cowl midbeam at a particular cross section should be small (less than 111°K (200°R)). It is concluded, therefore, that sliding beam-to-beam connections are not required because the differential thermal growth between beams will not be excessive. A rigid joint can be made between beams and the resultant stresses can be held within the elastic limit.

Honeycomb behavior.--As noted above, a high temperature gradient can be developed across the honeycomb primary structure during a thermal transient and this will produce a high stress. Estimated temperature gradients in the honeycomb panel are shown in fig. 50. Maximum temperature differential across the panel is 514°R (925°R) and occurs at 125 seconds. Panel temperatures across the width are assumed constant.

Additional thermal transient analyses are currently being performed. The high  $\Delta T$  across the honeycomb could produce a primary structure stress above the elastic limit. This is not desirable and would require special consideration to assure acceptability with respect to the overall design criteria.

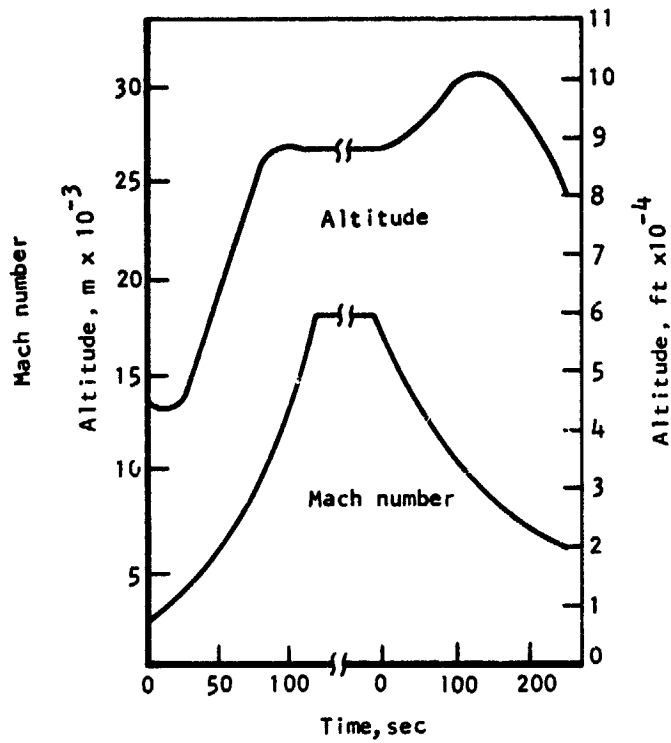


Figure 47.--Mission Profile.

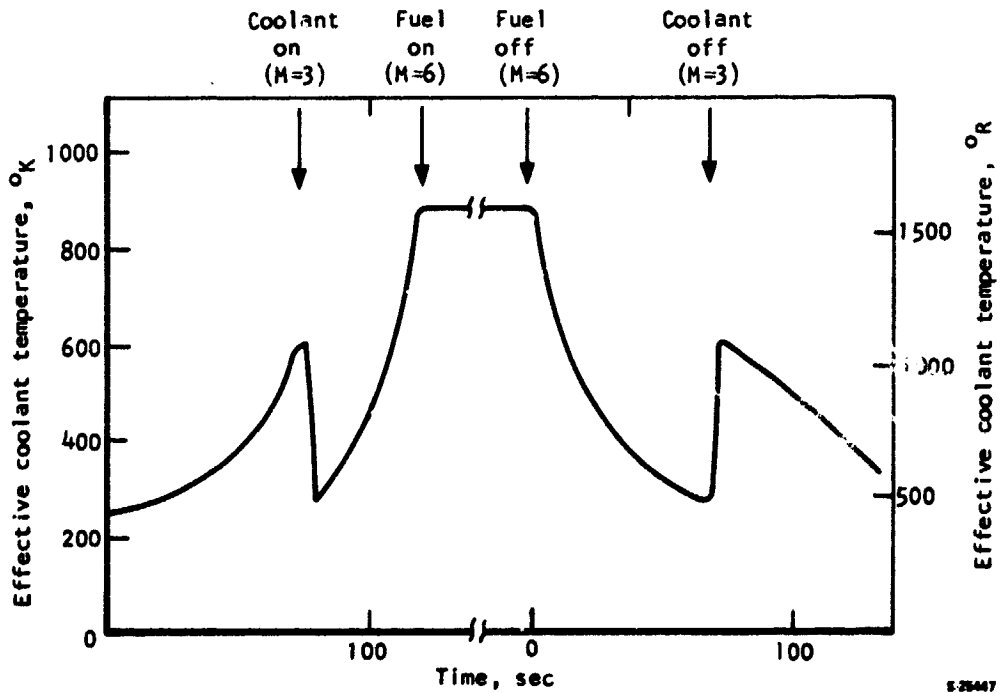
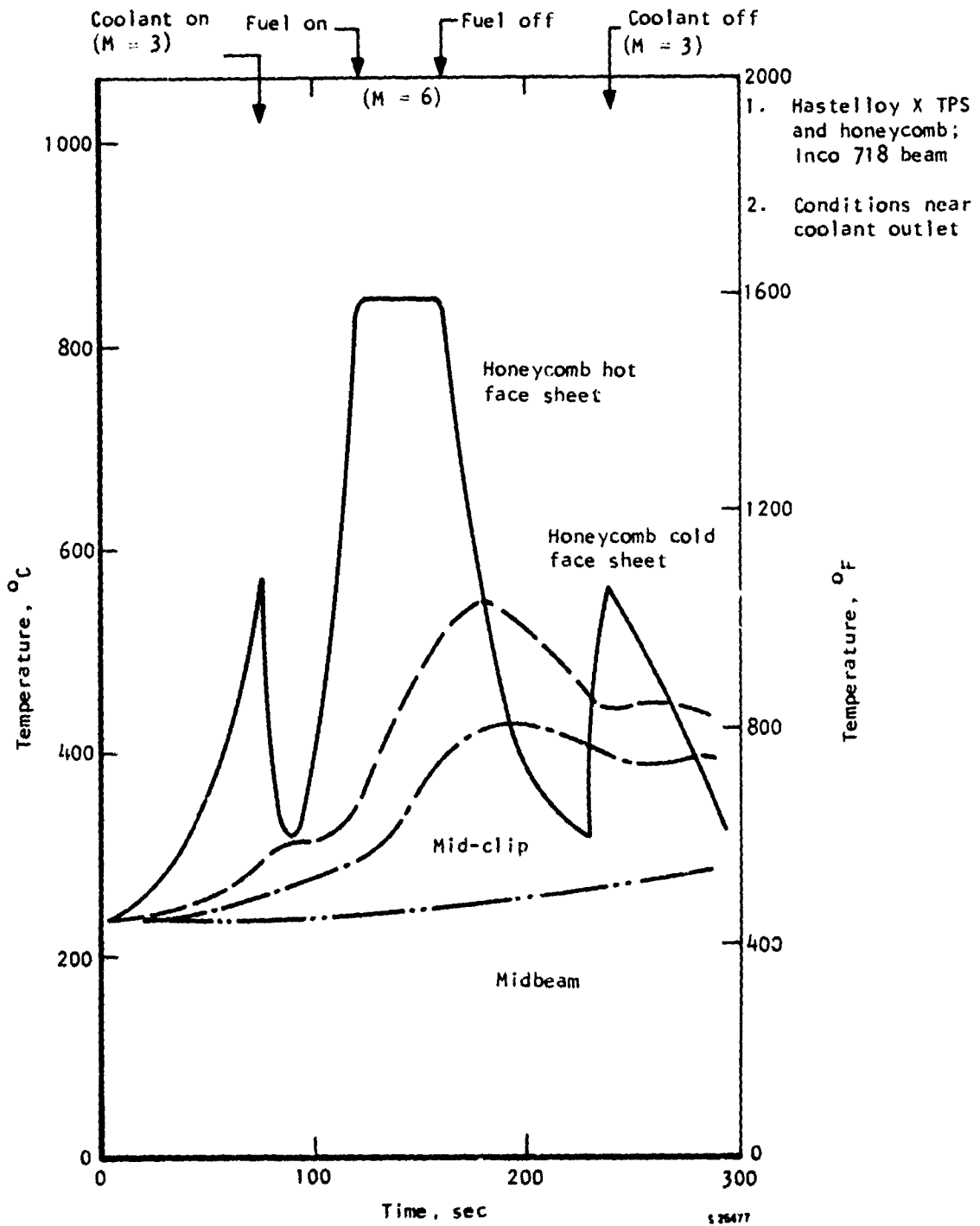
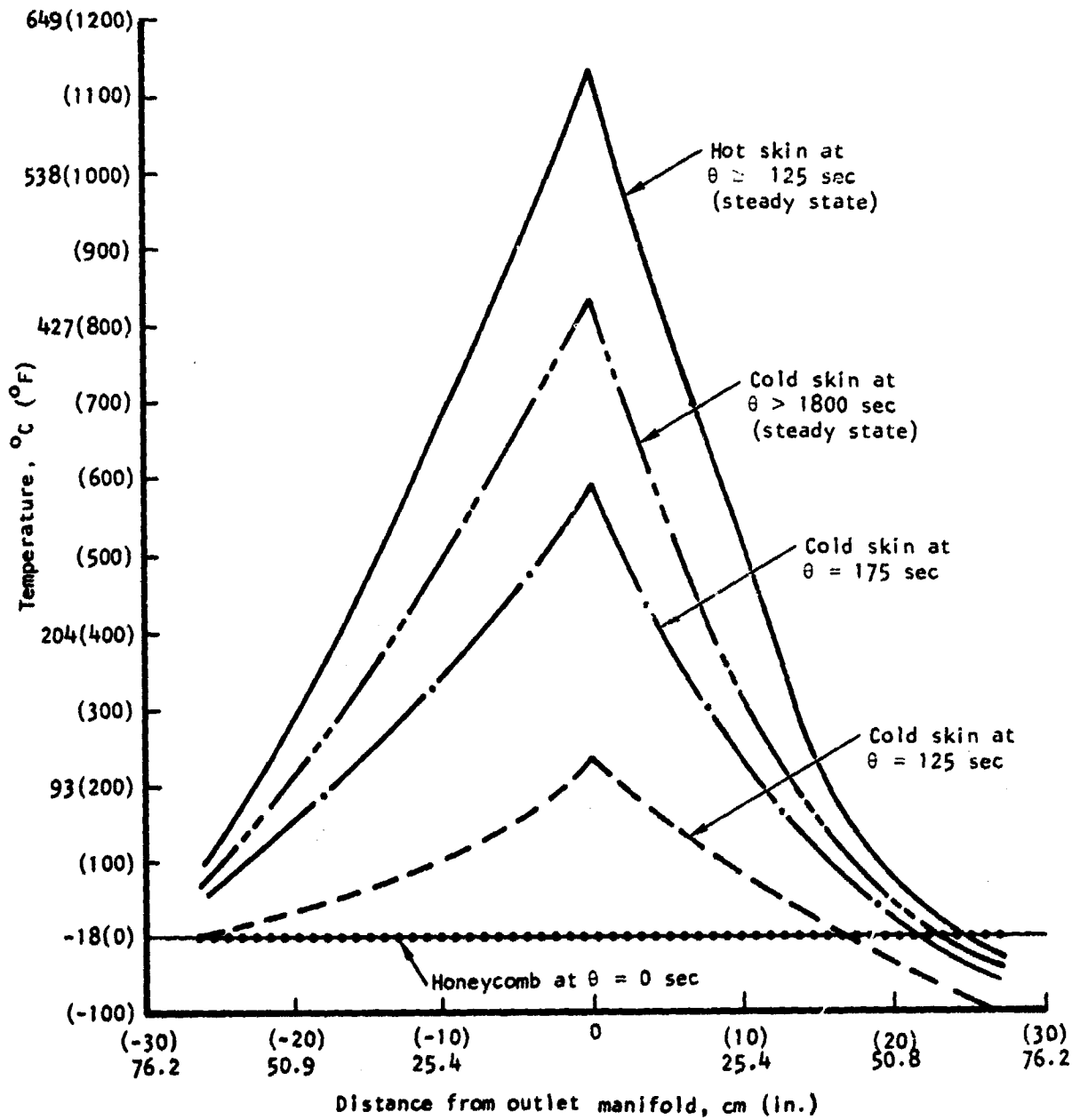


Figure 48.--Coolant Outlet Temperature.

S-25447





8-24832

Figure 50.--Sidewall Honeycomb Panel Temperature Profiles.

## ENGINE-AIRCRAFT INTERFACE

A separate mounting frame is used to join the engine modules to the aircraft. Module loads are transmitted through the topwall honeycomb structure to the mounting frame. The frame transmits engine thrust, drag, and inertial loads to the aircraft and should, therefore, be stiff to prevent excessive deflections. The airframe attachment links should be greater than three to satisfy fail-safe criteria. Truss arrangements are effective in meeting the stiffness/weight goals, but the cross members interfere with the hydrogen ducting. The frame must accommodate module thermal growth and must not impose excessive thermal deflections on the airframe.

The selected concept is shown in fig. 51. In this case, a total of six modules comprise the engine assembly. The frame is rectangular with cross members at the module split line. It was assumed that the maximum temperature of the mounting frame will not exceed 316°C (600°F). Inconel 718 was selected as the preferred material.

Six mounts join the engine frame to the airframe. All mounts carry vertical loads; thrust loads are through the three forward mounts; the two center mounts carry lateral loads (see fig. 51(b)). Swing and sliding links are used to accommodate thermal growth. An alternative is to use only the four outboard mounts. This may be necessary because of limited accessibility to the center mounts.

The spacing between the fore and aft mounting frame beams ("wheelbase") should be maximized to reduce deflections between leading and trailing edges and aircraft outer skin. The corresponding fore and aft module attachment points should be located where the primary structure temperatures are equal. This locating scheme will minimize differential thermal growth between fore and aft mount points, thereby keeping the module axial centerlines parallel during operation. These criteria can be met by locating the frame beams shown in fig. 51(a) at stations 29 and 85 where the topwall primary structure is about 24°C (75°F) during normal operation.

As shown in Figure 51(c), the aft module mounts are fixed axially while the forward mounts are free to slide axially. The central modules are fixed laterally along the inboard sidewall at both fore and aft mounts. Lateral growth of an individual module is outward from the engine centerline, and is cumulative.

The engine compartment must be sealed to prevent ingress of hot gas. Required sliding seals are indicated on Figure 51(d). The fore and aft seals must also accommodate vertical deflection due to fuselage bending. As previously noted, the effect of this deflection is minimized by increasing the mounting frame wheelbase.

The space surrounding the mounting frame must be kept clear for hydrogen manifolding. An additional area above the mounting frame, about 15 to 30 cm (6 to 12 in.) in height, is desirable for installation of the hydrogen fuel and

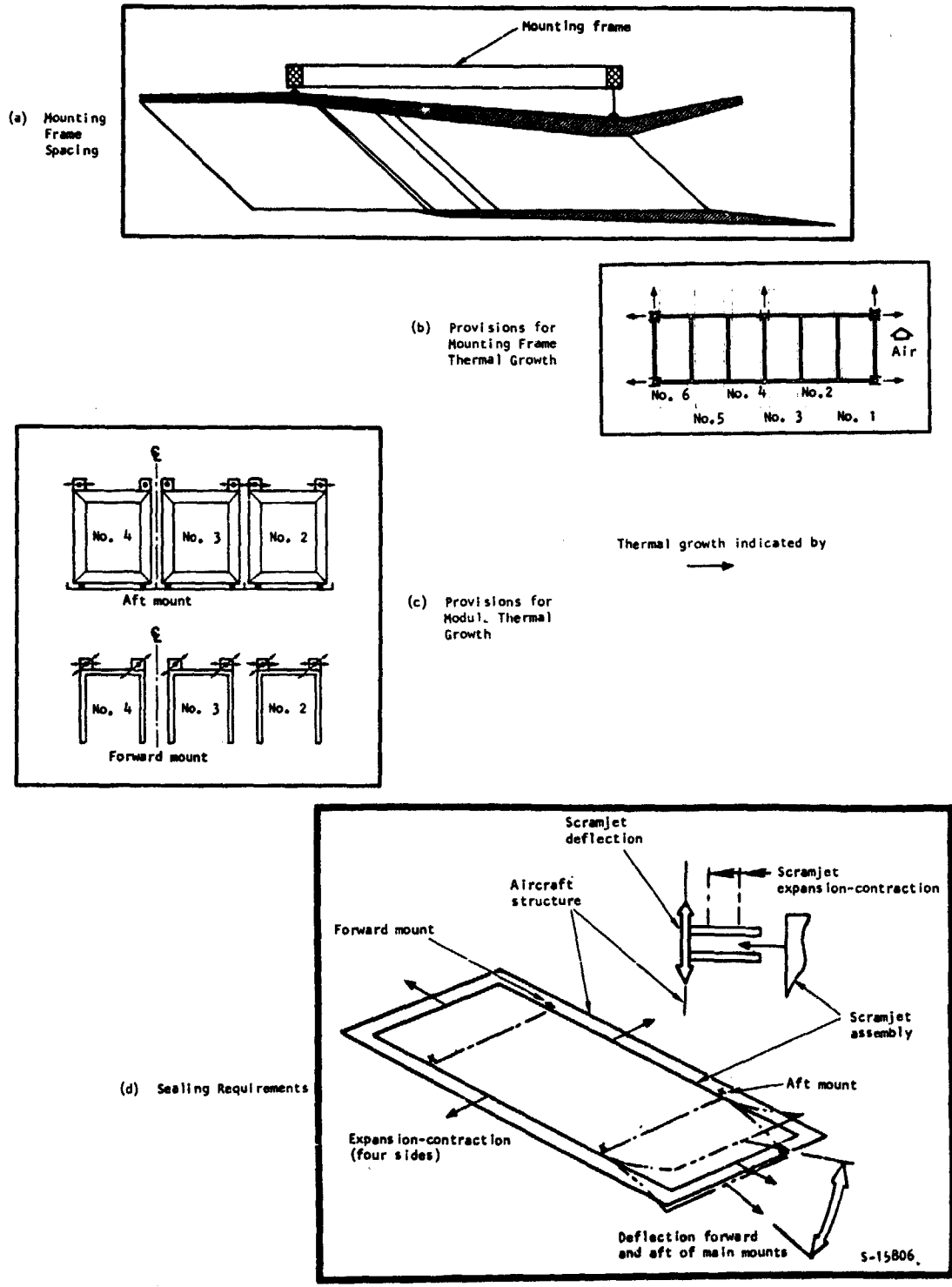


Figure 51.--Engine Mounting Considerations.

ORIGINAL PAGE IS  
OF POOR QUALITY



coolant valves. These valves should be installed close to the engine modules to obtain optimum control response and to minimize the plumbing and the number of firewall penetrations. The entire engine compartment cavity should be purged for safety. Overboard vents will be required for dumping hydrogen during engine shutdown, i.e., whenever coolant flow rates exceed combustion fuel flow rates.

The engine is modularized; however, because common sidewall leading and trailing edges are used and because of limited access in general, a complete single module assembly cannot be separated from the engine cluster. Repair of an individual panel, except for the external cowl, will also require removal of the engine assembly from the aircraft. Strut removal is through the top wall only. Access to the cowl interior and the space between sidewalls with the engine installed on the aircraft is possible by removing a panel on the external cowl.

## HYDROGEN FLOW CONTROL

### Coolant Flow Routing

As previously discussed, the proportion of the total heat load absorbed by any individual flow circuit is not constant throughout the flight envelope. To achieve maximum coolant utilization, active controls will be required to maintain the coolant outlet temperature close to the 890°K (1600°R) limit. The number of controls (coolant flow regulating valves) is dependent on how closely the 890°K (1600°R) limit must be met. A minimum number of valves will be required to ensure that the desired interpanel temperature differentials are not exceeded and that the matching is close to that shown in Figure 12(c).

Maximum coolant utilization can be achieved by using a valve to control coolant flow to each individual module flow route--at least seven valves per module; a total of 42 valves for a six-module engine. Mission analyses are necessary to assess the resulting savings in coolant utilization as compared with control concepts using fewer valves.

The least complex approach is to valve all forward-flow routes in parallel and all aft-flow routes in parallel among the six modules. A third valve controls all strut flow routes. This concept divides the engine into three sections: (1) the inlet section, (2) the combustor/nozzle section, and (3) the struts. It is assumed that there is no large difference in heating rate between modules.

Calibrated orificing is used to establish the basic flow split between the topwall, sidewalls, and cowl within the forward and aft circuits. This approach presumes that the heat load split between panels will remain in a reasonably fixed proportion for all flight conditions. Temperature sensors are imbedded in the thermal protection system panels near the outlet of the flow circuit and adjacent to the outlet manifold. During operation, it is expected that the coolant temperatures at the exits of the parallel flow routes will not necessarily be equal. A computer (microprocessor) will monitor all temperature sensors and will drive the coolant regulating valve (CRV) to maintain the sensor with the maximum temperature reading at 890°K (1600°R). Thus, one of the panel flow circuits within the forward or aft sections can be slightly overcooled.

As noted, the entire cooling capacity in the fuel is not utilized ( $\phi_c$  is less than 1.0 at all conditions). If the remaining capacity is not used for airframe cooling, then it would be possible to operate the engine structure at a lower temperature level by using the entire flow rather than just the portion based on a 890°K (1600°R) outlet temperature. Control valves would still be required to regulate the flow split. This scheme does offer potential improvements. It was not considered except for the struts because one of the goals of the study is to conserve coolant.

No provision has been made to shut down a single module in the event of an unstart or other abnormal condition. Since the transient conditions in the engine are severe for even normal operation, operation without combustion in one of the modules may prove feasible as is. Control system response, in turn, may be too slow to prevent the imposition of the large  $\Delta T$ 's associated with combustion shutdown in one module. Additional valving might be of no benefit in such a case. Further detailed study will be required to evaluate the effects of these conditions on both the engine structure and control system configuration.

## Fuel System

A preliminary study was conducted to define the Scramjet fuel system. Estimates of the component sizes and weights were made. To permit selection and sizing of the turbopump system, it was assumed that the equipment would be used in a research airplane in which the flight duration is 40 sec of cruise at Mach 6.

All hydrogen lines have been sized on the basis of a total fuel flow of 3.85 kg/sec (8.5 lb/sec) and 0.644 kg/sec (1.42 lb/sec). This is the fuel flow for six modules.

Fuel system schematic.--A schematic diagram of the installation is shown in Figure 52. The modules are grouped in two sets of three. A separate turbopump, coolant regulating valves, and fuel valves are used for each set of three modules. This arrangement permits testing either a three- or six-module cluster on the research airplane.

For maximum response rate, the coolant regulating and fuel control valves should be located adjacent to the engine modules. It is possible, however, to locate the turbopumps in a remote location, closer to the hydrogen supply tank. The computer should be installed in a controlled environment.

Overall dimensions and weights of the system components are summarized in Table 14. Each valve will consume 2.7 watts except for the purge and shutoff valve that will consume 35 watts when energized. Component descriptions are presented below.

Hydrogen supply.--The hydrogen supply in the tank is very close to saturation. It has been assumed that the turbopump can be designed to operate at this condition by using a specially designed inducer. A separate boost pump may be required. Alternatively, the hydrogen supply tank could be maintained at 0.34 MPa (50 psig).

Helium supply.--A separate helium supply tank is utilized to purge the hydrogen system after use and to provide a flow of purge gas in the payload bay after the research airplane drops from the B-52. A helium supply line is also routed to the engine compartment to supply helium to the fuel control valve actuators.

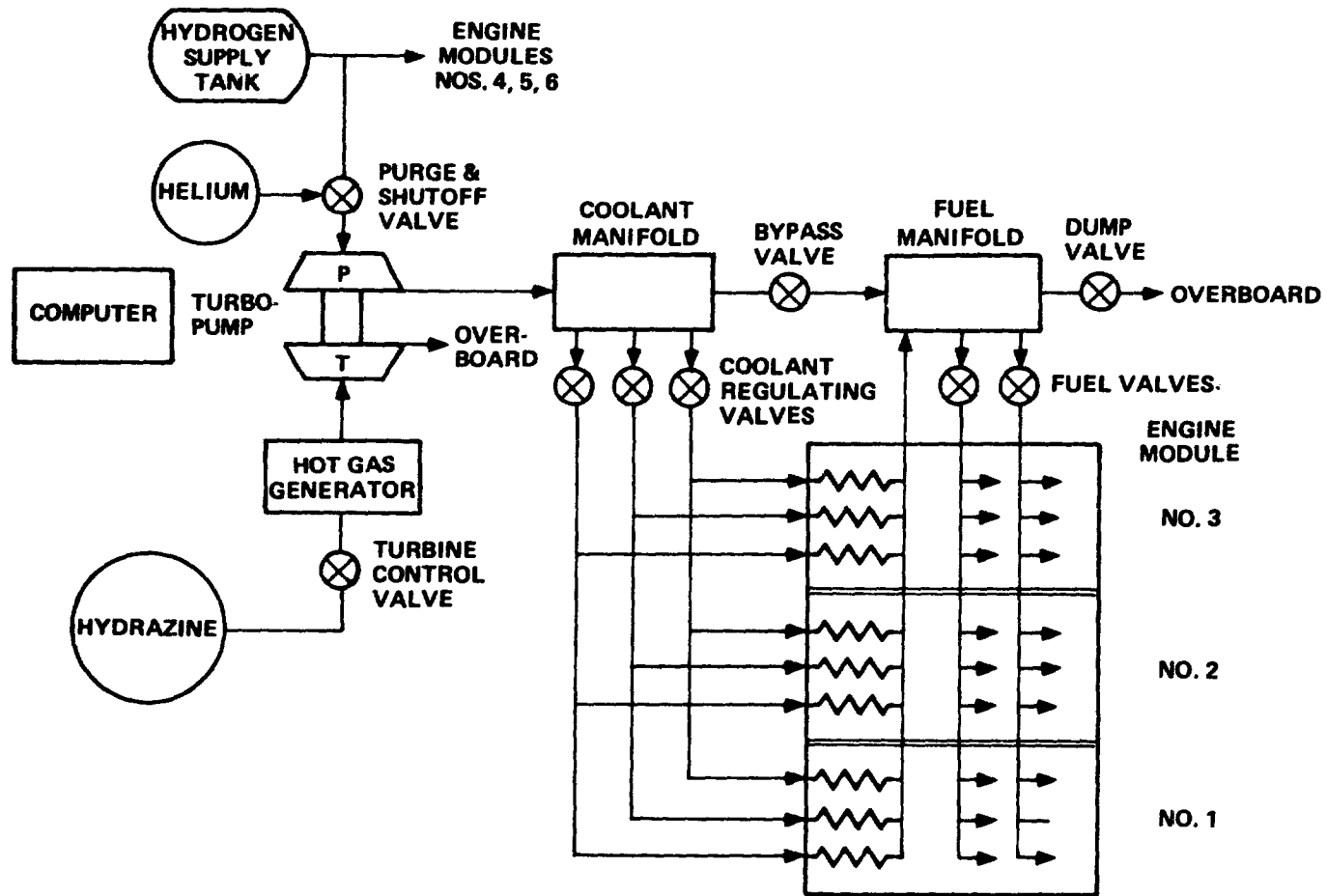


Figure 52.--Engine Fuel System.

TABLE 14.--FUEL SYSTEM COMPONENTS (TWO GROUPS OF THREE MODULES; SIX MODULES TOTAL)

Component	Envelope		Unit Weight		Total Weight	
	cm	in.	kg	lb	kg	lb
<b>Valve</b>						
Coolant regulating (6)	17.8 dia x 22.9 lg	7.0 dia x 9.0 lg	5.1	11.3	30.8	67.8
Fuel control - parallel injector (2)	17.8 dia x 22.9 lg	7.0 dia x 9.0 lg	5.1	11.3	10.3	22.6
Fuel control - perpendicular injector (2)	20.3 dia x 22.9 lg	8.0 dia x 9.0 lg	5.8	12.8	11.6	25.6
Bypass (2)	15.2 dia x 23.9 lg	6.0 dia x 9.4 lg	3.6	8.0	7.3	16.0
Dump (1)	15.2 dia x 22.9 lg	6.0 dia x 9.0 lg	8.2	18.0	8.2	18.0
Purge and shutoff (1)	15.7 x 22.9 x 31.5	6.2 x 9.0 x 12.4	6.4	14.0	6.4	14.0
Turbine control (2)	5.8 x 13.5 x 13.7	2.3 x 5.3 x 5.4	2.7	6.0	5.4	12.0
Computer (1)	12.7 x 20.3 x 34.8	5.0 x 8.0 x 12.5	13.6	30.0	13.6	30.0
He supply tank (1)	45.7 dia	18.0 dia	72.6	160.0	72.6	160.0
Turbopump (2)	23.4 dia x 25.9	9.2 dia x 10.2	29.5	65.0	59.0	130.0
Gas generator (2)	13.0 dia x 10.2 lg	5.1 dia x 4.0 lg	3.4	7.5	6.8	15.0
Total weight					232	511

The tank is assumed to be spherical with an operating pressure of 34.5 MPa (5000 psia). The volume is 42.5 liters (1.5 cu ft) and the tank weight is 72.5 kg (160 lb), including 4.5 kg (10 lb) of helium.

Computer.--The basic control system approach is to utilize a central programmable digital computer that will handle upwards of 300 input parameters and control some 30 output control variables. All valves in the various hydrogen circuits will be under the command of the digital computer. The computer provides all logic and control signals necessary for (1) operating the combustor fuel feed and distribution as required by speed and altitude for desired equivalence ratios, (2) regulating coolant flows to the engine module panels to maintain the desired skin temperatures, and (3) performing numerous safety and self-checking functions.

Estimated size is that of a 1/2-ATR (short) standard size case, 12.4 cm (4.88 in.) wide by 31.8 cm (12.52 in.) long by 19.4 cm (7.62 in.) high. Total volume is equal to 8500 cc (0.3 cu ft). Estimated power requirement is 40 watts, 28 vdc. The estimated weight is 13.6 kg (30 lb).

Turbopump subsystem.--A hot-gas-driven turbopump is recommended rather than a bootstrap-type design as used on the HRE. The reasons are:

- (1) The coolant  $\phi$  is less than 1.0 compared to about 3.0 on the HRE. Hence, additional hydrogen would be required to drive the turbopump. A bootstrap design may be feasible if the coolant  $\phi$  is maintained at unity at all conditions.
- (2) The plumbing required to supply hot hydrogen from the modules to the turbopump is eliminated. This is especially important if the turbopump is in a remote location.
- (3) A separate hot gas supply may still be required to start the turbopump in addition to the bootstrap arrangement.
- (4) Greater flexibility for research testing.

The characteristics of the hydrogen turbopump and hot gas generator are summarized in Table 15. This particular design is for a fuel flow of 2.56 kg/sec (5.65 lb/sec), which occurs with four modules at a Mach 6 condition. Thus the turbopump has growth capability and would be suitable for an 8-module engine cluster.

Two different hot gases were considered--hydrazine\* ( $H_2N_2$ ) and hydrogen peroxide ( $H_2O_2$ ). The resultant turbine and gas generator sizes are about equal. For a given mission duration, less hydrazine is required, and considering that oxygen is a decomposition product of hydrogen peroxide, it is believed that hydrazine is safer to use with hydrogen.

\*Hydrazine is currently used by the Concorde and F-16 emergency power units and the Space Shuttle APU.

TABLE 15.--TURBOPUMP SUBSYSTEM, THREE MODULES

Turbopump	Hydrogen pump	Hot gas turbine	
		H <sub>2</sub> O <sub>2</sub>	N <sub>2</sub> H <sub>2</sub>
Inlet temperature, °K (°R)	20.6 (37)	1006 (1810)	1200 (2160)
Inlet pressure, MPa (psia)	0.21 (30)	2.76 (400)	2.76 (400)
Discharge pressure, MPa (psia)	7.58 (1100)	0.14 (20)	0.14 (20)
Flow, kg/sec (lb/sec)	2.56 (5.65)	0.62 (1.37)	0.40 (0.88)
Efficiency, percent	79	71	58
Power, MW (hp)	0.350 (470)	0.373 (500)	0.373 (500)
Impeller dia, cm (in.)	104 (4.1)	11.9 (4.7)	11.7 (4.6)
Housing dia, cm (in.)	23.4 (9.2)	19.1 (7.5)	18.0 (7.1)
Total weight, kg (lb)	29.5 (65)		
Gas generator		H <sub>2</sub> O <sub>2</sub>	N <sub>2</sub> H <sub>2</sub>
Diameter, cm (in.)		14.0 (5.5)	13.0 (5.1)
Length, cm (in.)		10.2 (4.0)	10.2 (4.0)
Weight (each), kg (lb)		3.9 (8.6)	3.4 (7.5)

It was determined that by using two turbopumps in parallel rather than a single unit for all six modules, a weight savings of 10.4 kg (23 lb) could be achieved.

Valves.--The designs are electropneumatic poppet valves and were scaled from existing designs originally developed for the HRE program.

Coolant regulating valves: Three CRV's are shown in fig. 50 with one valve controlling the same flow circuit in each module (a parallel-flow arrangement).

Fuel control valves: For minimum complexity, only one valve is used for each set of parallel and perpendicular injectors. With a single set of fuel valves, however, it will be necessary to shut down the entire set of three modules in the event of an off-limit condition (e.g., unstart). The cost of a research flight as well as flight safety considerations in any ultimate application will probably dictate the ability to shut down an individual module. Hence, two fuel control valves will be required for each module.

Bypass valve: A bypass valve is utilized because the fuel flow required by the Scramjet exceeds the coolant flow requirement ( $\phi_c < 1.0$ ). The coolant regulating valves will be controlled to maintain the hydrogen outlet temperature (at the fuel manifold) at 89.0°K (1600°R). The bypass valve will be controlled to maintain the fuel manifold pressure at 5.2 MPa (750 psia).

Fuel dump valve: The fuel dump valve has been sized to handle the total coolant flow requirement. That is, it has been assumed that at the end of the Scramjet cruise, the fuel flow will be turned off, but the engine will still require full cooling for a short period of time.

Line size: Line size and hydrogen conditions for each location are summarized in Table 16. The helium supply line to the engine compartment is 9.5 mm (3/8-in.) diameter.



TABLE 16.--FUEL SYSTEM PLUMBING LINE SIZE

Location	Flow		Pressure		Temperature		Outside dia	
	kg/sec	lb/sec	MPa	psia	°K	°R	cm	in.
Pump inlet	4.15	9.15	0.14	20	21	37	8.9	3.5
Pump discharge	4.15	9.15	7.58	1100	56	100	5.1	2.0
Coolant regulating valve outlet	0.17	0.38	6.55	950	56	100	1.9	0.75
Bypass valve outlet	1.54	3.40	5.52	800	111	200	6.4	2.5
Turbine inlet	0.29	0.65	4.14	600	889	1600	5.1	2.0
Turbine discharge	0.29	0.65	0.14	20	556	1000	11.4	4.5
Dump valve discharge	2.31	5.10	0.69	100	889	1600	10.2	4.0

## CONCLUDING REMARKS

Overall objectives for the Scramjet engine design can be met. It is possible to attain a life of 100 hours and 1000 cycles, which is the goal for the intended research application. The coolant equivalence ratio is less than 1.0 throughout the engine operating envelope; however, at the maximum altitude and Mach number conditions a fuel equivalence ratio of 1.5 was used. Estimated coolant equivalence ratios for stoichiometric combustion at these conditions indicated a coolant equivalence ratio increase to 1.239. Thus, stoichiometric combustion requires the use of additional fuel for cooling at the Mach 10 condition with a 2-g turn. The mechanical design is feasible for manufacture using conventional materials. For the cooled structures in a six-module engine, the mass per unit capture area is  $12.4 \text{ KN/m}^2$  ( $259 \text{ lb/ft}^2$ ). The total weight of a six-module engine assembly including the fuel system is  $14.73 \text{ KN}$  ( $3311 \text{ lb}$ ).

### Cooled Structure

An all-honeycomb primary structure is better than beam and honeycomb combinations in terms of minimum deflection and complexity for equal weight. The required honeycomb material, cell dimensions, overall size, and contour are feasible for manufacture. The engine panels, i.e., the topwall, sidewall, and cowl, may be rigidly joined at the corners and no dynamic hot gas seals are required. Selected materials are: honeycomb primary structure--Inconel 718; TPS--Hastelloy X or Nickel-200; and leading edges--Nickel-200.

### Coolant Flow Routing

It is best to introduce coolant at the leading and trailing edges and let it flow toward the engine throat, where it is withdrawn. This basic flow scheme must be adjusted, however, to achieve temperature matching between panels. Uniformity in temperature gradients between panels is crucial in meeting thermal stress limitations. Active controls will be required to obtain maximum coolant utilization. The minimum number of flow routes to be controlled is three--forward and aft portions of the panels and a separate control for the struts.

### Thermal Protection System

In the HRE program, low-cycle fatigue of the offset-fin plate fin TPS was identified as the primary limitation on structural life. For the Scramjet, two heat exchanger geometries were determined to yield significantly better fatigue life. For the panels, topwall, sidewalls, and cowl, a machined channel design is specified. For the struts a pin-fin surface is recommended. Experimental data are required to substantiate the predicted low-cycle fatigue life and creep-rupture behavior of the selected TPS structures. A NASA-sponsored fabrication and material technology development program presently in progress is expected to provide such data. Test data are also required to confirm that the corner heat flux is not significantly higher than that at the engine centerline.

## Leading Edges

Low-cycle fatigue is the controlling design parameter. High performance is achieved by impinging the entire panel flow at the minimum supply temperature, 100°R, on the respective leading edges. Nickel-200 was specified because of its high thermal conductivity and ductility, two factors that contribute to increased fatigue life. The one-dimensional analysis (on which results in this report are based) should be extended to two dimensions to more precisely define the problem. Experimental data are required because of the intensity of the heat flux, complexity of the flow path, and the impact of brazing and other manufacturing operations on fatigue life.

## Fuel Injection Struts

External pressure loads, such as occur during an unsymmetrical unstart, combined with thermal stresses, impose major design problems for the slender struts. Design feasibility was proven, however. A midspan tie between struts is necessary to withstand unstart loads using minimal coolant flow. A possible alternate that eliminates the tie is to overcool the struts.

The limited space within the struts dictates the fuel and coolant flow routing. Integral manifolding with flow from one end of the strut remains as the most feasible approach.

The dynamic response of the struts to the unstart transient should be evaluated. Significant load amplification could occur because the pressure pulse period is close to the strut natural frequency.

## Engine-Aircraft Interface

Hydrogen flow control valves and manifolding should be located on the module mounting frame to provide an integral assembly, especially for a research application, and to achieve optimum control response. Behavior of the overall module cluster and the assembly response to an individual module shutdown deserve further attention to define the sealing problem and interface thermal stresses.

## Hydrogen Flow Control

The minimum number of valves has been specified. Additional valves may be required to provide for shutdown of an individual module or closer regulation of coolant temperatures.